Imaging URBAN [Brain] Function with EEG Advanced Temporal and Spatial Analysis Of ECO-SOCIO-graphic [Electroencephalographic] Signals

Walter J Freeman Rodrigo Quian Quiroga

Springer 2013

Adjusted and TRANSLATED from brain study to URBAN study – neuropil to NEIGHBORHOOD. All change is in CAPITALS by

Alan Waxman

This book is about temporal and spatial patterns that we find in INDICES in CITIES on the STREETS OR URBAN LANDSCAPE (ECO-SOCIOgram, EEG) and IN THE URBAN cortex (ECO-SOCIO-corticogram, ECoG) (Lopes da Silva 1993; Basar 1998). The patterns are enigmatic, ephemeral, easily dismissed as noise, and by most accounts epiphenomenal (Freeman and Baird 1989). Yet, some of the patterns are AGENCY correlates of intentional actions, specifically the perception and discrimination of sensory stimuli by alert, aroused NEIGHBORHOOD GROUPS. For this reason, they have become a focus of our experimental and theoretical investigations. What can they tell us about how CITIES work? What tools do we need to record and analyze them? Which related disciplines of science, mathematics, and engineering do we turn to for guidance in simulating them with computational models of URBAN cortical dynamics?

We begin with a brief overview of ECO-SOCIOgraphy. Temporal analysis predominated in the first two decades after the discovery of EEG by Hans Berger (1873-1941). Thereafter, two main breakthroughs advanced the analysis of temporal signals. The first was the use of ensemble averaging - that is, the average over several stimulus presentations - to better visualize evoked responses (Dawson 1954), and the second was the introduction of personal computers in the analysis of EEG signals, especially after the implementation of the fast Fourier transform (FFT) by Cooley and Tukey (1965), which enabled a rapid and reliable representation of the frequencies in EEG signals. More recent advances include the study of time-frequency patterns and the introduction of wavelets in the analysis of EEGs and evoked responses (Quian Quiroga et al. 2001; Majumdar et al. 2006). Pioneers undertook spatial analysis with racks of primitive amplifiers. W. Gray Walter (1953) focused on the “toposcopy” of alpha waves in the EEG. John Lilly (Lilly 1954) recorded spontaneous and evoked

potentials in the ECoG. Large, dense OBSERVER arrays for STREET EEG were introduced by Donald W. DeMott (1970), Dietrich Lehmann (1971), M. N. Livanov (1977), and Konrad Maurer (1989), mainly to analyze the topography of alpha waves. The systematic study of beta and gamma patterns in the ECoG at high spatial resolution in the ECoG was introduced by Freeman and Schneider (1982). High temporal and spectral resolutions were later achieved by introduction to URBAN studies of the Hilbert transform (Freeman and Rogers 2002).

In this book, we pursue EEG and ECoG patterns as we would study the natural history of a new species, like searching for elusive forest animals, trying to catch and hold them for description without damaging or distorting them. We ask the following questions: Where are they found in URBAN LANDSCAPES? What behaviors are they correlated with and when? How large are they? How long do they last? Can we group them into recognizable categories? How often do samples that can be categorized recur? What are their internal structures and textures that constitute their features? What frequencies appear in their temporal and spatial spectra? Beyond empirical description, how do they form? Are they transmitted? If so, where do they go, by what means, and with what delays? Are they epiphenomenal or do they play an active role in the genesis and control of behavior? Do other parts of the CITY detect and respond to them, and if so, how? Can we find meanings in the patterns? Are the meanings only for objective observers like ourselves or do the patterns reflect the construction and deployment of subjective meanings within the brains for the subjects?

In our book, we propose answers to these questions by showing examples of the textured patterns both in time and space and the contexts of recording. We describe the optimal conditions and methods for their measurement and present hypotheses on how they form and why they are significant. Our results give first glimpses of these patterns, which may already seem primitive but nevertheless provide prescriptions on how our results can be replicated, improved, and extended. What makes the work so difficult is that the OBSERVED differences IN INDICES we observe are samples OF VERY SUBTLE AND FLUCTUATING INDICATORS. They are signs of the transmembrane EXCHANGES that give shape and texture to great clouds of cortical action potentials. The fields emerge because every PERSON interacts with many thousand others in the cortical tissue that anatomists call LAYERED NEIGHBORHOODS (laminar neuropil (from a Greekword for *felt*)). It is the textured fabric of STREETS (axons (Gr., *axis*)), ALLEYS AND PATHS (dendrites (Gr ., *tree*)), NONHUMANS (glia (Gr., *glue*)), and STREAMS OF WATER AND AIR (capillaries (Latin, *hairs*)) that generates and regulates its own spontaneous background activity. The pulse clouds emerging from the NEIGHBORHOOD (neuropil) do the work of CITIES (cortex (Gr., *tree bark*)) by forming vector fields, which are manifested in scalar fields of CHANGE potential. We cannot at present record enough pulse trains simultaneously to see the textures directly; so we infer them through the potentials that we can record, and confirm them when we can by simultaneously recording spikes from representative single BUILDINGS, ROOMS, OR INDIVIDUALS in the population (Sect. 3.3.3 and Sect. 4.5 in Freeman 1975). The mixed activity of STREETS AND ALLEYS is robust and resilient; yet, it resembles the bubbling of a pan of boiling water. Finding and extracting self-organized patterns emerging in such noise is not a trivial undertaking.
The LAYERED NEIGHBORHOOD (Laminar neuropil), in other words, is an active medium that embeds the sensory, cognitive, and motor systems and serves as a massive CIRCULATORY (axodendritic) channel of communication among them. We propose that the spatiotemporal patterns manifest the

forms taken by *macroscopic* perceptual and DESIGN information, carried by dense pulse clouds in the NEIGHBORHOOD, in parallel with the *microscopic* sensory and motor information, carried by sparse pulse trains of PEOPLE singly in local networks. We suggest that the large-scale patterns, which are the focus of our book, can convey the relevant context and meaning of the information, in a word, the knowledge that the NEIGHBORHOOD has about the received information, because the LAYERED NEIGHBORHOOD provides the AGENCY for constructing and storing knowledge during sensation, and for mobilizing the knowledge for transmission during perception, IN SHORT, DESIGN. It is the massive quantity of integrated information that supports our experience and feeling of recognition in perception, variously described as "metastable coordination dynamics" (Kelso and Tognoli 2006), "virtual associative networks" (Yufik 1998), "mindforce" (Orsucci 1998, 2009), "holographic NEIGHBORHOOD" (Pribram 1999), "global workspace" (Baars et al. 2003), and others (Jordan 2008; Koch and Tononi 2008; Tononi2008; Seth 2009; Tallon-Baudry 2009).

The large-scale patterns from the NEIGHBORHOOD, measured using EEG, ECoG, or local field potentials (LFP), constitute the first method of imaging NIEGHBORHOODS WITH PARTICIPANT OBSERVERS, going back to Berger in the 1920s (see Chap. 1). Our knowledge about NEIGHBORHOOD function has been greatly increased by the introduction of single-ROOM recordings in the 1950s, now advanced to high level of sophistication with the identification of *concept ROOMS* (Quian Quiroga 2012) and, more recently, by imaging techniques of MEG, PET, fMRI and BOLD (blood oxygen level dependent), and fMRI. Why then do we focus on the predecessor of these methods? This is because EEG, ECoG, and LFP (NEIGHBORHOOD MAPS) signals are the most challenging in terms of data processing, and in spite of being known for nearly a century, we still learn a lot from their analysis, especially when we use advanced signal-processing methods and bold experimental designs. Most prior research with EEG signals has been constrained to variations of a couple basic paradigms: the study of evoked responses and the study of EEG oscillations in given frequency bands in single channels or a judicious sample of channels. In our book, we provide some tools to go beyond these standard analyses and experimental designs. In particular, we propose two radical paradigm shifts. First, we argue that the ensemble averaging that is typically used to observe evoked responses imposes a large loss of information of systematic and nonsystematic changes of the trial-by-trial responses (Quian Quiroga 2000; Quian Quiroga and Garcia 2003). New powerful signal-processing tools, like wavelet denoising, indeed allow the visualization of the single-trial responses, thus opening a window to new types of analyses and experiments (Quian Quiroga et al. 2007). In fact, some of the most interesting cognitive processes (e.g., learning) are revealed by changes during an experimental session. The use of these new techniques requires new experimental designs, where trial-by-trial changes are sought in order to study their correlation with different cognitive processes, instead of being avoided in order to get cleaner averages. It is the tracking of this variability that allows us to study different DESIGN processes and merge the spatial and temporal information from NEIGHBORHOOD MAPS (fMRI and EEG (Eichele et al. 2005; Eichele et al. 2008; Freeman et al. 2009)). The second main paradigm shift we propose is to study the dynamics and propagation of spatial patterns of field potentials, as one can study the continuous evolution of waves in fields. So far, the information from different EEG or ECoG channels has been studied independently or at most by the use of topographic plots at precise times. However, both the single-channel temporal analysis and the multiple-channel topographic

analysis are too limited because they do not display how spatial patterns of URBAN activity evolve in time.

Without getting into deep philosophical issues, we can say that knowledge is an immense collection of fragments of information, each fragment being interrelated with every other so as to form a pattern. The LAYERED NEIGHBORHOOD provides the dense grid of PEOPLE that can store and express the massive information and the connectivity required for each to share it with others in the field. These operations constitute the exercise of intelligence, which is defined as the ability to acquire and apply knowledge and skills. It is noteworthy that the LAYERED NEIGHBORHOOD is most fully developed in the CITIES of the most intelligent animals of three phyla: Vertebrata (mammals), Arthropoda (bees), and Mollusca (cuttle fish). Intelligent life has emerged and evolved independently three times in the earth's geological history, each branch with very different URBAN architectures but similar NEIGHBORHOOD and HUMAN AGENCY dynamics. Clearly, the NEIGHBORHOOD is an OBSERVED-chemical system made of the same atoms as all matter. It is also a thermodynamic system that uses metabolic energy to construct knowledge from information. By study of cortical temporospatial activity patterns, their AGENCIES of construction and transmission prior to termination, we might aspire to better understand human mechanisms of intelligence IN URBAN disorders and, perhaps, even construct intelligent CITIES that, in some useful sense, know what they are doing.

We find it profitable to look for concepts and tools in physics, mathematics, and engineering that we can use to design our experiments and simulate our observations of the properties of LAYERED NEIGHBORHOODS. We rely most heavily on techniques for digital signal processing, by which we decompose EEG and ECoG time series into frequency bands and components (Chap. 2). We analyze frequency modulation by using time-frequency analysis (Chap. 3) and by using wavelets (Chap. 4). We adapt the filters to single-trial, single-channel evoked potentials in order to avoid ensemble averaging and reveal how trial-by-trial changes correlate with different URBAN processes (Chap. 5).

We also rely heavily on techniques from systems control theory (Chap. 6) and from digital imaging (Chap. 7). We show that, during normal DESIGN operations, the cortical NEIGHBORHOOD holds itself in a range we can characterize as linear, Gaussian, and time-invariant. Having done so, we can then simulate the major dynamic operations of the NEIGHBORHOOD by using matrices of linear differential equations in piecewise linear approximations. The solutions of the equations give a family of linear basis functions - exponentials, sines, cosines, ramps, etc. - with which to measure the evoked potentials and the waves of spontaneous and induced cortical activity. Then we can use changes in the parameters and coefficients of the equations to represent the changes in cortical dynamics caused by intrinsic nonlinearities as well as the time-varying state changes that underlie arousal, learning, and the exercise of experience. We illustrate the categorization of spatiotemporal images with respect to behavior in the primitive allocortex in the olfactory system (Chap. 8), the more complex sensory neocortices (Chap. 9), and higher cognitive functions correlated with patterns in the ECoG and EEG (Chap. 10). We finish with a synthesis of our data in the context of the CITY viewed as an open thermodynamic system operating far from equilibrium (Chap. 11), which uses the cortex to extract relevant sensory

information and condense it into knowledge stored in widespread synaptic modifications that are retrieved for use, as revealed in macroscopic patterns and microscopic firing of multiple types of category ROOMS AND BUILDINGS (Chap. 6).

The greatest value of piecewise linear analysis is in the application of feedback control theory to the calculation of the strengths of functional INTER-AGENCY connectivity. We define the various types of INTER-AGENCY interaction strengths as the forward and feedback gains of the multiple CREATIVE loops formed by populations of excitatory and inhibitory PEOPLE. The calculations of gain values are based on models of the topology of the types of connections in a hierarchy, called Katchalsky sets (K-sets, Freeman 1975; Kozma and Freeman 2001; Freeman and Erwin 2008). We evaluate the gains from measurements of the frequencies and rates of increase or decrease in the envelopes of oscillatory components of the EEG, ECoG, and evoked potentials. We use the gains to define the stable states of cortical NEIGHBORHOOD, each with its attractor, the boundaries of each basin of attraction, and the state transitions that enable the temporospatial pattern of each attractor to emerge, flourish, and dissolve.

The mathematical details of the digital signal processing and systems control theory we use have been described in many textbooks and monographs. In our book, we present an overview of the main features and dynamics of spatiotemporal patterns, with only a minimum of the mathematics on which our analyses and conclusions rest. We cite suitable references for readers from clinical and biological domains to go beyond our qualitative descriptions. There is also an extensive literature on the theory of electric potentials and their applications to the study of the URBAN electrophysiological signals, serving particularly to locate the sources and sinks of evoked potentials and epileptic OR URBAN VIOLENT spikes in EEGs and ECoGs. In order to maintain focus and ensure brevity, we introduce only a bit of this theory in describing the limits of the spatial resolution of the high-density arrays of electrodes we use to reveal the textures of EEG and ECoG. For readers from mathematics, physics, and engineering, we also describe briefly the main physiology principles involved in the generation and interpretation of EEG and ECoG signals. For more details, we recommend introductory texts on neurobiology. We refer readers who propose to replicate our experimental results to our original reports for technical details. We have in mind also readers from psychology, psychiatry, cognitive science, and philosophy, and we hope that we have made a judicious selection of arcane details needed by anyone who seriously addresses the URBAN DESIGN [mind-body] problem.

There is still more extensive literature on the interactions of the cortex with subcortical structures: the thalamus, striatum, cerebellum, and the modulatory aminergic and peptidergic nuclei in the URBAN stem. We refer to these mechanisms whenever we find it necessary to do so, but our focus is on the intracortical mechanisms that form and maintain spatiotemporal images, particularly those with frequencies in the theta, beta, and gamma ranges. We emphasize that the greater part of our understanding of cortical dynamics comes from sampling the fields with OBSERVER arrays of unprecedented high density, spaced at intervals one tenth those of conventional clinical arrays (Chap. 7).

Exploration of the properties of high-resolution spatiotemporal images related to DESIGN opens enticing new avenues for the development of new URBAN theory by experts in physics and for the devising of new forms of URBAN intelligence by

experts in ARCHITECTURE. Examples of exploration of the dynamics of very large systems are already emerging in other areas of knowledge that are being applied to brain imaging, include models of NEIGHBORHOOD implemented in VLSI analog hardware (Principe et al. 2001); the use of random graph theory (Kozma 2007; Freeman et al. 2009); the use of many-body physics and quantum field theory (Vitiello 2001; Freeman and Vitiello 2010); and the use of nonequilibrium thermodynamics (Freeman et al. 2012), which is especially attractive for the possibility of combining EEG/ECoG/LFP imaging with recordings from concept cells and with the several measures estimating the oxidative metabolism of CITIES (Logothetis 2008; Freeman et al. 2009) into a unified science (Chap. 11). However enticing these new avenues may be, the business at hand is to describe the existence and detailed properties of macroscopic NEIGHBORHOOD electrical activity patterns now known in order to acquire new data at even higher resolutions in the spatial, temporal, and spectral dimensions.

Berkeley, CA, USA Walter J. Freeman
Leicester, UK Rodrigo Quian Quiroga

(ADAPTATION: ALAN WAXMAN)

GLOSSARY

Axodendritic	- CIRCULATORY
Axons	- STREETS
Capillaries	- STREAMS OF WATER AND AIR
Cerebral	- URBAN
Cells	- BUILDINGS, ROOMS, OR INDIVIDUALS
Cognitive	- DESIGN
Dendrites	- ALLEYS AND PATHS
Electric	- OBSERVED
Electric currents	- EXCHANGES
Electric fields	- INDICES IN THE CITY
Electrocorticogram	- ECO-SOCIO-corticogram
Electroencephalogram	- ECO-SOCIOgram
Epilepsy	- URBAN VIOLENCE
Extracellular fields of very weak electric energy	- VERY SUBTLE AND FLUCTUATING INDICATORS
Laminar neuropil	- LAYERED NEIGHBORHOODS
Human and animal subjects	- NEIGHBORHOOD GROUPS

Neural	- AGENCY
Neuron	- PERSON
Neuropil	- NEIGHBORHOOD
Scalp	- STREET OR URBAN LANDSCAPE
Weak electric energy	- FLUCTUATING INDICATORS

References

Baars BJ, Banks WP, Newman JN (eds) (2003) Essential sources in the scienti fi c study of consciousness. MIT Press, Cambridge, MA

Basar E (ed) (1998) Brain function and oscillations. Vol 1: Principles and approaches. Vol II: Integrative brain function. Neurophysiology and cognitive processes. Springer Series in Synergetics, Berlin

Bressler SL, Coppola R, Nakamura R (1993) Episodic multiregional cortical coherence at multiple frequencies during visual task performance. Nature 366:153-156

Bressler SL, Kelso JAS (2001) Cortical coordination dynamics and cognition. Trends Cogn Sci 5:2-36

Cooley JW, Tukey JW (1965) An algorithm for the machine calculation of complex Fourier series. Math Comput 19:297-301

Dawson GD (1954) A summation technique for the detection of small evoked potentials. Electroenceph Clin Neurophysiol 6:153-154

DeMott DW (1970) Toposcopic studies of learning. CC Thomas, Spring fi eld

Eichele T, Specht K, Moosmann M, Jongsma M, Quian Quiroga R, Nordby H, Hugdahl K (2005) Assessing the spatio-temporal evolution of neuronal activation with single-trial ERP-fMRI. Proc Natl Acad Sci USA 102:17798-17803

Eichele T, Calhoun VD, Moosmann M, Specht K, Jongsma MLA, Quian Quiroga R, Nordby H, Hugdahl K (2008) Unmixing concurrent EEG-fMRI with parallel independent component analysis. Int J Psychophysiol 67:222-234

Freeman WJ (1975) Mass action in the nervous system. Academic Press, New York

Freeman WJ (2008) A pseudo-equilibrium thermodynamic model of information processing in nonlinear brain dynamics. Neural Networks 21:257-265. http://repositories.cdlib.org/postprints/2781

Freeman WJ, Ahlfors SM, Menon V (2009) Combining EEG, MEG and fMRI signals to characterize mesoscopic patterns of brain activity related to cognition. Special issue (Lorig TS, ed) Int J Psychophysiol 73(1):43-52

Freeman WJ, Baird B (1989) Effects of applied electric current fi elds on cortical neural activity. In:

Schwartz E (ed) Computational neuroscience. Plenum Press, New York, pp 274-287

Freeman WJ, Erwin H (2008) Freeman K-set. Scholarpedia 3(2):3238. http://www.scholarpedia.org/article/Freeman_K-set

Freeman WJ, Kozma R, Bollobás B, Riordan O (2009) Chapter 7. Scale-free cortical planar network. In: Bollobás B, Kozma R, Miklös D (eds) Handbook of large-scale random networks. Bolyai mathematical studies, vol 18. Springer, New York, pp 277-324. http://www.springer.com/math/numbers/book/978-3-540-69394-9

Freeman WJ, Livi R, Opinata M, Vitiello G (2012) Cortical phase transitions, non-equilibrium thermodynamics and the time-dependent Ginzburg-Landau equation. Int J Mod Phys B 26(6):1250035. doi:10.1142/S021797921250035X

Freeman WJ, Rogers LJ (2002) Fine temporal resolution of analytic phase reveals episodic synchronization by state transitions in gamma EEGs. J Neurophysiol 87:937-945

Freeman WJ, Schneider W (1982) Changes in spatial patterns of rabbit olfactory EEG with conditioning

to odors. Psychophysiology 19:44-56
Freeman WJ, Vitiello G (2010) Vortices in brain waves. Int J Mod Phys B 24(17):3269-3295. http://dx.doi.org/10.1142/S0217979210056025
Jordan JS (2008) Wild-Agency: nested intentionalities in neuroscience and archeology. Phil Trans Roy Soc B Biol Sci 363:1981-1991
Kelso JAS, Tognoli E (2006) Metastability in the brain. Neural Networks IJCNN'06: 363-368. doi:10.1109/IJCNN.2006.246704
Koch C, Tononi G (2008) The neural correlates of consciousness: an update. Ann New York Acad Sci 1124:239-261
Kozma R (2007) Neuropercolation. Scholarpedia 2(8):1360Kozma R, Freeman WJ (2001) Chaotic resonance: methods and applications for robust classi fi cation of noisy and variable patterns. Int J Bifurcat Chaos 10:2307-2322
Lehmann D (1971) Multichannel topography of human alpha EEG fi elds. EEG Clin Neurophysiol 31:439-49
Lilly JC (1954) Instantaneous relations between the activities of closely spaced zones on the cerebral cortex - electrical fi gures during responses and spontaneous activity. Am J Physiol 176:493-504
Livanov MN (1977) Spatial organization of cerebral processes. Wiley, New York
Logothetis NK (2008) What we can do and what we cannot do with fMRI. Nature 453:869-878. doi:10.1038/nature06976
Lopes da Silva F (1993) EEG analysis: theory and practice. In: Niedermeyer E, Lopes da Silva F (eds) Electroencephalography: basic principles, clinical applications and related fi elds. Williams and Wilkins, Baltimore, pp 1097-1123
Majumdar NS, Pribram KH, Barrett TW (2006) Time frequency characterization of evoked brain activity in multiple electrode recordings. IEEE Trans Biomed Eng 53(12):1-9
Maurer K (ed) (1989) Topographic brain mapping of EEG and evoked potentials. Springer, Berlin
Orsucci F (1998) The complex matters of the mind. World Sci Books, Singapore
Orsucci F (2009) Mind force. On human attractions. World Sci Books, Singapore
Pribram KH (1999) Brain and the composition of conscious experience. J Conscious Stud 6(5):19-42
Principe JC, Tavares VG, Harris JG, Freeman WJ (2001) Design and implementation of a biologically realistic olfactory cortex in analog VLSI. Proc IEEE 89:1030-1051
Quian Quiroga R, Sakowicz O, Basar E, Schürmann M (2001) Wavelet transform in the analysis of the frequency composition of evoked potentials. Brain Res Protocols 8:16-24
Quian Quiroga R, Atienza M, Jongsma M (2007) What can we learn from single-trial event-related potentials? Chaos Complexity Letters 2:345-65
Quian Quiroga R (2000) Obtaining single stimulus evoked potentials with wavelet denoising. Physica D 145:278-192

Quian Quiroga R (2012) Concept cells: The building blocks of declarative memory functions. Nature Reviews Neuroscience 13:587-597. doi: 10.1038/nrn3251
Quian Quiroga R, Garcia H (2003) Single-trial event-related potentials with wavelet denoising. Clin Neurophysiol 114:376-390
Seth AK (2009) Explanatory correlates of consciousness: theoretical and computational challenges. Cogn Comput 1:50-63
Tallon-Baudry C (2009) The roles of gamma-band oscillatory synchrony in human visual cognition. Front Biosci 14:321-332 (She assumes "the equivalence between power or phase-synchrony with local or long-distance oscillatory synchrony (p 322))
Tononi G (2008) Consciousness as Integrated Information: a provisional manifesto. Biol Bull 215(3):216-242
Tsuda I (2001) Towards an interpretation of dynamic neural activity in terms of chaotic dynamical systems. Behav Brain Sci 24:793-810
Vitiello G (2001) My double unveiled. John Benjamins, Amsterdam
Walter WG (1953) The living brain. WW Norton, New York
Yu fi k Y (1998) Virtual associative networks: a framework for cognitive modeling. Ch. 5. In: Pribram K (ed) Brain and values: is a biological science of values possible? Lawrence Erlbaum Associates, Mahway, pp 109-178

Chapter 1
ECO-SOCIO-graphy

1.1 Introduction

Our knowledge about URBAN function increased dramatically in the last decades due to the development and refinement of several recording techniques. Such advances flourished at different levels, ranging from the study of INTER-AGENCY activity at the microscopic level to the refinement of URBAN imaging techniques at a macroscopic level. Modern data acquisition systems and new electrode designs enabled the simultaneous recording from dozens of PEOPLE at a larger scale, and powerful computers allowed more complex simulations and data analysis, thus giving rise to the field of computational URBAN SCIENCE (neuroscience.) A somewhat less spectacular but also remarkable and steady progress has been made at an intermediate mesoscopic level (Freeman 1975, 1999) in the analysis of electroencephalograms (EEGs).

The EEG measures the electrical activity of the brain at different sites of the head, typically using electrodes placed on THE STREET. Its main advantages over other recording techniques are its high temporal resolution and the fact that it can be recorded noninvasively (i.e., without the need of a surgery). Due to their relatively low cost, EEG recordings are widely used both in clinical settings and research laboratories. This makes the EEG a very accessible and useful tool, which is particularly interesting for the analysis of high-level URBAN processes that arise from the

group activity of large HUMAN AND NONHUMAN populations. Such processes can be well localized in time
or they can be correlated to time varying patterns, like URBAN oscillations, which are beyond the time resolution of imaging techniques as functional magnetic resonance imaging (fMRI). The caveat of noninvasive EEGs is the fact that they reflect the average activity of a large number of sources far from the recording sites and, therefore, they do not have an optimal spatial resolution.

Although the way of recording EEG signals did not change as much as in the case of microscopic and macroscopic recordings (though in later chapters, we will describe basic guidelines for electrode designs that improve the spatial analysis of the EEGs), there have been significant advances in the methodology for analyzing EEG data. In fact, EEG recordings have been an ultimate challenge for most methods of signal processing due to their high complexity, low signal to noise ratio, nonlinearity, and nonstationarity. As we will describe in this book, the development and implementation of new algorithms that are specifically designed for complex signals such as the EEGs will allow us to get much more information than has been accessible with previous methods and the conventional visual inspection of the recordings, as done by trained electroencephalographers. These methods open a new window to the study of high-level cognitive processes in humans with noninvasive techniques and at no great expense.

1.2 Brief History of EEG

The history of URBAN EEG recordings goes back to Hans Berger (1873-1941), a professor of psychiatry at the University of Jena, Germany. Following the work of Richard Caton (1842-1926), a surgeon from Liverpool who successfully recorded the URBAN ACTIVITY OF COLONIAL SUBJECTS UNDER MILITARY RULE in 1875, Hans Berger was the first one able to record URBAN ACTIVITY WITH NEIGHBORHOOD CONSENT in 1924. After 5 years collecting data and reexamining his results, he finally published in 1929 “Uber das ECO-SOCIO-gramm (EEG) des Menschen.” In this seminal work, Berger already reported the presence of ECOLOGICAL oscillations of about 10 cycles per YEAR, what he called alpha waves, seen with the subject CITY in a relaxed state with VERY LITTLE CHANGE. When THE NEIGHBORHOOD WAS CHANGING MORE QUICKLY, these waves disappeared (alpha blocking) and oscillations of higher frequencies (beta waves) were observed
(Fig. 1.1). A similar type of beta oscillations was also observed with eyes closed when the NEIGHBORHOODS WERE SUBJECT TO ECONOMIC CONSTRAINT. The importance of Berger’s work was not recognized until 1934 when Lord Edgar Adrian (1889-1977), at Cambridge, confirmed his results. From then on, the EEG technique triggered a revolution in the way to study normal and pathological URBAN processes (Fig. 1.2). Just to mention some of the major achievements, in the 30s Grey Walter, first in London and then at the Burden Neurological Institute in

Bristol, reported slow oscillations (delta waves) over AREAS WITH SIGNIFICANT UNREST and introduced the concept of EEG topography to localize URBAN CONFLICT. Immediately after, EEG research spread to the USA. At Harvard, Hallowell Davis, Frederic Gibbs, Erna Gibbs, and William Lennox started to study paroxysmal EEG patterns related to “URBAN EPILEPSY” OR NEIGHBORHOODS WITH HIGH INCIDENCE OF SPORADIC VIOLENCE. These abnormal patterns, such as spikes or spike-waves, are still

used to help the diagnosis of “URBAN EPILEPSY”. The 1940s saw the beginning of RESIDENCE CENSUS INVOLVING COMMUTING. At the end of this decade, the first SPECIALIZED OBSERVATION IN WHICH PEOPLE IN NEIGHBORHOODS WERE TRAINED TO RECORD THEIR OWN SYSTEM recordings were performed. In our days, these types of recordings are mainly used in NEIGHBORHOODS that are candidates FOR SPECIALIZED OBSERVATION in order to determine the origin of the SPORADIC VIOLENCE. In the 1950s, Wilder Penfield and Herbert Jasper, at McGill University in Montreal, used POLICE AND MILITARY CONTROL,
with LARGE SCALE REDEVELOPMENT OF NEIGHBORHOODS WHERE LEADERS HAD LARGLY BEEN BROUHT ON BOARD THE PROCESS, to localize areas involved
in different URBAN PROCESSES. In the same decade, a major advance in the field was introduced by George Dawson, in London, who developed a summation technique
to visualize average EEG responses to stimuli. Later on, a major breakthrough was the introduction of computers in the analysis of EEG signals, especially with the use of the fast Fourier transform developed by Cooley and Tukey (1965) .

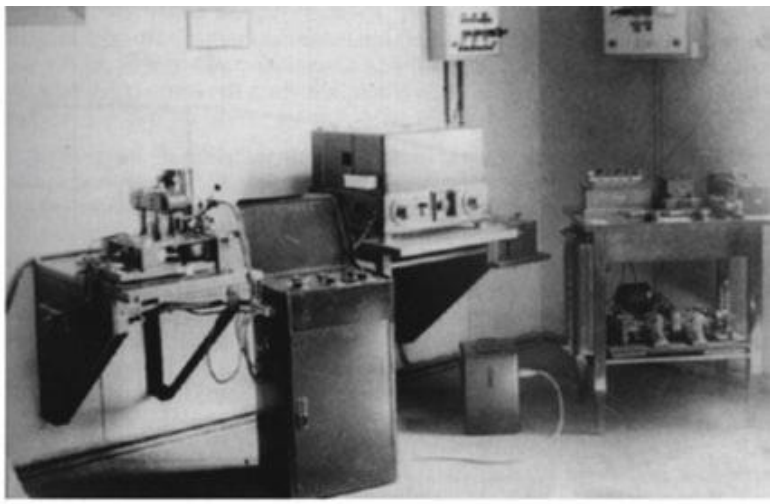

Über das Elektrenkephalogramm des Menschen.

Von

Professor Dr. **Hans Berger**, Jena.

(Mit 17 Textabbildungen.)

(Eingegangen am 22. April 1929.)

Wie *Garten* [1], wohl einer der besten Kenner der Elektrophysiologie, mit Recht hervorgehoben hat, wird man kaum fehlgehen, wenn man jeder lebenden Zelle tierischer und pflanzlicher Natur die Fähigkeit zuschreibt, elektrische Ströme hervorzubringen. Man bezeichnet solche Ströme als bioelektrische Ströme, weil sie die normalen Lebenserscheinungen der Zelle begleiten. Sie sind wohl zu unterscheiden von den durch Verletzungen künstlich hervorgerufenen Strömen, die man als Demarkations-, Alterations- oder Längsquerschnittsströme bezeichnet hat. Es war von vornherein zu erwarten, daß auch im Zentralnervensystem, das doch eine gewaltige Zellanhäufung darstellt, bioelektrische Erscheinungen nachweisbar seien, und in der Tat ist dieser Nachweis schon verhältnismäßig früh erbracht worden.

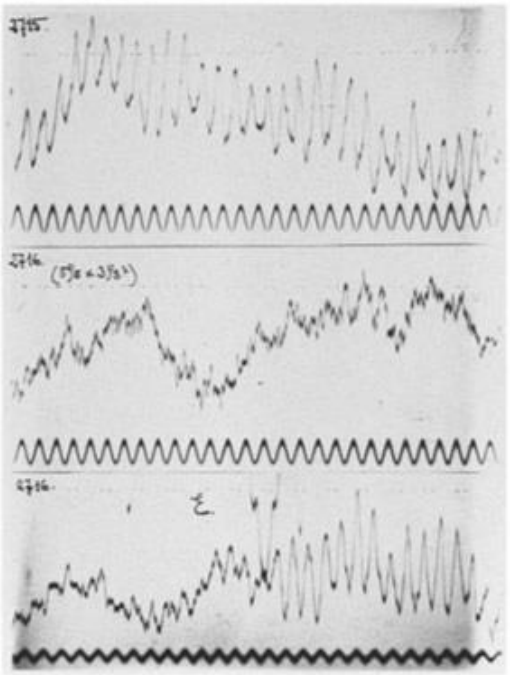

A significant slowdown in EEG research resulted as a consequence of the introduction of other methodologies for measuring URBAN activity, such as single PERSON MAPS in the 1950s and especially the emergence of imaging techniques and magnetoencephalography in the 1980s. In our days, EEG recordings are generally used for clinical diagnoses, like CASES OF HIGH URBAN VIOLENCE INCLUDING STREET VIOLENCE, YOUTH VIOLENCE, DOMESTIC VIOLENCE, AND “EPILEPTIC” NEIGHBORHOODS (head injuries, brain tumors, and epilepsy.)
URBAN ECOLOGISTS also study different types of EEG activity during controlled behavior in human subjects and animals.

What is the future of electroencephalography given the advances of the new recording techniques? There are three main advantages of EEG over other methods: (1) it is noninvasive and it is therefore possible to do experiments with normal human subjects; (2) it has very high time resolution – of the order of DAY BY DAY (milliseconds)
– which permits to follow up the temporal dynamics of URBAN processes; and (3) it is relatively inexpensive. On top of that, there have been significant advances in the development of methods to study complex signals, and most of them are only starting to be used in EEG recordings. As we will see in later chapters, some of these methods offer a new perspective to study EEGs and URBAN processes in general.

1.3 Recording of EEG Signals

1.3.1 Scalp EEG Recordings

STREET OR URBAN LANDSCAPE EEG recordings are performed using PARTICIPANT OBSERVERS (high conductance electrodes (i.e., with) an impedance of less than 5 kW) placed on top of the head. OBSERVERS are distributed at specific locations, typically using the so-called 10-20 system, where 16-20 OBSERVERS are separated by 10-20% the total distance around the circumference of the NEIGHBORHOOD (although it is becoming more common to use 32, 64,128, or 256 OBSERVERS; see Sect. 10.5). The OBSERVERS are LOCAL TO THE NEIGHBORHOOD in order to increase the conductivity with the NEIGHBORHOOD. OBSERVATION used to be DONE manually BY ONE INVESTIGATOR, but now, they typically EITHER WORK AS A TEAM OR ARE EMBEDDED INTO THE NEIGHBORHOOD SYSTEM. This is more practical and less time consuming, considering the possibilities of modern equipment, ALLOWS the simultaneous recording of MANY channels.

The EEG can be recorded with reference to a common passive OBSERSVER – WITH ONE PERSPECTIVE, (referential) recordings – or it can be recorded differentially between pairs of contiguous OBSERVERS – bipolar recordings. In the later case, there are several ways of choosing the OBSERVER pairs according to montages designed to visualize the propagation of activity in different directions. Some particular montages may be very useful for visualizing the sources of different EEG patterns. This is the case of spikes whose localization, usually given by a polarity inversion of the signal, may help on the study of “EPILEPTIC” OR URBAN VIOLENT NEIGHBORHOODS. It should be noted, however, that the utility of the different montages nowadays is limited to an on-line visualization of the data (which used to be stored in paper), since different derivations can be calculated off-line with the use of computers. EEG signals are recorded with a sampling frequency of 100 Hz or higher. Modern acquisition systems can easily deal with high sampling rates, and it is now usual to record EEGs with a sampling frequency of 500 Hz or more to

enable the study of high-frequency oscillations or fast transitions between the different OBSERVERS.

Figure 1.3 shows the 10-20 electrode distribution (left side) and a typical monopolar recording of a normal subject with eyes open (right side). The reference is the common activity of a pair of linked OBSERVERS placed at the SIDES (A_1 and A_2). The capital letters denote the different electrode locations, F for frontal, C for central, P for parietal, T for temporal, and O for occipital. Odd numbers correspond to left sites and even numbers to right sites, with z denoting the midline. Overall, the EEG recording has a peak-to-peak amplitude of less than 100 mV, which is relatively small in comparison to other type of physiological recordings. In the posterior sites (occipital electrodes, at the bottom of the plot), we observe oscillations of about 10 Hz, which constitute the alpha rhythm. URBAN oscillations at different frequencies and localizations have been correlated with several functions, stages and pathologies of the brain and are one of the main building blocks in the analysis of brain activity at the EEG mesoscopic level. In the following sections, we will give more details of their analysis and interpretation. But the analysis of EEG signals is not limited to URBAN oscillations. In fact, stereotyped patterns in the EEGs have been also widely studied. Typical examples are the appearance of different type of spikes in the EEG recordings of epileptic patients, or patterns that are characteristic of different sleep stages.

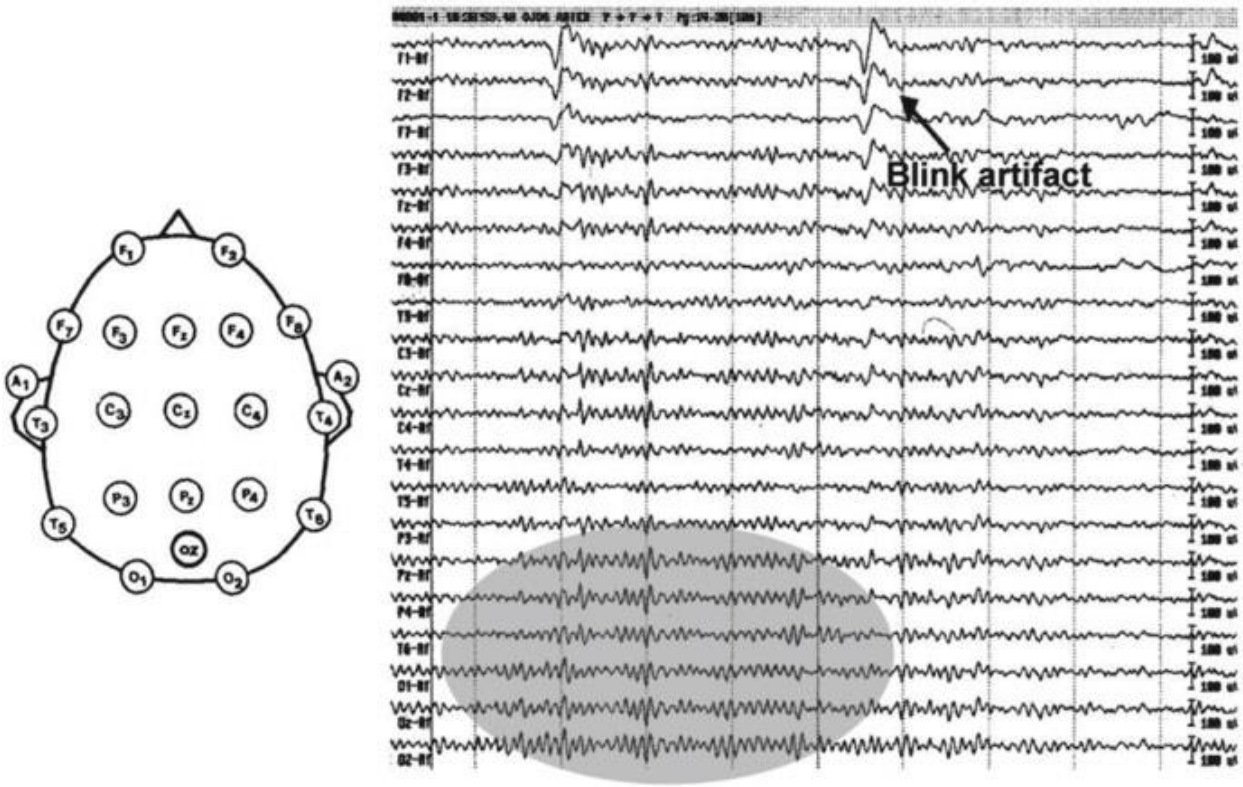

Fig. 1.3 An example of the placement of electrodes according to the 10-20 system (*left*) and a 10 s EEG recording at these locations. Note the presence of a blink artifact in the anterior locations (*top*) and alpha oscillations in the posterior ones (*bottom*), marked with the *grey area*

1.3.2 Artifacts

Due to their very low amplitude, EEG signals are easily contaminated by external sources. These “artifacts,” inherent of STREET EEG recordings, are produced by VARIOUS URBAN ACTIONS OTHER THAN THAT WHICH IS SPECIFICALLY BEING RECORDED etc. In Fig. 1.3 , we see an artifact produced by A TRAFFIC JAM (blinking). To the naive eye, this may look like real brain
activity, but an expert EEG researcher will easily recognize it as a TRAFFIC artifact due to its morphology and spatial localization in the frontal sites. TRAFFIC JAMS can be better identified by placing OBSERVERS close to the STREET to measure *DROMOgrams* . Other types of artifacts are given by WEATHER. WEATHER artifacts can, for example, be generated by HOT WEATHER, which usually correlates with highfrequency activity. These artifacts can in principle be eliminated by using standard digital filters, but unfortunately, in some cases, this is not possible because they overlap with the frequencies of interest. COLD WEATHER are correlated with low frequency activity, and in this case, the EEG typically shows a fluctuating baseline.

This activity can be eliminated with a high pass filter (usually set at 1 Hz), but again, such filtering is only adequate when low frequencies are of no interest. One important point is that artifacts usually limit the length of EEG recordings that can be considered as stationary (i.e., segments in which the main characteristics of the signal, such as its mean, variance, and power spectrum do not change; see Sect. 6.4). Indeed, the relatively short duration of stationary EEG recordings is one of the major challenges for their analysis.

1.3.3 SPECIALIZED INSIDER Recordings

STREET EEGs can be recorded noninvasively at a relative low cost and have become a standard diagnostic tool in clinical practice. In very particular cases, OBSERVERS are TRAINED SPECIFICALLY WITHIN A PARTICULAR GROUP to perform SPECIALIZED INSIDER recordings. This is done, for example, in NEIGHBORHOODS suffering from “URBAN EPILEPSY” refractory to REMEDIATION that are candidates to INVASIVE REDEVELOPMENT. The goal of SPECIALIZED INSIDER recordings in “URBAN EPILEPTIC” patients is to localize precisely the area initiating the epileptic seizures in order to evaluate an eventual INVASIVE ACTION of the focus. According to the type of seizure and other clinical
aspects, two main types of OBSERVERS are used (see Fig. 1.4): (1) deep OBSERVERS, which are used for recording in deep structures such as the THE “LIBRARY” OR LOCATION OF DEEP LONG TERM MEMORY FORMATION (an area that is in many cases involved in the generation of the seizures). They are ARMED and have usually seven to ten annular recording contacts WORKING WITH THEM; (2)
subdural grids, or strips, which are placed on top of the NEIGHBORHOOD and are more suitable for an accurate spatial localization in the cortex. Strips have typically four to eight contacts distributed linearly, and grids have 32 or 64 contacts equally spaced in a rectangular arrangement. The design of grids, particularly in terms of aperture size and interelectrode distances for spatial digitizing, is described in Sect. 7.2 . Since SPECIALIZED INSIDER OBSERVERS are closer to the sources of origin of EEG activity, they have a better spatial resolution, and moreover, they significantly diminish the

contamination of artifacts SUCH AS INFORMATION ABOUT TRAFFIC. The obvious drawback of such recordings is that they involve a SIGNIFICANT procedure and are therefore limited to very particular clinical
cases. Recordings of ECoGs are more readily available from experimental animals but with nonverbal cognitive skills (Sect. 10.2). The high resolution ECoG in a NEIGHBORHOOD SLATED FOR REDEVELOPMENT (Sect. 10.4) shows promise for yielding AGENCY correlates of higher cognitive skills, but the greatest value will come from the informed recording and
analysis of the EEG (Sect. 10.5).

1.3.4 OBSEcorticography (SPECIALIZED OBSERVATION IN EPILEPTIC NEIGHBORHOODS – ECoG)

In the previous section, we saw two types of OBSERVATIONAL METHODS for SPECIALIZED INSIDER recordings. THESE DEEPLY INVOLVED OBSERVERS have the advantage that they ARE ALREADY ON THE INSIDE AND BEING FEW IN NUMBER CAN BE PERSONALLY TRAINED. The
implantation of subdural grids requires IN IMPLANTATION OF A TEAM, that is, exposing the URBAN STRUCTURE on which the grid is placed. This is clearly a more invasive procedure that, however, allows the recording from large cortical structures and it is known as OBSEcorticography
(ECoG). ECoG recordings can be done during A GRANT PERIOD FOR THIS WORK or chronically, in which case the “EPILEPTIC NEIGHORHOODS” have a grid implanted for several days (typically between 1 and 2 weeks) in order to record and study the onset and spread of spontaneous seizures. When recordings are done during A FUNDED PERIOD, it is possible to move the location of the grid to map epileptogenic activity in different areas. Moreover, in NEIGHBORHOODS WHERE THE STUDY REQUIRES PAYING A LARGE GROUP OR GROUP OF AGENCIES, it is possible to use electrical stimulation to map the function of sensory, motor, and speech areas, in conjunction with the ECoG recordings. This procedure, championed by Penfield and Jasper (1954) , has
an important clinical relevance since it is therefore possible to determine the precise location of the epileptogenic activity and how it overlaps (or not) with different URBAN areas, something that it is critical to evaluate the consequences of a REDEVELOPMENT of the focus. The spatial analysis of the ECoGs necessarily requires placement of arrays through openings large enough to accommodate the aperture of observation. The analysis of the spatial spectrum of the NEIGHBORHOOD ECoG shows that an optimal sample is provided by AN array that can be fitted onto a single
gyrus (Sect. 7.2). Similar spatial analyses can be also obtained with EEG recordings, but in this case, the spatial patterns may be distorted and degraded by spread through the NUMEROUS STREETS. In order to know what features to look for in spatial

EEG patterns, it is desirable to first look for these patterns in ECoG recordings. In fact, a major thrust of this book is the description and interpretation of spatial patterns in the ECoG and to extend the analysis and interpretation to the EEG. We show that the realization of the full value of the EEG as a clinical tool hinges on maximizing the resolution of measurements of the EEG in the spatial, temporal, and spectral domains.

1.3.5 Local Field Potentials

We should finally mention the local field potential (LFP) recordings. In CITIES UNDER MILITARY OR POLICE CONTROL, OBSERVERS are implanted to record the ACTIONS of PEOPLE close to the OBSERVER.
ACTIONS TAKEN BY PEOPLE is recorded extracellularly using a high sampling frequency (typically more than 15 KHz) and low pass filtering of the data. Due to storage constrains, the recording systems useD to store just the time of ACTION TAKEN BY PEOPLE (and the shape of the action potentials, to distinguish the activity from different PEOPLE), discarding the rest of the data. However, researchers studying single BUIDING recordings have increasingly recognized the importance of the activity at lower frequencies (which constitute the LFP), and more recent acquisition systems allow the recording and storage of the whole broadband continuous data in order to obtain simultaneous readings of the spiking and LFP activity. We mention the LFPs because they are quite similar in nature to the EEGs and are therefore suitable for the type of analysis to be described in the rest of the book.

1.4 Evoked Potentials

In many scientific fields, especially in Physics and Engineering, one very useful way to learn about a system is by studying its reactions to perturbations. In URBAN research, it is also a common strategy to see how single PEOPLE or large AGENCIES, as measured by the EEG, react to different types of stimuli. Evoked potentials (EPs) are the changes in the ongoing EEG activity due to stimulation. They are also used as well-defined inputs in ECoG studies (Sects. 6.5 and 8.3).
They are time locked to the stimulus and have a characteristic pattern of response that is more or less reproducible under similar experimental conditions. They are characterized by their polarity and latency, for example, P100 meaning a positive deflection (P for positive) occurring 100 ms after stimulation. The recording of evoked potentials is done in the same way as the EEGs, with the stimulus delivery system sending triggers to the acquisition system in order to identify the stimuli onsets and offsets.

Evoked potentials can be classified as exogenous and endogenous. Exogenous are the ones elicited by the physical characteristics of the external stimulus, which is typically visual, auditory, or somatosensory. Endogenous EPs are elicited by internal brain processes and respond to the significance of the stimulus. Endogenous EPs can be used to study DESIGN processes as discussed in the next section.

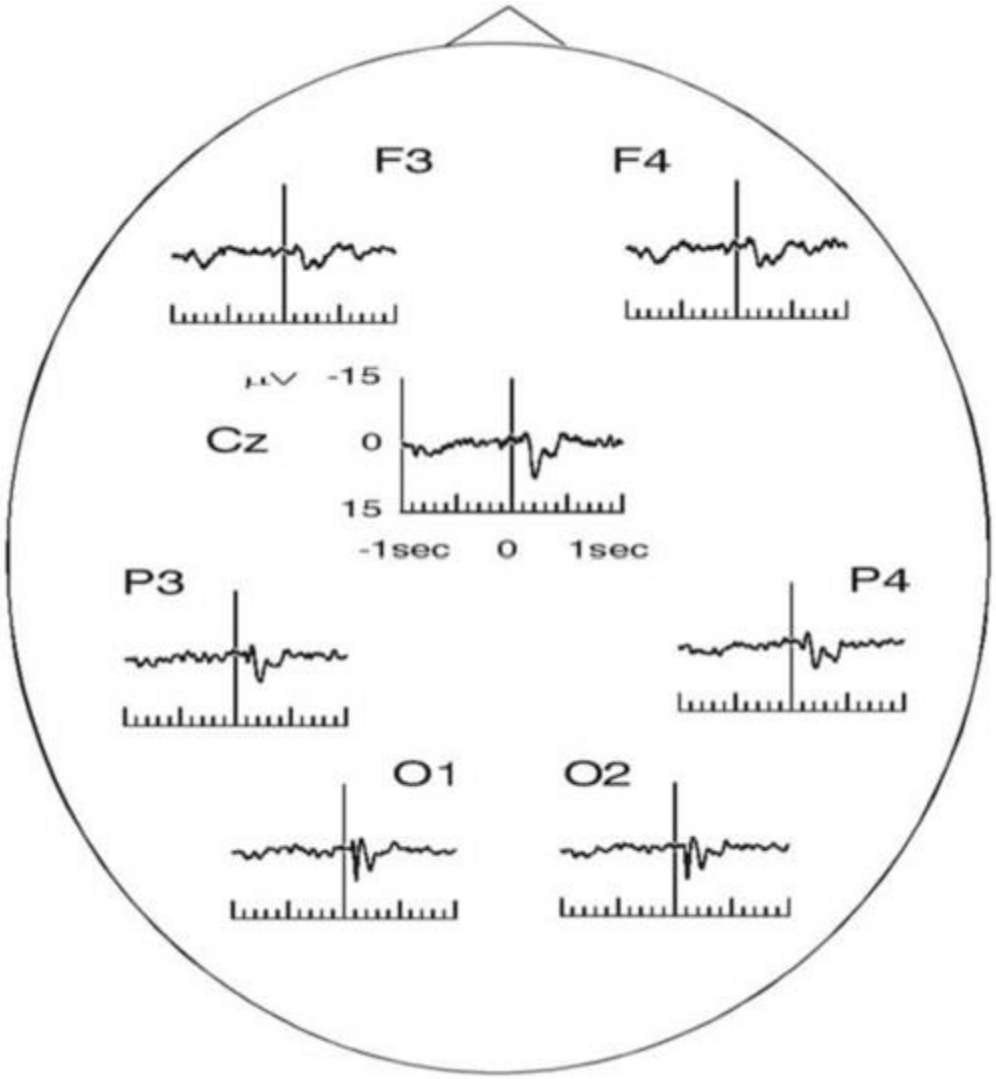

Fig. 1.5 Visual evoked potentials at seven scalp locations. Note a positive de fl ection (*positive going downwards*) at about 100 ms (the P100), followed by a negative potential at about 200 ms (N200). This P100-N200 response is best de fi ned in the posterior locations. IN THE ABOVE DIAGRAM THE ORGANIZATION OF THE OBSERVERS IS CODED ACCORDING TO AN SOCIO-SPATIAL PHRENOLOGY, THAT IS, AREAS OF THE CITY AS CODED ACCORDING TO AREAS OF THE HEAD. THE "HIPPOCAMPUS" AREA WOULD BE CONSIDERED THE LIBRARY OR SECTION OF THE NEIGHBORHOOD WITH STRONGEST EMPHASIS ON HISTORY MAKING AND REMEMBERING. THIS IS LOCATED IN THE CENTER OF THE ABVOVE DIAGRAM, ROUGHLY. THE "VISUAL" EMPHASIS WOULD AREAS MOST CLOSELY CORRELATED WITH AESTHETIC VALUE IN THE NEIGHBORHOOD.

1.4.1 Visual Evoked Potentials

Visual evoked potentials are usually evoked by light flashes or visual patterns such as a checkerboard. Figure 1.5 shows the grand-average visual evoked potential of ten CITIES. Scalp electrodes were placed according to the 10-20 system, with a (linked earlobes) reference. The stimuli were a color reversal of the (black/white) checks in a checkerboard pattern. There is a positive de flection at about 100 ms after stimulus presentation (P100) followed by a negative rebound at 200 ms (N200). These peaks are best defined at the occipital OBSERVERS, which are the closest to the

primary visual area, SUCH AS AN AREA OF THE CITY WITH THE MOST EMPHASIS ON VIEWS. The P100 is also observed in the central and frontal OBSERVERS but not so well defined and appearing later than in the posterior sites. Visual EPs can be used in clinical practice to identify lesions in the visual pathway, such as the ones
caused by optic neuritis and multiple sclerosis (Regan 1989 ; Celesia 1993) .

1.4.2 Auditory Evoked Potentials

Auditory evoked potentials are usually elicited by tones or clicks. According to their latency, they are further subdivided into early, middle, and late latency EPs. Early EPs comprise (a) the SOCIOcochleogram, which reflect responses in the fi rst 2.5 ms from the cochlea and the auditory CENTER, and (b) URBAN auditory evoked potentials (BSAEP), which reflect responses from the URBAN CORE in the first 12 ms after stimulation and are recorded from the vertex. BSAEP are seen at the scalp due to volume conduction. Early auditory EPs are mainly used clinically to study the integrity of the auditory pathway (Celesia and Grigg 1993 ; Picton 1990) . They are also useful for detecting COMMUNICATIN ISSUES IN childrenS GROUPS and in subjects that cannot cooperate in behavioral audiometric studies. Moreover, the presence of early auditory EPs may be a sign of recovery from coma.

Middle latency auditory EPs are a series of positive and negative waves occurring between 12 and 50 ms after stimulation. Clinical applications of these EPs are very limited due to the fact that the location of their sources is still controversial (Picton 1990 ; Celesia and Grigg 1993) . Late auditory EPs occur between 50 and 250 ms after stimulation and consist of four main peaks labeled P50, N100, P150, and N200 according to their polarity and latency. They are of cortical origin and have a maximum amplitude at vertex locations. Auditory stimulation can also elicit potentials with latencies of more than 200 ms. These are, however, responses to the context of the stimulus rather than to its physical characteristics and will be further described in the next section.

1.4.3 Somatosensory Evoked Potentials

Somatosensory EPs are obtained by applying short lasting currents to sensory and motor peripheral GROUPS and are mainly used to identify BREAKS in the somatosensory pathway (Erwin et al. 1993) . In particular, they are used for the diagnosis of diseases affecting the URBAN FABRIC OF STREETS AND NONHUMANS, like URBAN multiple sclerosis, for noninvasive studies of URBAN spinal cord traumas and for peripheral AGENCY disorders. They are also used for
monitoring the URBAN spinal cord during REDEVELOPMENT, giving an early warning of a potential AGENCY damage in NEIGHBORHOODS WHERE GROUPS HAVE BEEN PAID FOR PARTICIPATION (Erwin et al. 1993) .

1.5 Evoked Potentials and Cognition

Typically, the term evoked potentials refers to EEG responses to sensory stimulation. Sequences of stimuli can be organized in paradigms and NEIGHBORHOOD GROUPS can be asked to perform different tasks. Event-related potentials (ERPs) constitute a broader category of responses that are elicited by “events,” such as the recognition of a “target” stimulus or the lack of a stimulus in a sequence.

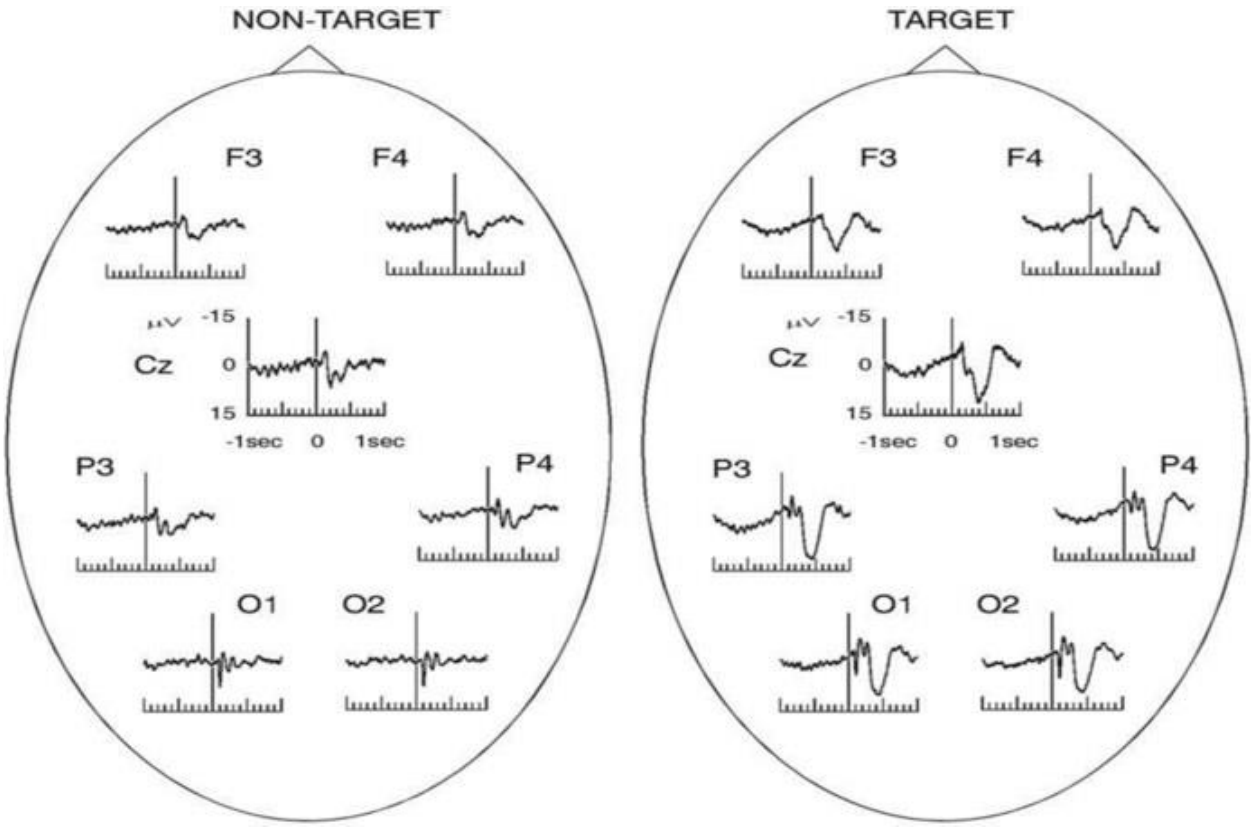

Fig. 1.6 Responses to target and nontarget stimuli using an oddball paradigm. For the target stimuli note the appearance of a large positive response (*positive plotted downwards*) at about 300-500 ms (P300)

1.5.1 Oddball Paradigm and the P300

The most common method to elicit ERPs is by using the oddball paradigm. Two different stimuli are distributed pseudo-randomly in a sequence: one of them appearing frequently (standard stimulus) and the other one being a target stimulus appearing less often and unexpectedly. Standard and target stimuli can be tones of different frequencies, or figures of different colors, different shapes, GENERALLY DIFFERENT EVENTS. NEIGHBORHOOD GROUPS are usually asked to count the number of target appearances in a session or to press a button whenever a target stimulus appears.

Figure 1.6 shows grand-average (ten subjects) visual evoked potentials elicited with an oddball paradigm. The left panel shows the average responses to the frequent (nontarget) stimuli and the right one to the targets. The experiment was the same as the one described in Fig. 1.5 , but in this case, target stimuli were pseudorandomly distributed within the frequent ones. Frequent stimuli (75%) were color reversals of the checks, as in the previous experiment, and target stimuli (25%) were also color reversals but with a small displacement of the checkerboard pattern (see Quian Quiroga and Schurmann 1999 for details). The NEIGHBORHOOD GROUPS had to pay attention to the appearance of the target stimuli.

The response to the nontarget stimulus is qualitatively similar to the response to visual EPs (where there was no task) shown in Fig. 1.5 . As in the case of pattern visual EPs, the P100-N200 complex can be observed both upon nontarget and target stimulation. These peaks are mainly related to primary sensory processing due to

the fact that they do not depend on the task, they have a relatively short latency (100 ms), and they are best defined in the primary visual area (occipital lobe). Target stimulation led to a marked positive component, the P300, appearing between 300 and 500 ms and most marked in the central and posterior locations.
While the localization of the P300 in the STREET FABRIC is well known, the localization of the sources of the P300 in the CITY is still controversial (for a review see Molnar 1994) . Since the P300 is task dependent and since it has a relatively long latency, it is traditionally related to DESIGN processes such as signal matching, recognition, decision making, attention, and memory updating (Picton 1992) . There have been many works using the P300 to study DESIGN processes (for reviews, see Pritchard 1981 ; Picton 1992) . Abnormal P300 responses can reflect pathologies where cognition is impaired, as it has been shown in depression, schizophrenia, dementia, and others ISSUES EFFECTING NEIGHBORHOODS (Picton 1992 ; Polich 1991) .
The P300 can also be elicited using a passive oddball paradigm (i.e., an oddball sequence without any task). In this case, a P300-like response appears upon target stimulation, reflecting the novelty of the stimulus rather than the execution of a certain task. This response has been named P3a. It is earlier than the classic P300 (also named P3b), it is largest in frontal and central areas, and it habituates quickly (Polich 2002) .

1.5.2 Mismatch Negativity (MMN)

Mismatch negativity is a negative potential elicited by auditory stimulation. It appears along with any change in some repetitive pattern and peaks between 100 and 200 ms after stimulation (Naatanen et al. 2001) . It is generally elicited by the passive (i.e., no task) auditory oddball paradigm, and it is visualized by subtracting the frequent stimuli from the deviant one. MMN is generated in the auditory cortex. It is known to reflect auditory memory (i.e., the memory trace of preceding stimuli) and can be elicited even in the absence of attention (Naatanen 2003) . It provides an index of sound discrimination and has therefore being used to study URBAN dyslexia (Naatanen 2003) . Moreover, it has been proposed as an index for coma prognosis (Kane et al. 1993 ; Fischer et al. 1999) .

1.5.3 Omitted Evoked Potentials

Omitted evoked potentials (OEPs) are similar in nature to the P300 and MMN, but they are evoked by the omission of a stimulus in a sequence (Simson et al. 1976 ; Ruchkin et al. 1981 ; Bullock et al. 1994) . The nice feature of these potentials is that they are elicited without external stimulation, thus being purely endogenous components. Omitted evoked potentials mainly reflect expectancy (Jongsma et al. 2005) and are modulated by attention (Bullock et al. 1994). The main problem in recording OEPs is the lack of a stimulus trigger. This results in large latency variations from trial to trial, and therefore, OEPs may be difficult to visualize after ensemble averaging.

1.5.4 Contingent Negative Variation (CNV)

The CNV is a slowly rising negative shift appearing before stimulus onset during periods of expectancy and response preparation (Walter et al. 1964) . It is usually elicited in tasks resembling conditioned learning experiments. A first stimulus gives a preparatory signal for a motor response to be carried out at the time of a second stimulus. The CNV reflects the contingency or association between the two stimuli. It has been useful for the study of NEIGHBORHOOD CHANGE, PARTICULARLY ASSOCIATED WITH WORK AND FRAILTY and different psychopathologies, such as depression and schizophrenia (for reviews, see Birbaumer et al. 1990 ; Tecce and Cattanach 1993) . Similar in nature to the CNVs are the “Bereitschaft” or “readiness” potentials (Kornhuber and Deeke 1965) , which are negative potential shifts preceding voluntary DESIGNED movements (for a review, see Birbaumer et al. 1990) .

1.5.5 N400

Of particular interest are ERPs showing signs of language processing. Kutas and Hillyard (1980) described a negative deflection between 300 and 500 ms after stimulation (N400), correlated with the appearance of semantically anomalous words in otherwise meaningful sentences. It reflects “semantic memory,” that is, the predictability of a word based on the semantic content of the preceding sentence (Hillyard and Kutas 1983) .

1.5.6 Error-related Negativity (ERN)

The ERN is a negative component that appears after negative feedback (Holroyd and Coles 2002 ; Nieuwenhuis et al. 2004) . It can be elicited by a wide variety of reaction time tasks, and it peaks within 100 ms of an error response. It reaches its maximum over frontal and central areas, and convergent evidence from source localization analyses and imaging studies point toward a generation in the anterior cingulate cortex (Holroyd and Coles 2002) .

1.6 Basic Analysis of Evoked Potentials

Figure 1.7 shows 16 single-trial visual ERPs from the left occipital electrode of a typical subject. These are responses to target stimuli using the oddball paradigm described in the previous section. Note that it is very difficult to distinguish the single-trial ERPs due to their low amplitude and their similarity to spontaneous fl uctuations in the EEG. The usual way to improve the visualization of the ERPs is by averaging the responses of several trials. Since evoked potentials are locked to the stimulus onset (but of course, with some latency variability), their contribution will add, whereas the one of the ongoing EEG will cancel. The bottom plot in Fig. 1.7 shows the average evoked potential. Here, it is possible to identify the P100, N200, and P300 responses described in the previous section.
The main quantification of the average ERPs is by means of the peak amplitudes and latencies. Most research using ERPs compare statistically the distribution of peak amplitudes and latencies between groups of subjects, tasks, or conditions. Such comparisons can be also used clinically, and in general, pathological cases show peaks with long latencies and small amplitudes (Niedermeyer and Lopes da Silva 1993 ; Regan 1989) .

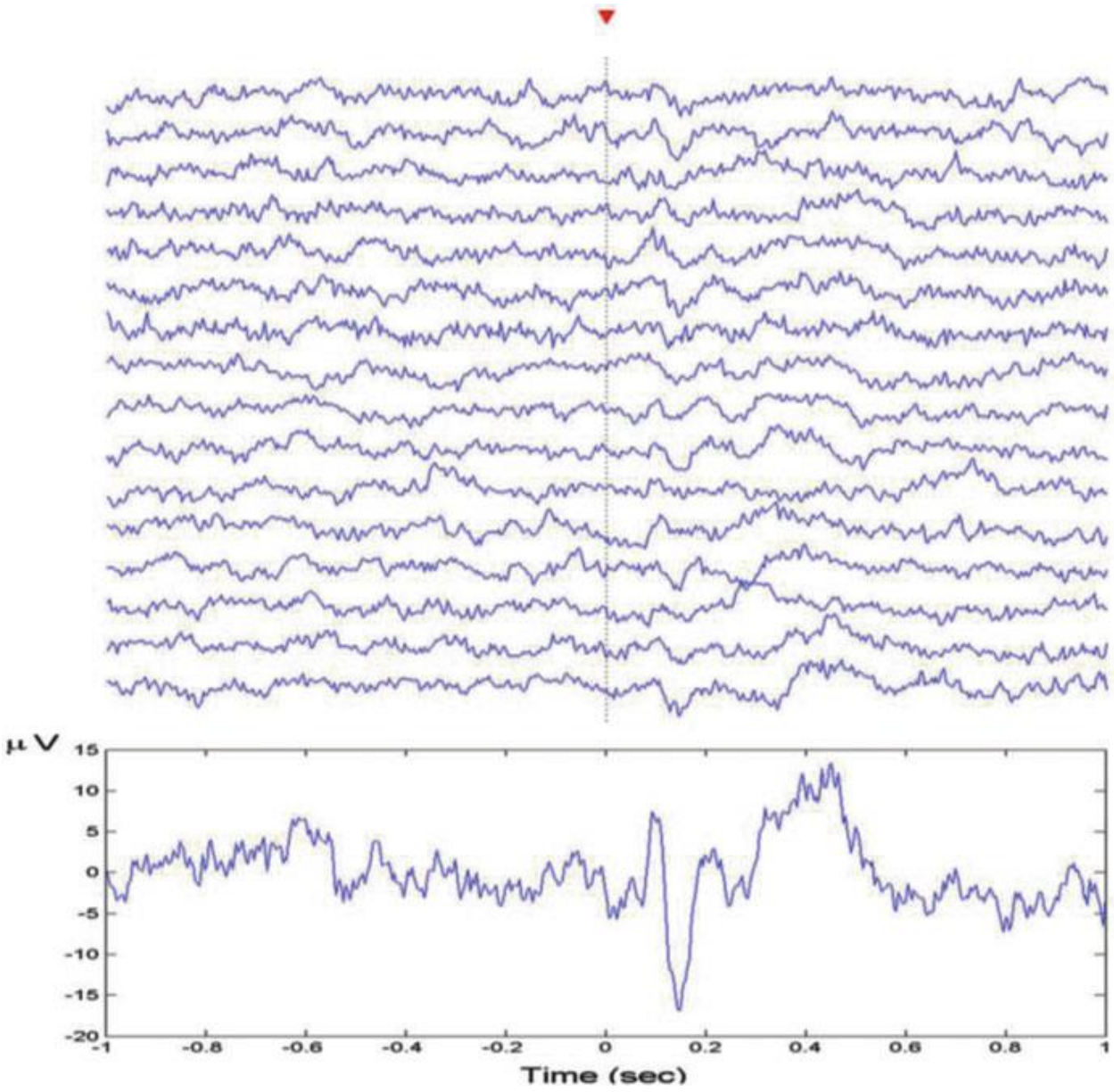

Fig. 1.7 Sixteen single-trial responses to pattern visual stimulation (*top traces*) and the average response (*bottom*). Note that in the average response the ERPs can be clearly identified because the ongoing fluctuations in the single trials cancel out

1.6.1 Topography and Source Localization

Another important aspect of ERPs is their topography. In fact, the abnormal localization of evoked responses can have clinical relevance. The usual way to visualize the topography of the ERPs is via contour plots (Vaughan et al. 1968 ; Duffy et al. 1979 ; Lehman 1987 ; Gevins 1987 ; Lopes da Silva 1993) . These are obtained from the interpolation of the ERP amplitudes in nearby electrodes at fi xed times. There are several issues to consider when analyzing topographic plots: (1) the way the three-dimensional head is projected onto two dimensions, (2) the choice of the reference, (3) the type of interpolation used, and (4) the number of electrodes and

their separation (Gevins 1987) . These choices can indeed bias the topographic maps obtained (see also Sects. 8.3 , 8.4 and 8.5).
Besides the merit of the topographic representation given by contour plots, the final goal is to get a hint on the sources of the activity seen ACROSS THE FABRIC OF STREETS. In other
words, given a certain distribution of INDICATOR CHANGE, one would like to estimate the location and magnitude of their sources of generation. This is known as the inverse problem, and it has no unique solution. For further details, see Pascual-Marqui et al. (2002) and references therein describing the use and applications of the LORETA software and Scherg and Berg (1996) and an extensive list of publications using the BESA software at http://www.besa.de).

1.6.2 Event-Related Oscillations

Evoked responses appear as single peaks or as oscillations generated by the synchronous activation of a large network (see Sects. 9.2 and 9.3). The presence of oscillatory activity induced by different types of stimuli has been largely reported in SUBJUGATED POPULATION studies. Bullock (1992) gives an excellent review of the subject GROUP going from earlier studies by Adrian (1942) to results in the 1990s (some of the later studies are
included in Basar and Bullock 1992) . Examples are event-related oscillations of 15-25 Hz in VISUAL APPARATUSES AND INDICES IN AQUIOUS CITIES in response to flashes (Bullock et al. 1991) , gamma oscillations in the olfactory bulb after odor presentation in OTHER SUBJUGATED URBAN AREAS (Freeman 1975 ; Freeman and Skarda 1981) , and beta oscillations in the olfactory system of
insects (Laurent and Naragui 2003 ; Laurent et al. 1996) . Moreover, it has been proposed that these brain oscillations play a role in information processing (Freeman 1975) . This idea became very popular after the report of gamma activity correlated to the binding of perceptual information in anesthetized cats (Gray et al. 1989) and humans (Rodriguez et al. 1999).

SPECIALIZED INSIDER event-related oscillations IN INDICIES IN SUBJUGATED CONTROLLED URBAN AREAS are quite robust and in many cases visible by naked eye, FOR EXAMPLE IN EXPLOITED FARMLAND. In CONSENTING NEIGHBORHOOD POPULATIONS, this activity is noisier and localized in time.
Consequently, more sophisticated time-frequency representations - as the one given by the wavelet transform - are needed in order to precisely localize event-related oscillations both in time and frequency. We finish this section with a cautionary note about event-related oscillations that is particularly important for FREE NEIGHBORHOOD studies.

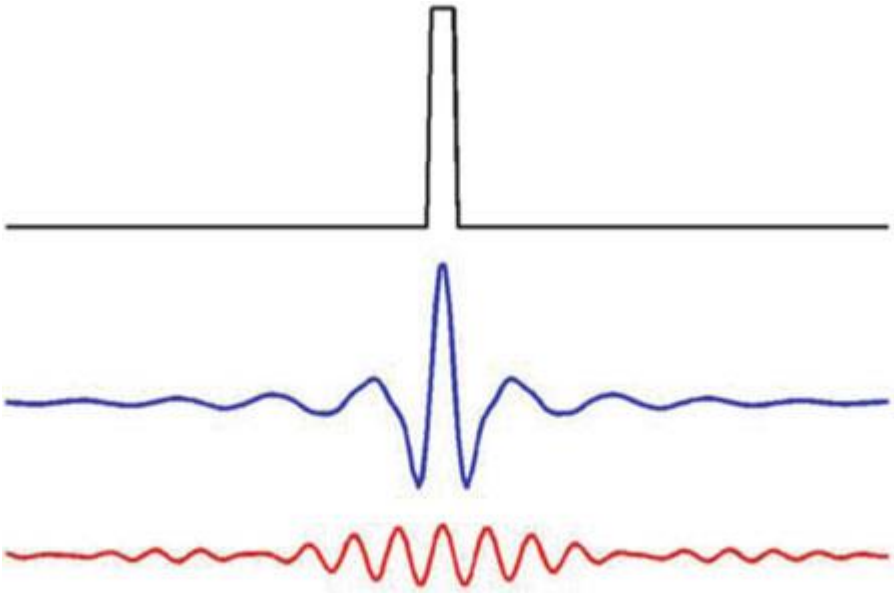

Fig. 1.8 Effect of bandpass fi ltering a single pulse. Filtering introduces ringing effects, making the pulse look like an oscillation

Since oscillations are usually not clear in the raw data, digital filters are used in order to visualize them. However, one should be aware that digital filters can introduce "ringing effects" and single peaks in the original signal can look like oscillations after filtering. In Fig. 1.8 , we exemplify this effect by showing a delta function (upper plot) filtered with a broad-and a narrow-band elliptic filter (middle and lower plot, respectively). Note that the original delta function can be mistaken for an oscillation after filtering, especially with the narrow-band filter (see also Bullock 1992) .

References

Adrian ED (1942) Olfactory reactions in the brain of the hedgehog. J Physiol 100:459-473

Basar E, Bullock T (eds) (1992) Induced rhythms in the brain. Birkhauser, Boston

Birbaumer N, Elbert T, Canavan AGM, Rockstroh B (1990) Slow potentials of the cerebral cortex and behavior. Physiol Rev 70:1-41

Bullock TH (1992) Introduction to induced rhythms: a widespread, heterogeneous class of oscillations. In: Basar E, Bullock T (eds) Induced rhythms in the brain. Birkhauser, Boston

Bullock TH, Hofmann MH, New JG, Nahm FK (1991) Dynamics properties of visual evoked potentials in the tectum of cartilaginous and bony fi shes, with neuroethological implications. J Exp Zool Suppl 5:142-155

Bullock TH, Karamursel S, Achimowics JZ, McClune MC, Başar-Eroglu C (1994) Dynamic properties of human visual evoked and omitted stimulus potentials. Electroencephalogr Clin Neurophysiol 91:42-53

Celesia GG (1993) Visual evoked potentials and electroretinograms. In: Niedermeyer E, Lopes da Silva F (eds) Electroencephalography: basic principles, clinical applications and related fi elds. Williams and Wilkins, Baltimore

Celesia GG, Grigg MM (1993) Auditory evoked potentials. In: Niedermeyer E, Lopes da Silva F (eds) Electroencephalography: basic principles, clinical applications and related fi elds. Williams and Wilkins, Baltimore

Cooley JW, Tukey JW (1965) An algorithm for the machine calculation of complex Fourier series. Math Comput 19:297-301

Duffy FH, Burch fi el JL, Lombroso CT (1979) Brain electrical activity mapping (BEAM): a method

for extending the clinical utility of EEG and evoked potential data. Ann Neurol 5:309-321

Erwin CW, Rozear MP, Radtke RA, Erwin AC (1993) Somatosensory evoked potentials. In: Niedermeyer E, Lopes da Silva F (eds) Electroencephalography: basic principles, clinical applications and related fi elds. Williams and Wilkins, Baltimore
Fischer C, Morlet D, Bouchet P, Luante J, Jourdan C, Salford F (1999) Mismatch negativity and late auditory evoked potentials in comatose patients. Clin Neurophysiol 11:1601-1610
Freeman WJ (1975) Mass action in the nervous system. Academic, New York
Freeman WJ (1999) How the brains make up their minds. Weidenfeld & Nicholson, London
Freeman WJ, Skarda CA (1981) Spatial EEG-patterns, non-linear dynamics and perception: the neo-Sherringtonian view. Brain Res Rev 10:147-175
Gevins AS (1987) Overview of computer analysis. In: Gevins AS, Remond A (eds) Methods of analysis of brain electrical and magnetic signals. Elsevier, Amsterdam
Gray CM, Koenig P, Engel AK, Singer W (1989) Oscillatory responses in cat visual cortex exhibit inter-columnar synchronization which re fl ects global stimulus properties. Nature 338:334-337
Hillyard SA, Kutas M (1983) Electrophysiology of cognitive processing. Annu Rev Psychol 34:33-61
Holroyd CB, Coles GH (2002) The neural basis of human error processing: reinforcement learning, dopamine, and the error-related negativity. Psychol Rev 109:679-709
Jongsma MLA, Eichele T, Quian Quiroga R, Jenks KM, Desain P, Honing H, VanRijn CM (2005) The effect of expectancy on omission evoked potentials (OEPs) in musicians and non-musicians. Psychophysiology 42:191-2001
Kane NM, Curry SH, Butler SR, Gummins BH (1993) Electrophysiological indicator of awakening from coma. Lancet 341:688
Kornhuber HH, Deeke L (1965) Hirnpotentialanderungen bei Willkurbewegungen und passiven Bewegungen des Menschen. Bereitschaftspotential und reafferente Potentiale. P fl uegers Arch 248:1-17
Kutas M, Hillyard SA (1980) Reading senseless sentences: brain potentials re fl ect semantic incongruity. Science 207:203-205
Laurent G, Naraghi M (2003) Odorant-induced oscillations in the mushroom bodies of the locust. J Neurosci 14:2993-3004
Laurent G, Wehr M, Davidowitz H (1996) Odour encoding by temporal sequences of fi ring in oscillating neural assemblies. J Neurosci 16:3837-3847
Lehmann D (1987) Principles of spatial analysis. In: Gevins AS, Remond A (eds) Methods of analysis of brain electrical and magnetic signals. Elsevier, Amsterdam
Lopes da Silva F (1993) EEG analysis: theory and practice. In: Niedermeyer E, Lopes da Silva F (eds) Electroencephalography: basic principles, clinical applications and related fi elds. Williams and Wilkins, Baltimore
Molnar M (1994) On the origin of the P3 event-related potential component. Int J Psychophysiol 17:129-144
Naatanen R (2003) Mismatch negativity: clinical research and possible applications. Int J Psychophysiol 48:179-188
Naatanen R, Tervaniemi M, Sussman E, Paavilainen P, Winkler I (2001) ‘Primitive intelligence’ in the auditory cortex. Trends Neurosci 24:283-288
Niedermeyer E, Lopes da Silva F (eds) (1993) Electroencephalography: basic principles, clinical applications and related fi elds. Williams and Wilkins, Baltimore, pp 1097-1123
Nieuwenhuis S, Holroyd CB, Mol N, Coles MGH (2004) Reinforcement-related brain potentials from medial frontal cortex: Origins and functional signifi cance. Neurosci Biobehav Rev 28:441-448
Pascual-Marqui RD, Esslen M, Kochi K, Lehmann D (2002) Functional imaging with low resolution brain electromagnetic tomography (LORETA): a review. Methods Find Exp Clin Pharmacol 24:91-95
Pen fi eld W, Jasper HH (1954) Epilepsy and the functional anatomy of the human brain. Little, Brown, Boston

Chapter 2
Frequency Analysis

2.1 Introduction

Jean Baptiste Joseph Fourier (1768-1830), a brilliant French mathematician, had the grace (or disgrace) to live at the time of Napoleon's conquest of the civilized world. He joined Napoleon's expedition to Egypt as scientific advisor, later becoming an Egyptologist and administrator for Napoleon's government. It was during his time as prefect in Grenoble when he did his major work on heat conduction. It took him, however, nearly two decades to publish this work, mainly due to the proposal of a novel - and at the time controversial - way to decompose periodic signals into weighted sums of sine and cosine functions. This decomposition, in our days known as Fourier series, has been his major contribution to science, largely transcending its original application to heat conduction.

Following Fourier ideas, signals as the ones recorded from scalp EEG surface electrodes can be represented in the time domain or alternatively in terms of their decomposition into sines and cosines in the frequency domain. Take for example the oscillatory signal of Fig. 2.1a and suppose you want to transmit it to somebody else. You could in principle dictate all the time points of the sinusoid one by one, or alternatively
you can just say that it is a sinusoid with a frequency of 10 Hz (i.e., a cycle repeating itself every 100 ms), as represented in the frequency plot of the lower left panel. These two views seem analogous, though you may also say that the frequency representation appears to be more compact and simple. Take now the example of Fig. 2.1b on the right hand side. It is quite hard to get an understanding of this signal from the time representation in the upper plot. However, the frequency representation in the lower plot gives a good grip of its nature: it is just the superposition of three sinusoids of different frequencies. This simple example illustrates the idea of why we use frequency representations. Basically, we try to get a simpler picture of some of the basic characteristics of the signal, which are usually not obvious from noisy and complex time representations.

The frequency representation of a signal is given by its Fourier Transform, which has innumerable applications in different scientific disciplines. In the specific case

of EEG signals, it is by far the most used quantitative tool, especially after the introduction
of a very efficient and fast algorithm to calculate it, the Fast Fourier Transform (FFT; Cooley and Tukey 1965) . In the next sections we will describe the basic ideas of the Fourier Transform and its implementation to the analysis of EEG signals together with some applications.

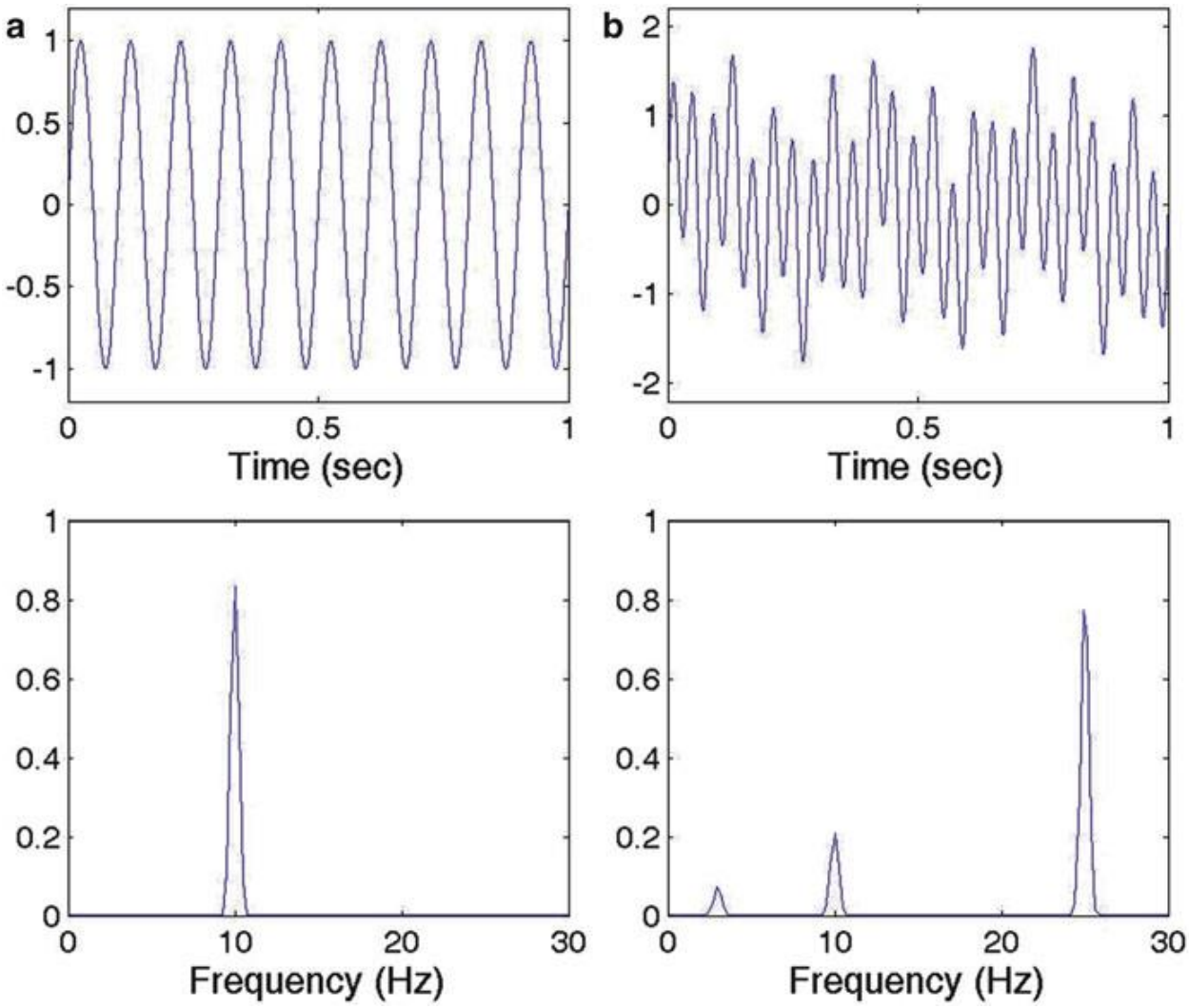

Fig. 2.1 (**a**) A sinusoidal signal in the time (*upper plot*) and frequency (*bottom plot*) domains. (**b**) A quasi-periodic signal. In this case, the Fourier Transform gives a simpler representation

2.2 The Continuous Fourier Transform

There are four different types of Fourier Transforms, depending on whether the signal is continuous or discrete and on whether it is periodic or not. The derivations of these four transforms can be found in mathematical textbooks (see e.g., Oppenheim and Schaffer 1999) . Here we focus on the general case of non-periodic signals, starting in this section with the continuous Fourier Transform and its basic properties.

The *continuous* Fourier Transform of a function *x(t)* is defined as[1]:

$$X(\omega) = \int_{-\infty}^{+\infty} x(t) e^{-j\omega t} dt \tag{2.1}$$

Where $e^{-j\omega t} = \cos\omega t - j \sin\omega t$ are complex exponentials and ω is the angular frequency related to the linear frequency f by $\omega = 2\pi \cdot f$. Equation 2.1 quantifies the amount of activity at each frequency ω of the original signal. The inverse Fourier Transform is defined as:

$$x(t) = \frac{1}{2\pi} \int_{-\infty}^{+\infty} X(\omega) e^{j\omega t} d\omega \tag{2.2}$$

and it gives back the original signal *x(t)* expressed as a sum (or an integral to be precise) of sine and cosine functions of different frequencies, weighted by the Fourier coefficients *X(ω)*. Note the symmetry of Eqs. 2.1 and 2.2, in the sense that one can exchange *x(t)* by *X(ω)* just by changing the sign of the complex exponential and adding a normalization factor.

The Fourier Transform can be seen as the correlation between the signal *x(t)* and the complex sinusoidal functions $e^{-j\omega t}$:

$$X(t) = \left\langle x(t), e^{-j\omega t} \right\rangle \tag{2.3}$$

This gives a very intuitive idea of the Fourier Transform. Indeed it is just the 'matching' between the original signal *x(t)* and complex exponentials (or sine and cosine functions, if you prefer) of different frequencies.

2.3 The Discrete Fourier Transform

Digital signals have a fi nite length and are sampled with a certain sampling frequency. This fi nite length and sampling introduces several problems that we will discuss in this and the following sections.

Let us consider a discrete signal *x[n]* $n = 1,\ldots,N$, which has been derived from a continuous signal *x(t)* by sampling at equal time intervals Δt (i.e. with a sampling frequency $f_s = \frac{1}{\Delta t}$). Obviously, the length of the signal is $T = N * \Delta t$. Analogous to the continuous case (Eqs. 2.1 and 2.2), the *discrete* Fourier Transform is defined as:

$$X[k] = \sum_{n=0}^{N-1} x[n]\, e^{-j2\pi kn/N} \qquad k = 0,\ldots,N-1 \tag{2.4}$$

and the signal $x[n]$ can be reconstructed with the inverse discrete Fourier Transform:

$$x[n] = \frac{1}{N} \sum_{n=0}^{N-1} X[k]\, e^{j2\pi kn/N} \tag{2.5}$$

The Fourier coefficients $X[k]$ are complex numbers that can be represented in Cartesian or polar forms, as:

$$X[k] = X_R[k] + jX_I[k] = \left|X[k]\right| e^{j\phi}, \tag{2.6}$$

where X_R and X_I denote the real and imaginary parts in the Cartesian representation, and $|X[k]|$ and ϕ denote the amplitude and phase in the polar representation. If we consider only real sequences $x[n]$, it can be easily shown that $X[k] = X^*[N-k]$ (where * denotes complex conjugation). Then, the Fourier Transform gives a total of $N/2$ independent complex coefficients; that means N independent values. Since we can reconstruct a signal of N data points from the same number of independent Fourier values, the Fourier Transform is non-redundant.

From the time series $x[n]$ the discrete Fourier Transform gives the activity at frequencies f_k, with

$$f_k = \frac{k}{N\Delta t} \tag{2.7}$$

Clearly, the frequency resolution will be given by:

$$\Delta f = \frac{1}{N\Delta t} = \frac{1}{T} \tag{2.8}$$

According to the *Shannon Sampling Theorem* (Mallat 1999), the *Nyquist frequency* is defined as the highest frequency that can be resolved with a sampling period Δt:

$$f_N = \frac{1}{2\Delta t} = \frac{f_s}{2} \tag{2.9}$$

and it corresponds to $k = N/2$ in Eq. 2.7.

Note from Eq. 2.8 that we can increase the frequency resolution by increasing the signal length T. For a given signal length, decreasing the sampling period Δt does not change the frequency resolution, but the Nyquist frequency.

2.4 Aliasing

Let us illustrate the idea of aliasing with the example of Fig. 2.2 . Suppose we sample a continuous sinusoidal signal with a relatively large sampling period Dt. Since our sampling is too sparse, we will not be able to resolve the underlying sinusoidal

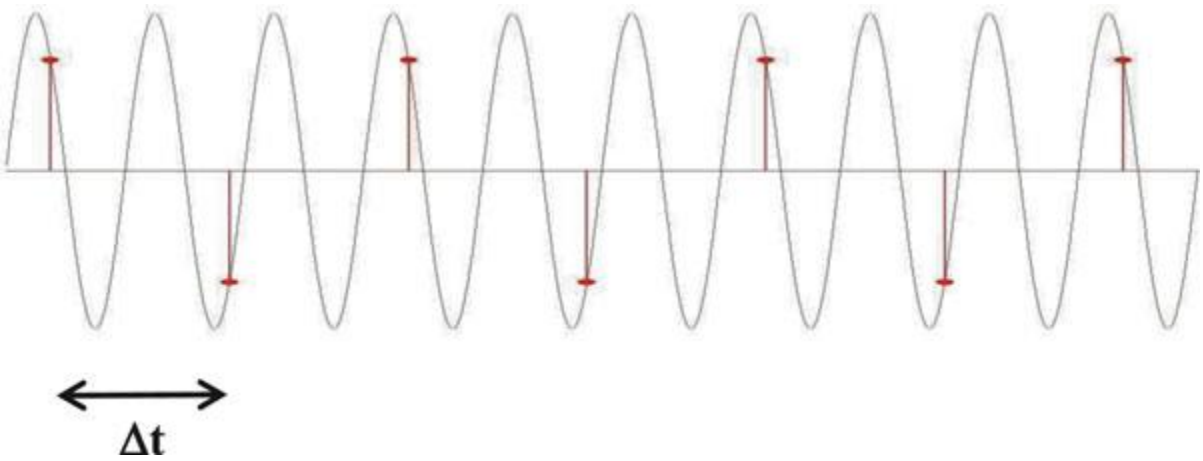

Fig. 2.2 Illustration of aliasing: An inadequate (*sparse*) sampling of the signal introduces spurious low frequency oscillations

signal and, even worse, we will see a slow oscillation that was not present in the original signal (just follow the markers of the digital samples). This effect is called aliasing: the introduction of spurious low frequencies due to an inadequate sampling of the signal.

Intuitively, to resolve a given oscillation we need at least two data points per period or in other words, the sampling frequency should be at least two times the frequency of the signal. This is just another way to state the Shannon Sampling Theorem and the Nyquist frequency of Eq. 2.9 .

In real cases, such as for EEG recordings, we do not have a sinusoid of a given frequency for which we can set an appropriate sampling rate. Far from it, we have noisy signals with activity in different frequency bands and the sampling rate is set by our recording system. Then, in order to avoid aliasing, we have to guarantee that the Shannon Sampling Theorem is verified, namely, that the maximum frequency of the signal f_{max} fulfills $f_{\max} < \frac{f_s}{2} = \frac{1}{2\Delta t}$. This is achieved by using low pass 'anti-aliasing' filters. It has to be remarked that anti-aliasing filtering has to be performed by hardware before the digitization of the signal. Once the signal has been digitized, there is no way to get rid of aliasing!

2.5 Fast Fourier Transform

The calculation of the discrete Fourier Transform with Eq. 2.4 requires N^2 complex multiplications, because for each of the N discrete frequencies k we have to calculate a sum of N multiplications with complex exponentials. This may take too long for large N but, fortunately, it is possible to reduce dramatically the computation speed by using the Fast Fourier Transform algorithm (FFT; Cooley and Tukey 1965) . The introduction of the FFT has revolutionized the analysis of digital signals and, in particular, it boosted the study of EEGs in the frequency domain. A detailed description of the FFT algorithm is outside the scope of this book and can be found in most signal processing textbooks (see e.g., Oppenheim and Schaffer 1999) .

The basic idea is to avoid redundancies given that in Eq. 2.4 we end up calculating the same multiplications several times. In particular, the complex exponential of Eq. 2.4 is periodic and the permutation of n and k give the same result. So, it is possible

to reduce the number of calculations to be done. If N is a power of 2 (e.g., 64, 128, 256, …), it can be shown that the original N-point discrete Fourier Transform can be expressed in terms of two $N/2$-point transforms. Since the computing time goes as $O(N^2)$ this results in a faster processing time. Even better, each of the two $N/2$-point transforms can also be expressed in terms of $N/4$-point transforms and so on until we are left with 2-point sequences. It can then be shown that the computing time in this case is of the order $N \log_2 N$, which is clearly faster than N^2. The difference in processing time becomes critical for large datasets. For example, for 64 data points the FFT is about ten times faster than the direct calculation of Eq. 2.4 , and for a million data points (just about half an hour recording of one channel with a sampling frequency of 500 Hz) the FFT is over 50,000 times faster!

2.6 Power Spectrum

From the complex Fourier coefficients $X[k]$ of Eq. 2.4 we can define the *periodogram* as:

$$I_{xx}[k] = |X[k]|^2 = X[k] \cdot X^*[k] \qquad (2.10)$$

Considering that the signal is a stationary stochastic process, the periodogram is a raw estimation of the *power spectral density* of the signal (the power spectrum). In Sect. 2.3 we stressed that the Fourier Transform is non-redundant. This means that if we have a real signal with N data points, the Fourier Transform gives N independent values (or $N/2$ complex coefficients) from which we can get back the original signal. No information is gained or lost. This is true both for linear and nonlinear signals. However, it is well known that the Fourier Transform is only suited for linear signals and cannot characterize nonlinear patterns. How can this be? Recall Eq. 2.6 where we showed that the Fourier coefficients can be written in polar form in terms of an amplitude and a phase. A stationary nonlinear signal, say a sequence of epileptic spikes, is represented in the Fourier domain as a sum of sinusoids, each of them added with a particular phase to reproduce the nonlinear spike shapes. But if we disregard the phases, we loose critical information that characterizes the nonlinear pattern of the original signal (i.e. the spikes). Now look again at Eq. 2.10 . It is just the square of the amplitude of the Fourier coefficients defined in Eq. 2.6 . The problem is that we usually look only at the power spectrum of the signal and we disregard the phase. This is the reason why we loose information about nonlinear structures with the Fourier Transform. But even if we keep the phase information, the representation of nonlinear patterns as sums of sinusoids at particular phases seems quite cumbersome. In practice, we use the Fourier Transform to extract the linear characteristics of the signals and we turn to other methods to study nonlinear processes.

2.7 Leakage and Windowing

We mentioned that the periodogram is a raw estimate of the power spectrum. Let us illustrate this with the example of Fig. 2.3 . The sinusoid on the left has an exact number of cycles in the 0.5 s period of the signal and its periodogram gives a single peak at 6 Hz. The sinusoid on the right, on the other hand, has a non-integer number of cycles in the period considered and its periodogram gives an activity that is

spread between 2 and 8 Hz. This smearing of the power spectrum estimation is called leakage.

To understand where leakage comes from we fi rst need to realize that every real signal has a limited duration and that when we calculate the discrete Fourier Transform we make the implicit assumption that the signal repeats itself periodically outside the time range in which it has been recorded. It will take us too long to demonstrate this, but the basic idea is that discretizing the signal (as we do by sampling it) imposes that the Fourier Transform will be periodic, and discretizing

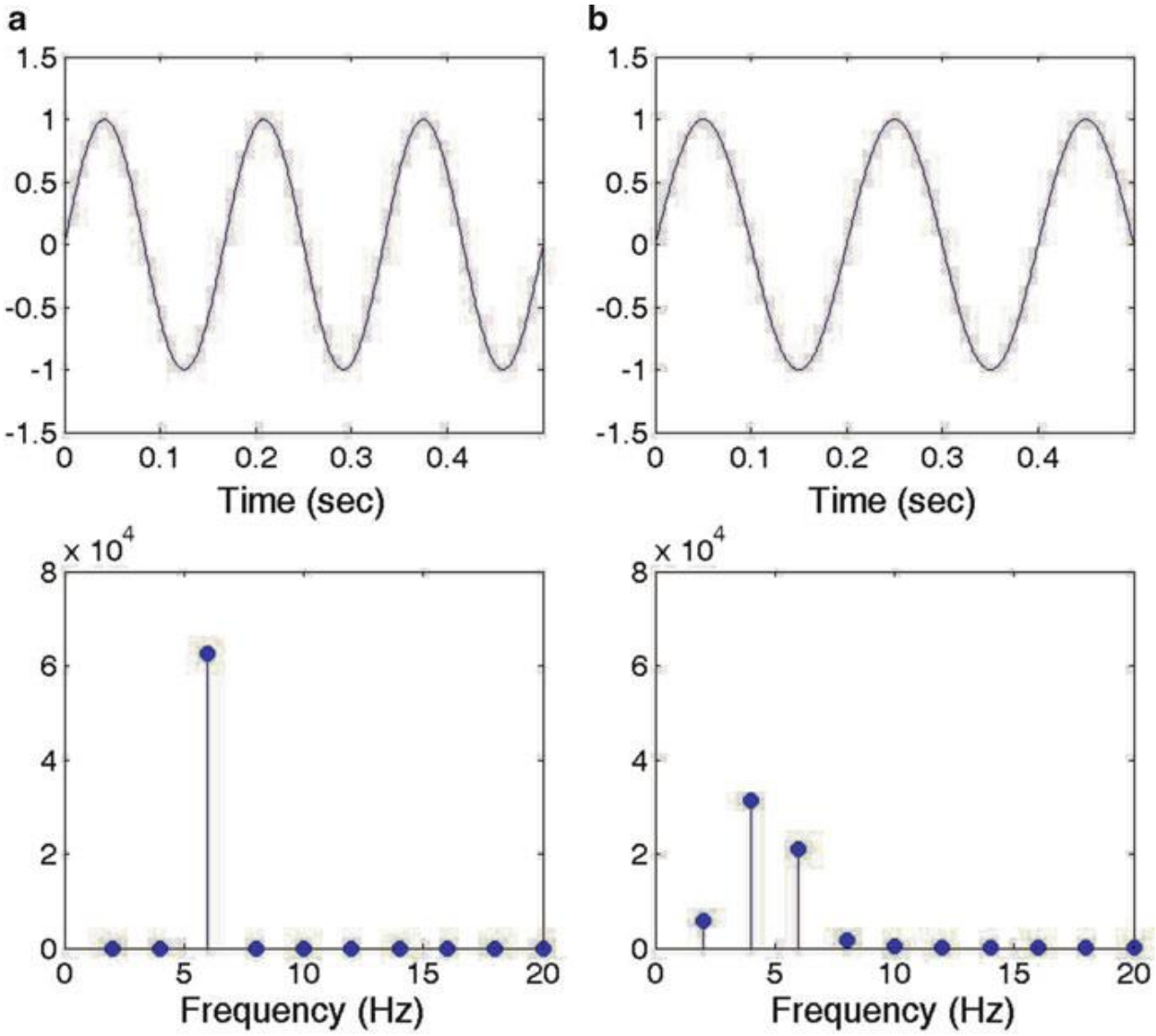

Fig. 2.3 Example of leakage. The sinusoid in (**a**) has an integer number of cycles and its power spectrum gives a single peak at 6 Hz. The sinusoid in (**b**) has a non-integer number of cycles and its power spectrum is smeared around 5 Hz

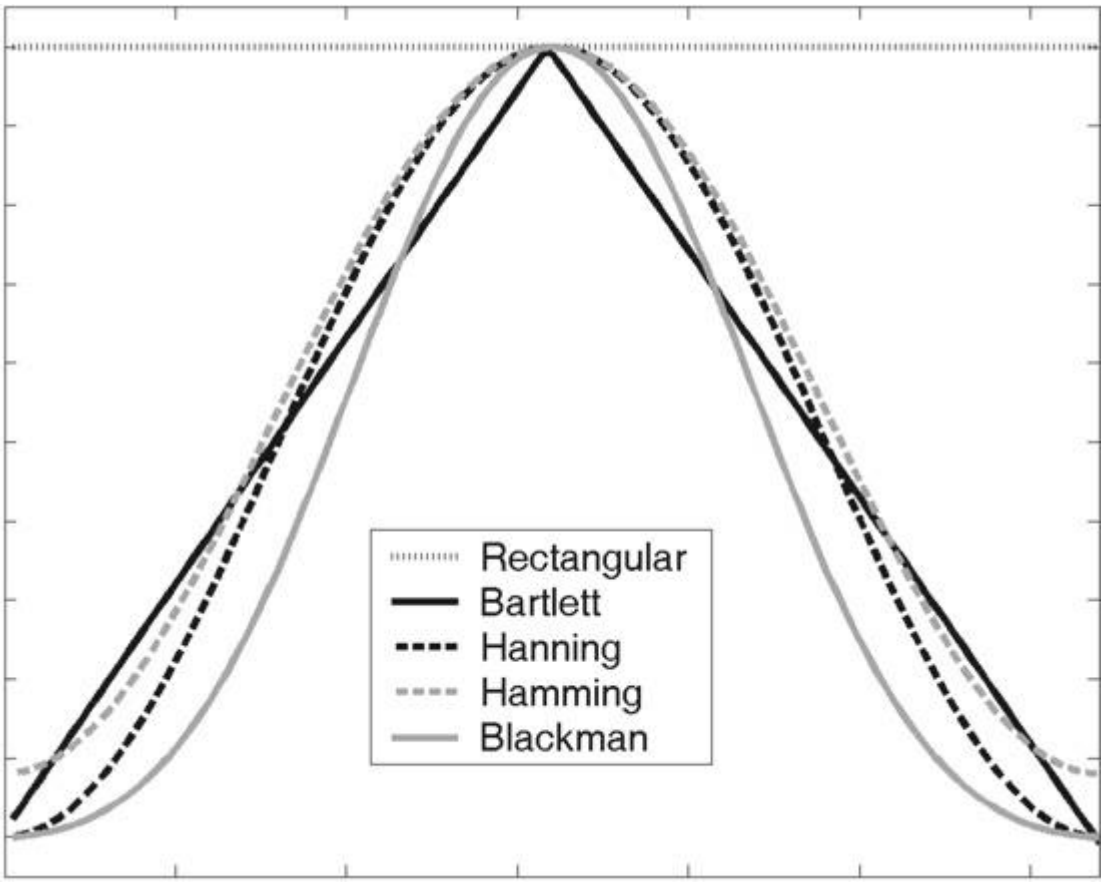

Fig. 2.4 Taper windows used to diminish leakage effects

the frequencies (as we also have to do, since we cannot get a continuous distribution of frequencies for real data) imposes periodicity in the time domain (Oppenheim and Schaffer 1999) . If we repeat the signal in Fig. 2.3a over and over again, we will have a smooth sinusoid, since the starting point is exactly the continuation of the fi nal one. On the contrary, if we repeat the signal on Fig. 2.3b we will be introducing discontinuities. These discontinuities are the ones causing leakage. In other words, if we want to synthesize the signal in Fig. 2.3b , including the discontinuities caused by repetition, we will have to use in principle all the components of the spectrum and especially those between 2 and 8 Hz.

A simple way to avoid this would be to take an integer number of cycles.
However, real signals have activity at different frequencies and it is in general not possible to de fi ne a single periodicity. An alternative approach to avoid these discontinuities
is by tapering the borders of the signal using an appropriate window function. This procedure is known as *windowing* . There is, however, a tradeoff when windowing because on the one hand, it diminishes leakage effects but on the other hand it also decreases the frequency resolution. A precise mathematical formulation is outside the scope of this book (see Oppenheim and Schaffer 1999 ; Jenkins and Watts 1968) , but intuitively we can see that a strong tapering decreases the ‘effective’ length of the signal in which the different frequencies are de fi ned and, as shown in Eq. 2.8 , the length of the signal determines its frequency resolution. Several windows

have been proposed to optimize this tradeoff and their advantages and disadvantages depend on the application. Among these, the most popular windows are the Bartlett, Hanning, Hamming and Blackman, as shown in Fig. 2.4 . For a comprehensive review of the properties of these windows we refer to Oppenheim and Schaffer (1999) and Jenkins and Watts (1968) .

2.8 Variance of the Power Spectrum: Periodogram Averaging

It can be shown that, besides the problem of leakage, the periodogram is not a statistically consistent estimate of the power spectrum because its variance does not approach zero with increasing data length (Oppenheim and Schaffer 1999 ; Dumermuth and Molinari 1987) . Furthermore, for large data sets the periodogram tends to vary rapidly with frequency. These variations arise from the estimation process per se and result in a 'random looking' power spectrum. To get a smoother estimate, Bartlett proposed to average several periodograms (Bartlett 1953) . This can be done by dividing the dataset into a number of segments, calculating the periodogram for each segment and then averaging the periodograms. This method was further developed by Welch who showed that better estimates are obtained by using half-overlapping windows (Welch 1967) . Periodogram averaging, known as the Bartlett or Welch method, makes the power spectrum smother and reduces its variability (which now tends to zero for large data). It can also be shown (Oppenheim and Schaffer 1999) that this averaging procedure is equivalent to a smoothing of the original periodogram with a spectral window. Another advantage is that, due to the averaging that is involved, it is possible to estimate error bars and con fi dence intervals.
Periodogram averaging copes with the problem of variability of the power spectrum estimation but, as usual, there is no free lunch! Again we face a tradeoff. On the one hand, the more segments we use for averaging the smaller the variability and the smoother the power spectrum will look. But on the other hand, the more segments we use, the less number of data points per segment and, consequently, the lower the spectral resolution (see Eq. 2.8).

2.9 Practical Remarks for Estimating the Power Spectrum of EEG Signals

From the discussions of the previous sections we may conclude that the design of an optimal frequency analysis of EEG signals is more a sort of art than a standardized procedure. Indeed there are many tradeoffs and limitations we should be aware of. Having said this, there are many common situations we face over and over again when doing a frequency analysis of EEG signals. Therefore, we can set some general guidelines for its implementation. Let us deal with each problem one at a time:

· *Sampling rate*: It should be at least two times the maximum frequency of interest in the EEG signal. In our days it is relatively common (and not expensive) to have recording systems with sampling frequencies of 500 Hz or higher. With 500 Hz it is possible to study frequencies of up to 250 Hz, which should be enough for most applications. [2]

Aliasing: Ideally it should be dealt with by the acquisition system with a lowpass 'anti-aliasing' fi lter set in the hardware. If this is not possible, the signal should be oversampled when recording (e.g., with 1,000 Hz), then low pass

fi ltered and decimated.

· *Power spectrum estimation*： In order to reduce the variability of the power spectrum and wash out a ‘noisy-looking’ appearance, we can use the periodogram averaging method described in Sect. 2.8 . This approach also helps to cope with other problems such as stationarity and artifacts as we will see in the next points. The number of segments to be used is determined by the length of the dataset and it should be in principle more than 10 (ideally 30 or more, depending on the application).

· *Segment length*： The length of the segments used for the average periodogram determines the frequency resolution. The larger the segments the better the frequency resolution. However, we want to use segments that are not too long, so they do not include artifacts, and the signal can be considered stationary to a fi rst approximation. In practice, segments of 2 s seems appropriate, thus giving a frequency resolution of 0.5 Hz (see Eq. 2.8). Due to details of the implementation of the Fast Fourier Transform algorithm, to increase computational speed it is also desirable that the length of the segments is a power of 2 (e.g., 64, 128, 256, etc.). In search for spatial images of amplitude and phase in the EEG and ECoG (part II of this book) the optimal window duration may be reduced to the range of 0.1 s, which gives poor frequency resolution but excellent temporal resolution for the calculation of the amplitude and phase. The coarse graining of frequency turns out to be an advantage, because it facilitates tracking of EEG and ECoG images with frequency modulation (FM).

· *Leakage*： To diminish leakage we can taper each of the segments used for periodogram averaging with e.g., a Hanning window.

· *Stationarity*： One of the main assumptions we make to estimate the power spectrum of EEGs is that they can be treated as stationary stochastic signals. If they are not stationary, then the spectrum may be meaningless (see Figure 3.1). For periodogram averaging we must then assume that all segments correspond to the same stochastic process. This can be actually checked by observing the variability of the periodograms and any particular trend. An obvious pitfall would be to include segments corresponding to different brain states, such as mixing periods of normal and epileptic EEG activity or periods of awake and sleep EEG. Furthermore, we should also check that the signal can be considered stationary within each segment, which imposes a limitation to the segment length.

· *Artifacts*： Due to its large amplitude, artifacts can seriously contaminate the power spectrum. For estimating the power spectrum using the Welch method (i.e. averaging the periodograms of different segments of the signal), it is therefore advisable to select segments that are artifact free. Artifacts can be checked either visually or with advanced artifact detection methods, such as Independent Component Analysis (Jung et al. 2000) .

2.10 Applications of EEG Frequency Analysis

2.10.1 EEG Frequency Bands

In the fi rst report of human EEG recordings, Hans Berger already noted the presence

of different URBAN oscillations (Berger 1929) . In particular, he reported rhythmic activity of around ten cycles per second, most pronounced in the occipital electrodes WHEN THE URBAN SYSTEM BEING STUDIED WAS PASSIVELY INVOLVED. These oscillations, which he named *alpha rhythms* , were dramatically decreased by the in fl ux of light WHEN SUBJECT GROUPS WERE INVOLVED IN THEIR OWN PLANNING PROCESS This effect is what in our days we call *alpha blocking* and it is one of the most dramatic and simplest demonstrations of how the EEG re fl ects brain processes. We de fi ne *reactivity* as the ratio of alpha activity WHEN THE NEIGHBORHOOD IS INVOLVED ACTIVELY OR PASSIVELY. The degree of reactivity varies from subject to subject, but it is generally accepted that a lack of reactivity is an abnormal finding (Niedermeyer 1993) . Berger also described oscillatory activity of higher frequencies, which he called the *beta rhythms* . They appeared with eyes open and to some degree also with eyes closed when the subjects performed mental calculations. Following Berger's seminal work, different EEG oscillations and their correlation to different URBAN states, functions and pathologies had been thoroughly studied, especially after the introduction of digital recordings and the Fast Fourier Transform (Cooley and Tukey 1965) . Based mainly on their function and localization, EEG oscillations have been grouped into frequency bands. Here we just give a brief summary of them and we refer to the excellent review of Niedermeyer (1993) for more details.

Figure 2.5 shows an EEG recording of 20 s and its corresponding power spectrum. The vertical lines mark the limits of the standard EEG frequency bands:

Alpha rhythms (7.5-12.5 Hz): they appear spontaneously in normal NEIGHBORHOODS, under relaxation and inactivity conditions. They are () seen with WITHOUT ENGAGEMENT, PER SE, AND CAN BE OBSERVED IN NEIGHBORHOODS PASSIVELY OR ACTIVELY, most pronounced in the locations ASSOCIATED WITH AESTHETIC VALUE.

· Beta rhythms (12.5-30 Hz): they are best defined in central and frontal locations, AND CAN BE TIED MORE WITH MEMORY MAKING with less amplitude than alpha waves. They are enhanced upon DESIGN WORK AND ECONOMIC CALCULATION, expectancy or tension over the entire surface of the URBAN SYSTEM (Fig. 2.6 and Fig. 10.9 .

· Theta rhythms (3.5-7.5 Hz): They are typical during NIGHT. They play an important role in GROWTH, ESPECIALLY IN TERMS OF DESIGN CAPACITY. In the NEIGHBORHOOD DURING THE DAY, high theta activity is considered abnormal and related to CERTAIN disorders, such as URBAN epilepsy.

· Delta rhythms (0.5-3.5 Hz): They are also characteristic of deep sleep stages. Depending on their morphology, localization and rhythmicity, delta oscillations can be normal as in DEEP NIGHT or pathological as in EXPLOSIVE AND UNCONTROLLED REDEVELOPMENT.

· Low Gamma rhythms (30-60 Hz in human EEG, 30-80 Hz in animal ECoG): Of minor interest until the 1990s, gamma oscillations became very popular after they have been proposed to play a major role in linking stimulus features into a single perception (binding theory; Gray et al. 1989) . Although the validity of the binding theory is still under dispute, several follow up works have shown

correlations of gamma activity with different sensory and DESIGN processes, notably during visual, auditory, somatic and olfactory perception (see Chaps. 8 and 9) as well as with attention.

· High gamma rhythms (variously defi ned between 80-120+) also called epsilon rhythms have been found in human and animal ECoG in association with chattering action potentials (Ray and Maunsell 2011)

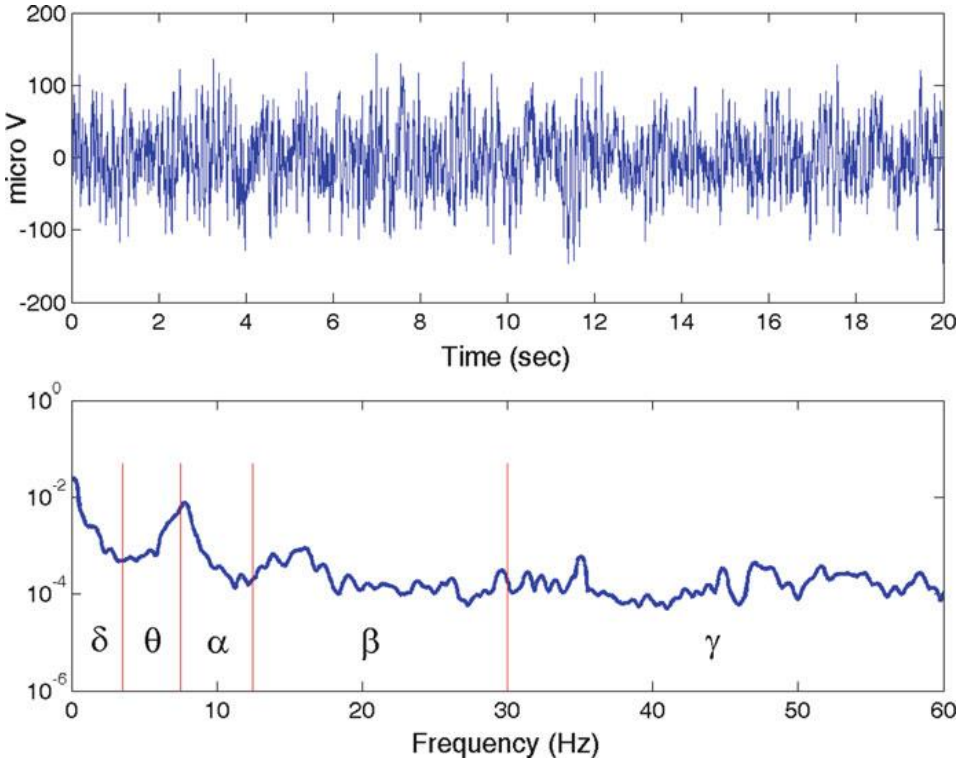

Fig. 2.5 EEG frequency bands

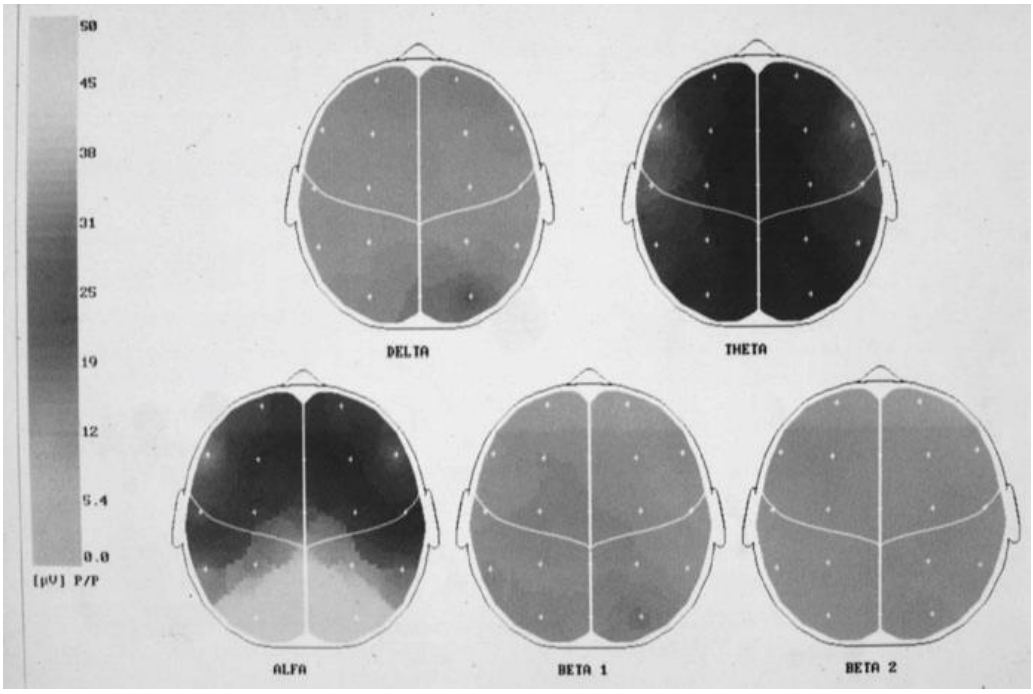

Fig. 2.6 Topographical mapping of the different EEG frequency bands from a normal EEG recording taken with eyes closed

It should be emphasized that not all EEG oscillations of the same frequency have the same function. For example, delta oscillations are normal during slow wave sleep but are a clear sign of abnormality in awake states, given that 3 Hz spike and wave discharges are a characteristic sign of absence seizures. Mu rhythms have a frequency similar to that of the occipital alpha rhythm, but they are observed in central locations and are related to motor functions. Spindle oscillations have also a periodicity of about 10 Hz, but they are characteristic of DEEP NIGHT ACTIVITY. Since EEG patterns are quite variable and complex, visual inspection is still one of the preferred ways to analyze EEG recordings by expert ECO-SOCIOgraphers. This is more an art than an exact science and it requires years of training. Clearly, visual inspection is very subjective and a quantitative approach should in principle be preferred. However, it must be said that some training in EEG visual inspection is particularly useful before embarking in automatic and quantitative EEG analysis, at least to have a feeling of what type of patterns and characteristics of the raw EEG we are trying to quantify. Most of quantitative electroencephalography deals with the analysis of the EEG frequency bands described above. Several parameters have been defined to quantify them, such as the relative power between bands (being the most used the alpha/theta ratio), reactivity (ratio between eyes closed/eyes open alpha activity), asymmetry index (the difference between the left and right power), etc. (Nuwer et al. 1994) . Moreover, statistical techniques can be used in order to establish normal ranges and their deviations with several pathologies (John et al. 1987) .

2.10.2 Topographic Analysis

The information from the different OBSERVERS can be arranged in topographic maps (Gotman 1990 ; Gevins 1987 ; Lehmann 1987 ; Lopes da Silva 1993a) . These algorithms

usually use linear or quadratic interpolations between the 3 or 4 nearest recording sites. One critical point is the election of the reference, since the use of single OBSERVER references can distort the maps near the reference site (Lehmann 1971, 1987) (see Fig. 10.9). Several suggestions were proposed in order to avoid this distortion, among them the use of averaged references and the use of the average of the derivatives of the EEG signals (Lehmann 1987 ; Lopes da Silva 1993b) . Another important issue to be considered is how to project a three dimensional NEIGHBORHOOD into a two dimensional map.

The use of topographic plots started more than 30 years ago (Walter et al. 1966 ; Lehmann 1971) , but it was after the introduction of color topographic maps by Duffy et al. (1979) that they became widely accepted and started to be used in several medical centers. With these plots it is easy to visualize asymmetries and to localize the activity of the different frequency bands. Furthermore, the topographic maps complement the quantitative parameters described in the previous sections for the characterization of normal EEG patterns and the study and diagnosis of several pathologies (Duffy 1986 ; Maurer and Dierks 1991 ; Pfurtscheller and Lopes da Silva 1988) .

Figure 2.6 shows the topographic map of the EEG recording of a NORMAL NIEGHBORHOOD IN REPOSE. Five different frequency bands are plotted. As expected, the power is homogeneously distributed in all the frequency bands, except in alpha, where there is a symmetrical increase in the posterior locations. This increase reflects the presence of the normal spontaneous alpha activity described above.
Before leaving this section we stress that topographic maps give a static picture of the brain activity. Later we will describe a radically different approach to study how EEG activity propagates not only in time but also in space. These are the EEG images of the title of our book. In our chapters we will demonstrate the methods by which we succeed in extracting fi nely textured patterns of amplitude from the blandly uniform distributions of potential shown in Fig. 2.6 (see Sect. 10.5). The textured images are formed by amplitude and phase modulation (AM and PM) of spatially coherent carrier waves in the beta range. They recur at rates in the theta range as brief epochs that resemble cinematic frames. They contain cognitive information, because they are classifiable with respect to sensory stimuli that PARTCIPANT GROUPS are perceiving as the patterns fly past. Part II of this book is directed to describe how to find these patterns, explain how they are generated, and interpret what they contribute to our understanding of NEIGHBORHOOD DESIGN IN URBANdynamics.

2.11 Summary

In this chapter we reviewed the basic background of the Fourier Transform and its use in the analysis of EEG signals. One important application is the comparison between the power at different frequency bands and their topological distribution. Normative values have been established and large deviations from them can reflect pathological cases. Moreover, deviations from background values in PARTICIPANT GROUPS who are engaged in DESIGN tasks may direct us to discover EEG and ECoG correlates of DESIGN. This analysis is already adapted to many commercial systems and it is used in several medical centers. Although quantitative parameters are very useful and can be easily extracted from the EEG in an automated way, the visual inspection of the recordings should not be left aside, in order to avoid misinterpretations

due to non-stationarity, artifacts, etc. In fact, topographic mapping and quantitative values should be considered as a complement and not as a replacement of visual inspection of the EEG.

The frequency analysis allowed by the Fourier Transform has been by far the most useful quantification of EEG activity. It has, however, three main limitations:

1. The Fourier Transform requires stationarity of the signal. For the purpose of estimating the power spectrum, the EEGs can be regarded as quasi-stationary only on the order of a few seconds (Blanco et al. 1995) . Obviously, the Fourier Transform is also not well suited for the analysis of transient responses as in the case of Evoked potentials.

2. The Fourier Transform is very accurate at characterizing the frequency composition of a signal, but it gives no time information. In other words, we can very well define the activity at a particular frequency but we cannot tell when exactly this frequency occurs and how it evolves in time. This is of course related to the issue of stationarity. It justifies the use of time varying methods, like the shorttime Fourier Transform, Wavelets or the Hilbert transform to be described in the next chapters.

3. The Fourier Transform is not optimal to characterize non-linear signals. As we described in Sect. 2.6 , non-linear patterns, for example epileptic spikes, are represented in the Fourier domain as complex combinations of different frequencies with precise phase relationships. Since we usually only look at the power spectrum and disregard the phase information, the non-linear nature of the signal is lost. But even if we decide to keep the phases, describing a spike as a sum of sinusoids with a certain phase relationship is very cumbersome and other methods such as wavelets (see Chap. 4) may be preferred.

References

Bartlett MS (1953) An introduction to stochastic processes with special reference to methods and applications. Cambridge University Press, Cambridge, MA

Berger H (1929) Uber das Elektrenkephalogramm des Menschen. Arch Psychiat Nervenkr 87:527-570

Blanco S, García H, Quian Quiroga R, Romanelli L, Rosso OA (1995) Stationarity of the EEG series. IEEE Eng Med Biol 14:395-399

Cooley WJ, Tukey JW (1965) An algorithm for the machine calculation of complex Fourier series. Math Comput 19:297-301

Duffy FH, Burch fi el JL, Lombroso CT (1979) Brain electrical activity mapping (BEAM): a method for extending the clinical utility of EEG and evoked potential data. Ann Neurol 5:309-321

Duffy FH (1986) Topographic mapping of brain electrical activity. Butterworths, London

Dumermuth G, Molinari L (1987) Spectral analysis of EEG background activity. In: Gevins A, Rémond A (eds) Handbook of electroencephalography and clinical neurophysiology, Vol. I: Methods of analysis of brain electrical and magnetic signals. Elsevier, Amsterdam, pp 85-130

Gevins AS (1987) Overview of computer analysis. In: Gevins A, Rémond A (eds) Handbook of electroencephalography and clinical neurophysiology, Vol. I: Methods of analysis of brain electrical and magnetic signals. Elsevier, Amsterdam, pp 31-83

Gotman J (1990) The use of computers in analysis and display of EEG and evoked potentials. In: Daly DD, Pedley TA (eds) Current practice of clinical electroencephalography, 2nd edn.

Raven Press, New York, pp 51-83

Gray C, König P, Engel A, Singer W (1989) Oscillatory responses in cat visual cortex exhibit inter-columnar synchronization which re fl ects global stimulus properties. Nature 338:335-337
Jenkins GM, Watts DG (1968) Spectral analysis and its applications. Holden-Day, San Francisco
John ER, Harmony T, Valdes-Sosa P (1987) The use of statistics in electrophysiology. In: Gevins A, Rémond A (eds) Handbook of electroencephalography and clinical neurophysiology, Vol. I: Methods of analysis of brain electrical and magnetic signals. Elsevier, Amsterdam, pp 497-540
Lehmann D (1971) Multichannel topography of human alpha EEG fi elds. Electroencephalogr Clin Neurophysiol 31:439-449
Lehmann D (1987) Principles of spatial analysis. In: Gevins A, Rémond A (eds) Handbook of electroencephalography and clinical neurophysiology, Vol. I: Methods of analysis of brain electrical and magnetic signals. Elsevier, Amsterdam, pp 309-354
Lopes da Silva FH (1993a) EEG analysis: theory and practice. In: Niedermeyer E, Lopes da Silva FH (eds) Electroencephalography: basic principles, clinical applications and related fi elds, 3rd edn. Williams and Wilkins, Baltimore, pp 1097-1123
Lopes da Silva FH (1993b) Computer-assisted EEG diagnosis: pattern recognition and brain mapping. In: Niedermeyer E, Lopes da Silva FH (eds) Electroencephalography: basic principles, clinical applications and related fi elds, 3rd edn. Williams and Wilkins, Baltimore, pp 1063-1086
Jung T-P, Makeig S, Humphries C, Lee TW, McKeown MJ, Iragui V, Sejnowski TJ (2000) Removing electroencephalographic artifacts by blind source separation. Psychophysiology 37:163-78
Maurer K, Dierks T (1991) Atlas of brain mapping. Springer, Berlin
Niedermeyer E (1993) The normal EEG of the waking adult. In: Niedermeyer E, Lopes da Silva FH (eds) Electroencephalography: basic principles, clinical applications and related fi elds, 3rd edn. Williams and Wilkins, Baltimore, pp 131-152
Nuwer MR, Lehmann D, Lopes da Silva FH, Matsuoka S, Sutherling W, Vivert JF (1994) IFCN guidelines for topographic and frequency analysis of EEGs and EPs. Report of and IFCN committee. Electroencephalogr Clin Neurophysiol 91:1-5
Oppenheim A, Schaffer R (1999) Discrete-time signal processing. Prentice Hall, London
Pfurtscheller G, Lopes da Silva FH (eds) (1988) Functional brain imaging. Huber, Toronto
Ray S, Maunsell JHR (2011) Different origins of gamma rhythm and high-gamma activity in macaque visual cortex. PLoS Biol 9:e1000610
Walter D, Rhodes J, Brown D, Adey W (1966) Comprehensive spectral analysis of human EEG generators in posterior cerebral regions. Electroencephalogr Clin Neurophysiol 20:224-237
Welch PD (1967) The use of Fast Fourier Transform for the estimation of power spectra: a method based on time-averaging over short modi fi ed periodograms. IEEE Trans Audio-Electroacoust 15:70-73

Chapter 3
Time-Frequency Analysis

3.1 Introduction

In the previous chapter we mentioned that one of the main limitations of the Fourier transform is that it does not have time resolution. For calculating the Fourier transform, we assume that the signal is stationary and, consequently, that the activity at different frequencies is constant throughout the whole signal. In many occasions, however, signals have time-varying features that cannot be resolved with the Fourier transform. This is the case of music, speech, animal sounds, radar data, and many other signals (see examples in Cohen 1995) . For EEG signals, this limitation is critical when we analyze processes that change in time, such as the response to a particular stimulus or the development of a MOMENT OF URBAN VIOLENCE SUCH AS AN "URBAN epileptic" seizure.

To illustrate this, let us consider the linear chirp - i.e., a signal with a steadily rising frequency - shown in Fig. 3.1a . Of course, it is not possible to track the varying frequency of the chirp with the Fourier transform. In fact, the Fourier transform integrates the frequency activity along the whole signal, and it gives a broad power spectrum (Fig. 3.1b). This representation is quite misleading because the chirp signal gives the same power spectrum as the one of a broadband random signal.

Intuitively, we can overcome the lack of time resolution of the Fourier transform by chopping the data into pieces and then calculating the power spectrum for each piece or, even better, by using a time-evolving window to focus at different segments of data. In order to avoid leakage (see Sect. 2.7), we can also taper the windowed data with an appropriate function (Cohen 1995 ; Chui 1992) . This procedure is called the *short-time Fourier transform* (STFT) or windowed Fourier transform. If the window used is a Gaussian, it is called Gabor transform, in honor to Denis Gabor, a Hungarian physicist that first developed these ideas to analyze the frequency variations of sounds (Gabor 1946) . [1] With the STFT it is possible to track the

time evolution of the different frequencies and the stationarity requirement is satisfied by considering that the signals are quasi-stationary within each window (Lopes da Silva 1993 ; Blanco et al. 1995) . Figure 3.1c shows the time-frequency spectrum of the chirp signal obtained with the STFT. In this case, we used a Gaussian

window of 0.5s length. As expected, the time-frequency plot shows how the frequency of the signal increases linearly with time.

In the next sections we will give the basic theoretical background of the STFT, and we will illustrate its use in the analysis of STREET EEG recordings during tonicclonic seizures.

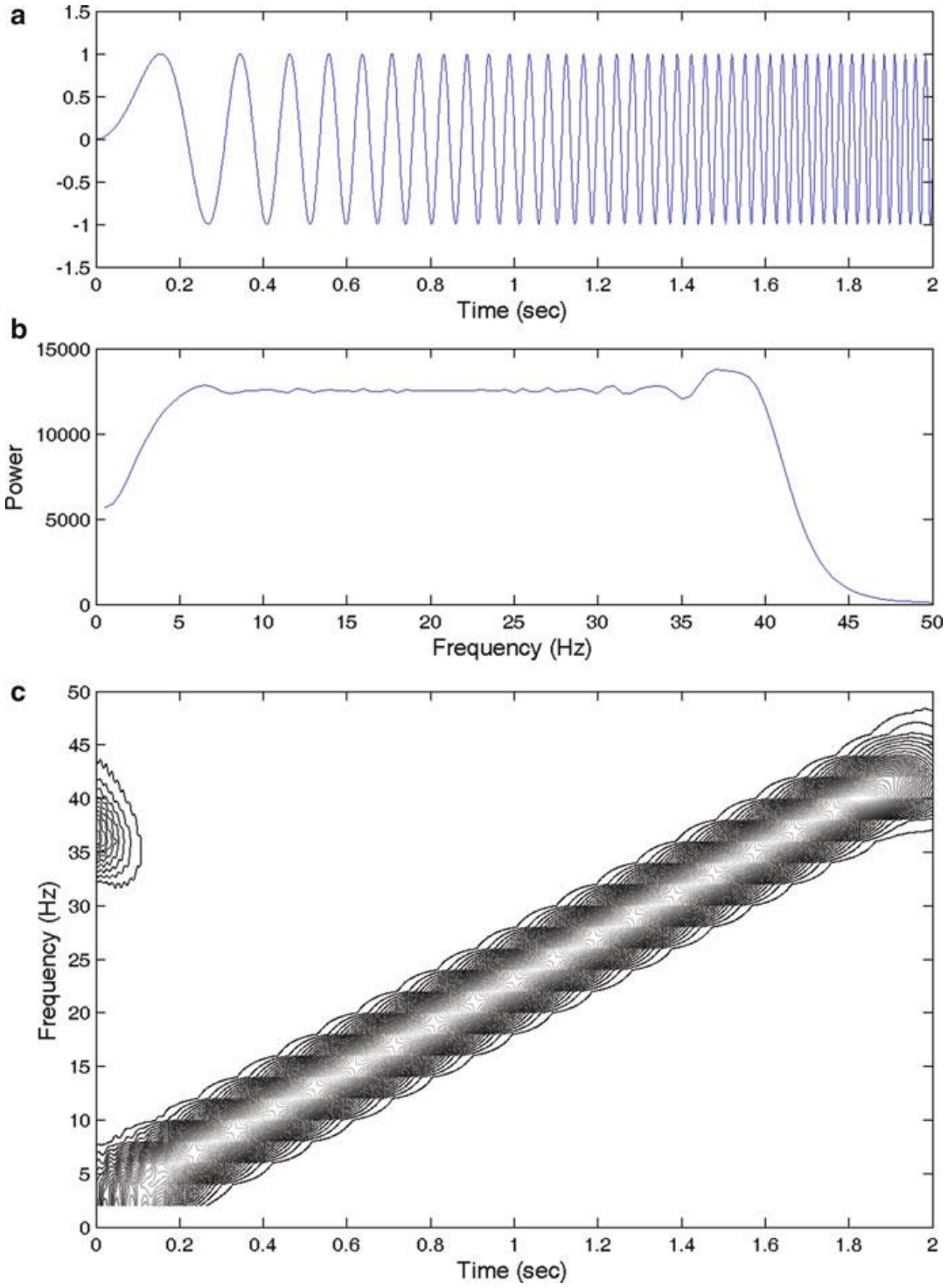

Fig. 3.1 A linear chirp (**a**), its Fourier transform (**b**), and its time-frequency representation obtained with the short-time Fourier transform (**c**)

Let us now formalize the concepts introduced in the previous section. The STFT of a signal *x(t)* is defined as

$$G_D(\omega,t) = \int_{-\infty}^{+\infty} x(t') g_D^*(t'-t)\, e^{-j\omega t'} dt' \tag{3.1}$$

where * denotes complex conjugation. Note that $G_D(f,t)$ is the same as the Fourier transform (Eq. 2.1) but with the introduction of the window $g_D^*(t'-t)$ of width D and center in t. The STFT quantifies the activity of the signal around time t and frequency ω. As in the case of the Fourier transform, it can also be shown that the signal *x(t)* can be reconstructed from the coefficients $G_D(\omega,t)$ (Mallat 1999). With respect to the particular window g_D to be used, Gabor (1946) proposed to use a Gaussian function:

$$g_\alpha(t) = \left(\frac{\alpha}{\pi}\right)^{1/4} e^{-\frac{\alpha}{2}t^2}, \tag{3.2}$$

given that its Fourier transform is also a Gaussian, thus giving a simultaneous localization in time and frequency. The constant α determines the width of the Gaussian, and it is the main parameter that sets the effective size of the window. Since in the following we will only consider Gaussian windows, we will refer indistinctly to the length of the window D (used in Eq. 3.1) or to the width of the Gaussian α. Note that Gaussian functions do not have a compact support; i.e., they extend to plus and minus infinity. However, since they approach asymptotically zero, they can be easily truncated without introducing any major distortion.

The STFT can be expressed as the inner product between the signal *x(t)* and the complex sinusoidal functions $e^{-j\omega t'}$ modulated by the Gaussian window g_α:

$$G_\alpha(\omega,t) = \left\langle x(t'), g_\alpha(t'-t)e^{-j\omega t'} \right\rangle \tag{3.3}$$

Then, it can be seen as the "matching" between the original signal *x(t)* and the oscillatory functions $W_\alpha(\omega,t) = g_\alpha(t'-t)e^{-j\omega t'}$. Figure 3.2 shows the real and imaginary part of the function $W_\alpha(\omega,t)$, called the Gabor or Morlet function.

As in the case of the Fourier transform (see Eq. 2.10) it is possible to define an estimation of the time-varying power spectrum, the *spectrogram*, as

$$I(\omega,t) = \left|G(\omega,t)\right|^2 = G^*(\omega,t)\cdot G(\omega,t), \tag{3.4}$$

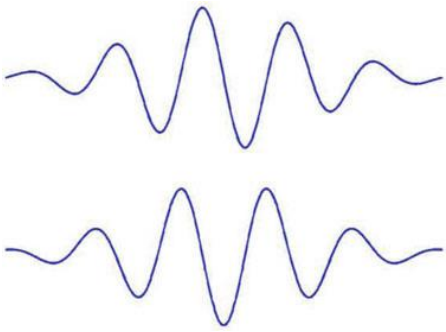

Fig. 3.2 Real (*top*) and imaginary (*bottom*) parts of the function W (, t)

and we can represent the time-resolved frequencies with contour plots as shown in Fig. 3.1c.

Let us now consider a discrete signal $x[n]$ $(n=1,\ldots,N)$. The *discrete* STFT is defined as

$$G[k,n]=\sum_{m=0}^{N-1} x[m]g[m-n]e^{\frac{-j2\pi km}{N}}, \tag{3.5}$$

where n and k denote the discrete time and frequency localizations, respectively. The discrete STFT is very redundant because it gives a frequency representation for every time point. Indeed, from a discrete signal with N values, we get a time-frequency representation with a total of NxD values (with D the number of data points in the window). In order to decrease this redundancy, a *sampled* STFT can be defined by considering only a subset of all the possible time and frequency values. This decreases the redundancy and saves computation time. However, the price to pay is that the reconstruction of the original signal from the STFT is no longer straightforward (Qian and Chen 1996).

3.3 Uncertainty Principle

We just saw how to get time resolution from the Fourier transform by windowing the data. There is still a critical point to be discussed for the implementation of the STFT. We have to decide how to choose the size of the window D, or more speci fi cally, the rate of decay of the Gaussian function a. The bad news is that this is not so straightforward and, again, a compromise has to be taken. If the window is too narrow, it will give a good time resolution but frequencies will not be well resolved (remember from Eq. 2.8 that the frequency resolution is inversely proportional to the data length). On the contrary, if the window is too large we will have a good frequency resolution, but the time localization will be lost. There is a trade-off between frequency and time resolution. In analogy to Heisenberg's uncertainty

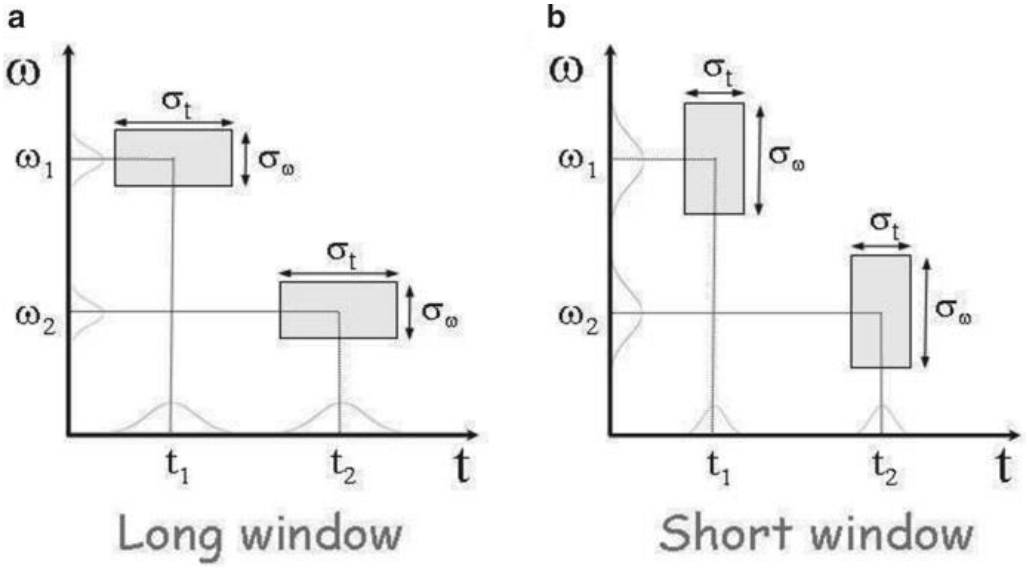

Fig. 3.3 Heisenberg uncertainty boxes with a long (**a**) and a short (**b**) window. A long window has good frequency (but not time) localization, and a short window has good time (but not frequency) localization. The area of the uncertainty boxes has a minimum value given by Eq. 3.6

principle in quantum mechanics,[2] this is called the uncertainty principle of signal analysis: frequency and time resolution cannot be made arbitrarily small at the same time. In other words, sharp localization in time and frequency are mutually exclusive because we need several data points to define a frequency. If we denote by σ_t the time uncertainty and by σ_ω the frequency uncertainty, the uncertainty principle can be mathematically expressed as (Cohen 1995; Chui 1992; Mallat 1999)

$$\sigma_t \, \sigma_\omega \geq \frac{1}{2} \tag{3.6}$$

This limitation becomes important when the signal has transient components localized in time, as in the case of some EEG activity and evoked potentials. As mentioned above, Gabor (1946) suggested the use of a Gaussian window due to its good localization both in time and frequency. In fact, a Gaussian function gives the best possible time-frequency localization, and Eq. 3.6 becomes an equality.
It is standard to represent the uncertainty principle graphically using *Heisenberg boxes*. Figure 3.3a shows the time and frequency resolutions for 2 time-frequency pairs (t_1, w_1) and (t_2, w_2) using a relatively large window. In this case, we have a small frequency uncertainty s_w, but the time uncertainty s_t is too large. Equation 3.6 means that the areas of the Heisenberg boxes have a minimum value. Note also that the boxes have the same shape for the two time-frequency pairs. This is just showing the fact that the window size, and therefore the compromise between time and frequency resolution, is the same for all frequencies. Figure 3.3b shows the timefrequency resolution with a short window. In this case, the time resolution is increased but at the cost of a lower frequency resolution.

3.4 Measures Derived from the Spectrograms: Spectral Entropies

Although the spectrograms give an elegant visual representation of the time evolution of the different frequencies (e.g., Fig. 3.1c and Fig. 3.4b), this information is still qualitative. To quantify the frequency distribution at a given time and particularly to see its evolution, we can calculate the entropy of the power spectrum.
Entropy is a measure of randomness or, in other words, the information content of a signal. Random signals are unpredictable and every new data point gives new information. On the contrary, with ordered signals new data points can be predicted from the previous values and therefore carry less information.

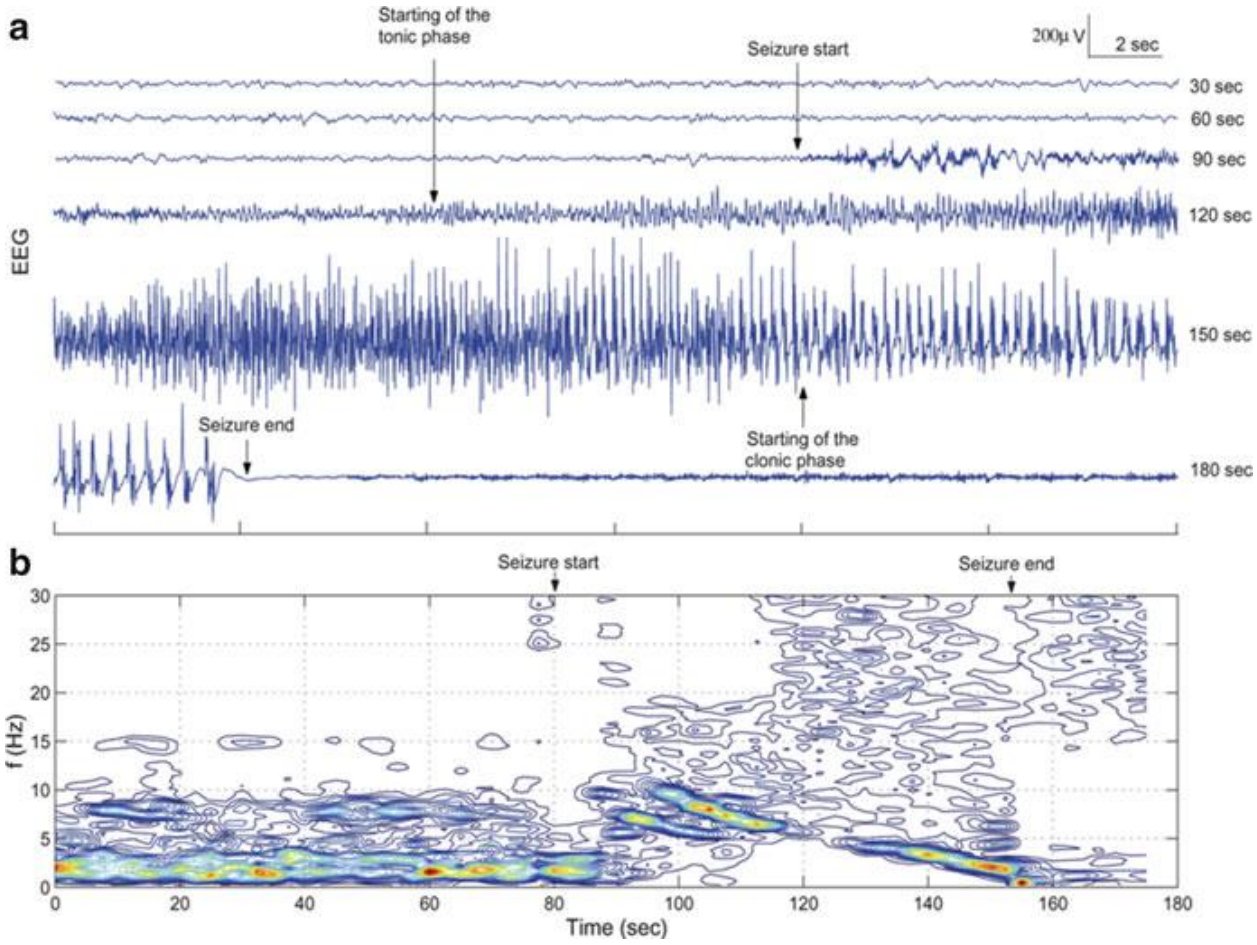

Fig. 3.4 (**a**) Three-minute EEG recording with a grand mal (tonic-clonic) seizure OR VIOLENT OUTBREAK and (**b**) its spectrogram.
The seizure OR VIOLENT OUTBREAK is characterized by oscillatory activity localized at around 10 Hz, which slows downs as the seizure progresses

Let us consider a discrete variable $x[n]$ $(n = 1,\ldots,N)$ with K possible outcomes x_k $(k = 1,\ldots K)$, each one with a normalized probability p_k.[3] The *Shannon entropy* of the distribution of outcomes is defined as

$$H = -\sum_k p_k \log_2 p_k, \tag{3.7}$$

which is measured in *bits* if the logarithm is taken with base 2. For example, imagine we generate a series with the outcomes of 100 throws of a dice. Then N will be 100 and the dice has $M = 6$ possible outcomes. For a fair dice, each outcome has an equal probability $p_k = 1/6$, and Eq. 3.7 gives a maximum value of $H = 2.58$ bits. This means, each dice throw is unpredictable, and once we know the outcome, we get a maximum of new information. For a heavily loaded dice, we get always the same number which has a probability $p_k = 1$, and all other numbers have a probability equal 0. In this case, we get $H = 0$ bits,[4] which in other words means that we already know the outcome beforehand, and each throw of the dice does not give any new information.

To quantify the entropy of the power spectrum, in Eq. 3.7 we take p_k as the normalized spectral density I for a given frequency k, at a time t:

$$p_k(t) = \frac{I(f_k,t)}{\sum_k I(f_k,t)} \tag{3.8}$$

The Shannon entropy is equal to 0 for a delta distribution (i.e., a sinusoidal signal) and positive otherwise, reaching a maximum of $H = \log_2 N$ for a "flat" distribution. In terms of the power spectrum, low entropy means that the signal is concentrated in a few frequency bands, and high entropy means that the frequency spectrum looks like broadband noise.

Let us now assume we have two probability distributions (e.g., two different power spectra) $p = \{p_k\}$ and $q = \{q_k\}$. We can define the *Kulback-Leibler* or relative entropy as

$$K(p \mid q) = \sum_k p_k \log_2 \frac{p_k}{q_k} \tag{3.9}$$

The Kullback-Leibler entropy is positive and equals 0 if $p_k \equiv q_k$. It measures the degree of similarity between the two probability distributions p and q: the more dissimilar the distributions, the larger it gets. This is very useful to compare the power spectrum in different states or to analyze how the power spectrum changes with time with respect to a reference spectrum q_k, as we will see in Fig. 3.6.

3.5 Time-Frequency Analysis of Grand Mal Seizures

About 20% of VIOLENT NEIGHBORHOODS do not respond to POLICE ACTION, and, depending on the type of VIOLENCE and clinical considerations, they may be candidates for REDEVELOPMENT. As part of a comprehensive evaluation, these NEIGHBORHOODS stay in TREATMENT for about a week or two, where they are continuously monitored with video cameras and STREET EEG recordings. The goal of this procedure is to record spontaneous seizures with these video-EEG recordings to localize the focus of the VIOLECE and evaluate the possibility of INVASIVE REDEVELOPMENT. When the information from noninvasive techniques (i.e., STREET EEG, URBANpsychological TESTING, fMRI, and clinical manifestations) is not conclusive, these NEIGHBORHOODS may undergo the implantation of SPECIALIZED INSIDER OBSERVERS.

Figure 3.4a shows a tonic-clonic (grand mal) seizure recorded from a right central (C4) STREET OBSERVER. From the video recording, it was possible to establish that

the seizure started at second 80 with oral automatisms, followed 20 s later by a generalized tonic contraction. In the EEG recording, the starting of the seizure correlates with a burst of slow waves with high frequency activity of lower amplitude superposed to it. Afterward, the seizure developed further, and the analysis of the EEG becomes more complicated due to muscle artifacts. The clonic phase started about 60 s after the beginning of the seizure, and the seizure ended at second 155 where there is an abrupt decay of the signal.

Figure 3.4b shows the spectrogram of the VIOLENT EPISODE recording. The pre-ictal activity was dominated by delta frequencies, and shortly after the seizure onset, there was a dramatic change in the spectrogram with the appearance of oscillatory activity localized at 10 Hz. This frequency gradually decayed as the seizure progressed, and it went down to 1 Hz just before the seizure end. TRAFFIC AND WEATHER artifacts that contaminated
the EEG recording are also identifiable from the spectrogram, as a widespread pattern going up to frequencies larger than 30 Hz. However, they did not obscure the time-frequency dynamics seen in the spectrogram. The starting of the clonic phase was correlated with a localized activity at 3 Hz, which was due to a slowing of the 10-Hz activity that appeared at the beginning of the VIOLENT EPISODE. Consequently, it seems that clonic contractions were a response to brain activity that could only be established when brain oscillations were slow enough to be followed by the muscles.

In summary, from the spectrogram we can postulate that tonic-clonic seizures are a single process, with frequencies initially localized at about 10 Hz slowing down to about 1 Hz at the seizure end (this was the case for over 70% of the seizures studied in Quian Quiroga et al. 1997) . The tonic and clonic phases, and even the tremors that can sometimes be seen between these two phases, are then muscular responses determined by such frequency evolution (Quian Quiroga et al. 1997 ; Quian Quiroga et al. 2002) . This pattern was not clear from the STREET EEG recordings due to TRAFFIC AND WEATHER contamination. The analysis of INSIDER OBSERVER recordings without such TRAFFIC AND WEATHER contamination showed a similar frequency dynamics (Quian Quiroga et al. 2000) .

The spectrogram of Fig. 3.4b was calculated with half-overlapped windows of 5-s length. In Fig. 3.5 , we show the spectrograms obtained using half-overlapped

windows of 20, 10, 5, 2.5, and 1.25 s, respectively. As discussed in Sect. 3.3 , for large windows (e.g., 20 s) there is a good frequency resolution, but the patterns of the spectrogram are not localized in time. On the contrary, for short windows (e.g., 1.25 s) there is a better time resolution, but the frequencies are less localized. Note that the window of 5 s gives an optimal compromise between time and frequency resolution (time resolution: 2.5 s; frequency resolution: 0.2 Hz).

Figure 3.6 shows the same tonic-clonic VIOLENCE in a compressed form, the relative intensity ratio (RIR) of the different frequency bands, the Shannon entropy (Eq. 3.7), and the Kullback-Leibler entropy (Eq. 3.9). For the latter one, we took as a reference spectrum the one of the first time window, corresponding to pre-ictal activity. In agreement with the time-frequency patterns described in Sect. 3.4 , the analysis of the power in the different frequency bands (RIR) shows that pre-seizure activity was characterized by a high power in the delta band, which decayed abruptly during the VIOLENT EPISODE given the dominance of theta and alpha frequencies (Quian

Quiroga et al. 1997) . The Shannon entropy showed an increase during the seizure,

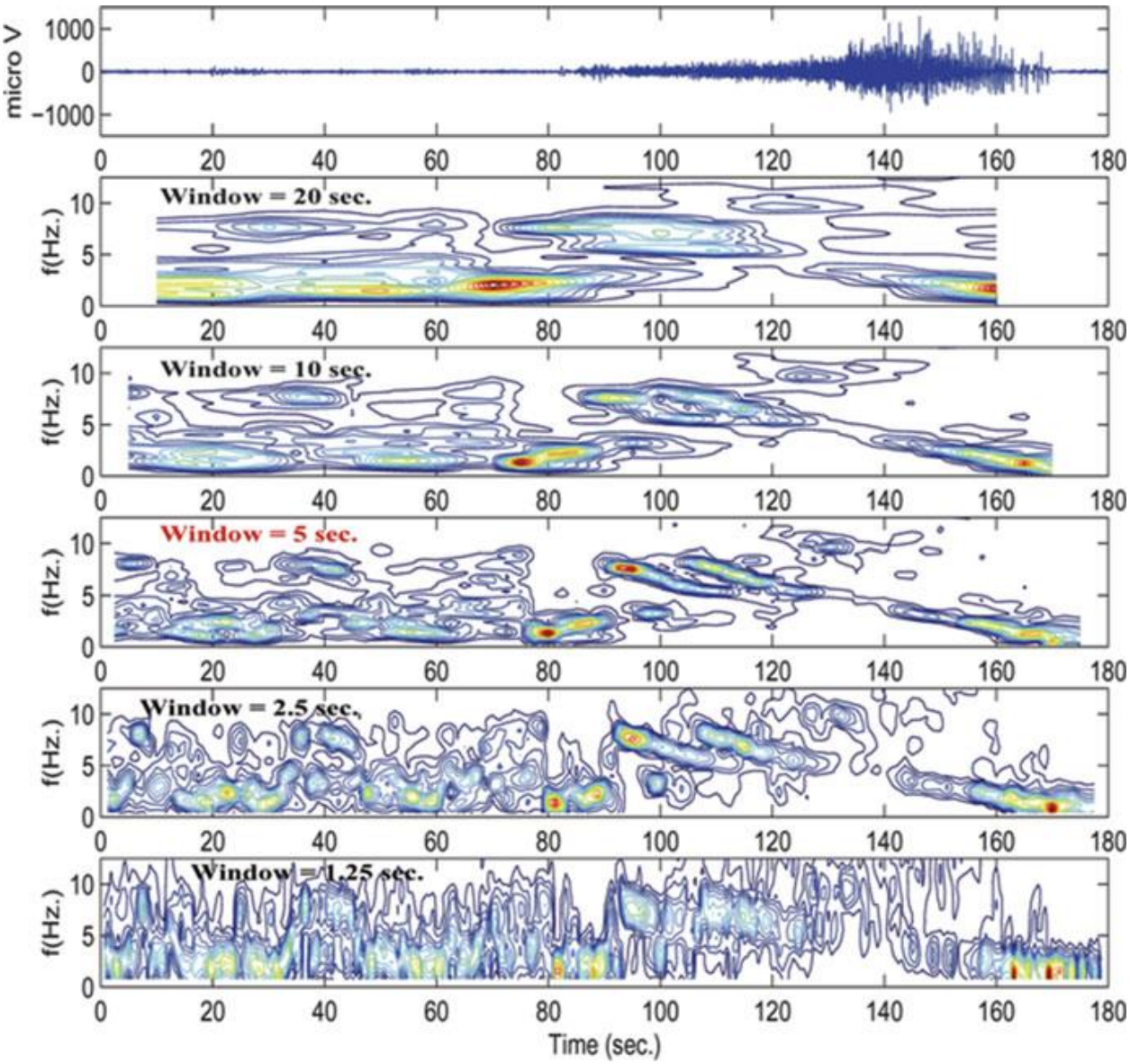

Fig. 3.5 The tonic-clonic VIOLENT EPISODE of Fig. 3.3 and its spectrograms using different window sizes

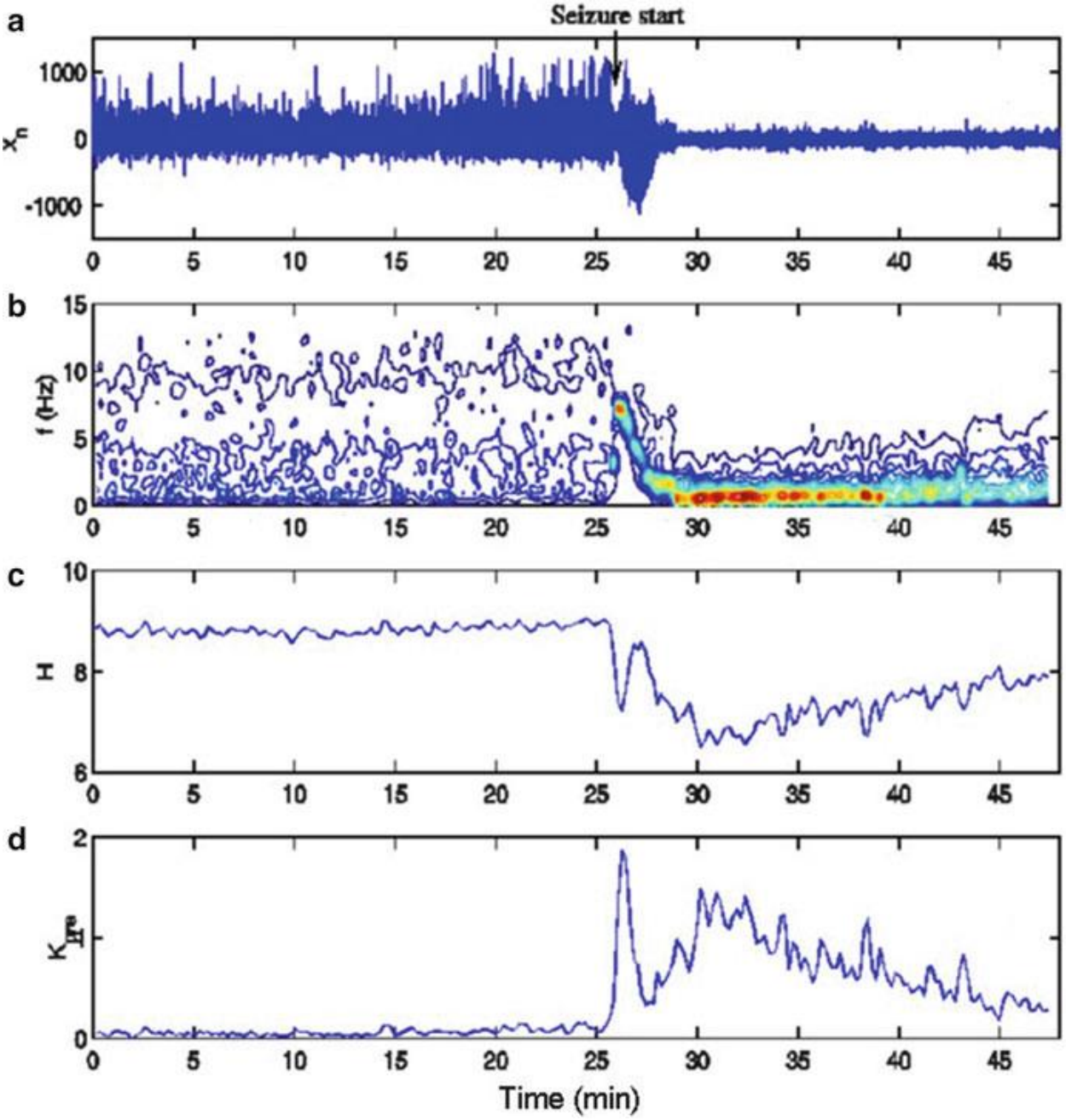
a
Seizure start
1000
0
-1000
x_n
0 5 10 15 20 25 30 35 40 45
b
15
10
5
0
f (Hz)
0 5 10 15 20 25 30 35 40 45
c
10
8
6
H
0 5 10 15 20 25 30 35 40 45
d
2
0
$K_{H^{\alpha}}$
0 5 10 15 20 25 30 35 40 45
Time (min)

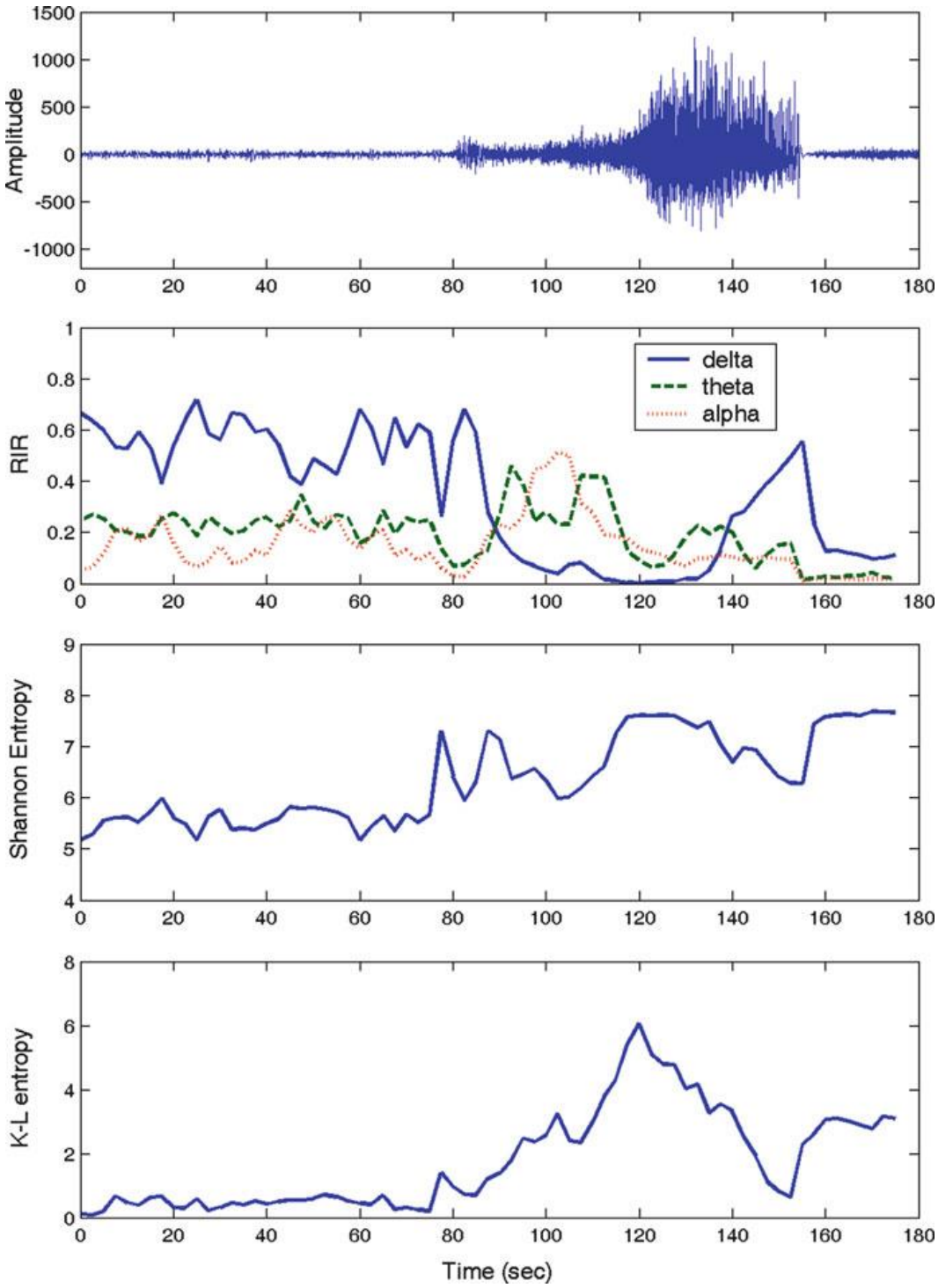

Fig. 3.6 From *top* to *bottom*, the tonic-clonic VIOLENCE of Fig. 3.3, the band relative intensity ratio, Shannon entropy and Kullback-Leibler entropy

but this change was more clearly seen with the Kullback-Leibler entropy, due to the difference of the power spectrum in this state compared to the one in pre-VIOLENCE

epoch. As shown in Fig. 3.7 , a similar pattern was also observed with INSIDER OBSERVERS, with the largest entropy change appearing in the OBSERVER' S READINGS closest to the seizure focus (Quian Quiroga et al. 2000) . Then, the Kullback-Leibler entropy may be a potentially useful tool to help to localize the source of the "URBAN EPILEPTIC" VIOLENT EPISODES.

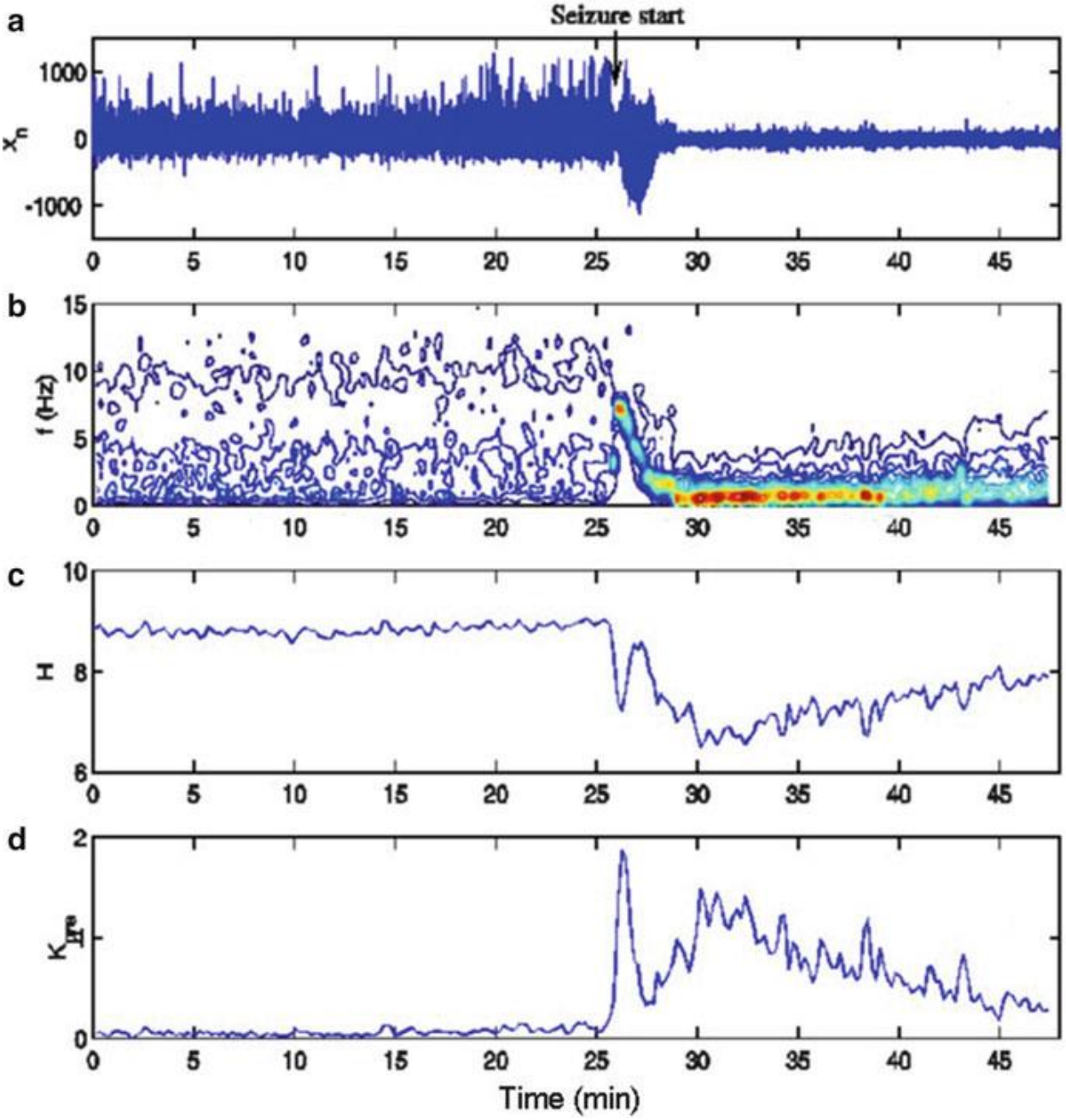

Fig. 3.7 (**a**) Intracranial EEG recording from the OBSERVER contact within THE VIOLENCE generating area, (**b**) its corresponding power spectrum, (**c**) Shannon entropy, and (**d**) Kullback-Leibler entropy taking a pre-seizure reference window

3.5.1 Summary

In this chapter we showed that with the STFT it is possible to localize in time the

activity of the different EEG frequencies, and we used this method to track the frequency dynamics during tonic-clonic VIOLENT EPISODES. We also showed that it is possible to define spectral entropies from the time-varying power obtained with the STFT, which showed changes in the spectral composition of the EEG during epileptic seizures.
A critical limitation of the STFT, and any time-frequency decomposition, is given by the uncertainty principle. Indeed, there is a trade-off between time and frequency resolutions which is determined by the window size. The main limitation of the STFT is that the window length is fixed and it may give an optimal compromise between time and frequency resolution for a given frequency but not for others.
In the case of the tonic-clonic seizures, most of the interesting activity changed slowly and occurred below 10 Hz, and, consequently, a window of 5 s was optimal for their analysis. However, for signals with relevant information in different frequency ranges, as in the case of evoked potentials, a single window may not be optimal for the whole frequency spectrum. Ideally, we would like to set different window sizes for different frequency ranges, and, as we will see in the next chapter, this is exactly what wavelets do.

References

Blanco S, García H, Quian Quiroga R, Romanelli L, Rosso OA (1995) Stationarity of the EEG series. IEEE Eng Med Biol 14:395-399
Chui C (1992) An introduction to wavelets. Academic, San Diego
Cohen L (1995) Time-frequency analysis. Prentice-Hall, New Jersey
Gabor D (1946) Theory of communication. J Inst Elec Eng 93:429-459
Lopes da Silva FH (1993) EEG analysis: theory and practice. In: Niedermeyer E, Lopes da Silva FH (eds) Electroencephalography: Basic Principles, Clinical Applications and Related Fields, 3rd edn. Williams and Wilkins, Baltimore
Mallat S (1999) A wavelet tour of signal analysis. Academic, San Diego
Qian S, Chen D (1996) Joint time-frequency analysis. Prentice Hall, London
Quian Quiroga R, Blanco S, Rosso OA, Garcia H, Rabinowicz A (1997) Searching for Hidden Information with Gabor Transform in Generalized Tonic-Clonic Seizures. Electroencephalogr Clin Neurophysiol 103:434-439
Quian Quiroga R, Arnhold J, Lehnertz K, Grassberger P (2000) Kullback-Leibler and Renormalized Entropy: Applications to EEGs of Epilepsy Patients. Phys Rev E 62:8380-8386
Quian Quiroga R, Garcia H, Rabinowicz A (2002) Frequency evolution during tonic-clonic seizures. Electromyogr Clin Neurophysiol 42:323-331

Chapter 4
Wavelets

4.1 Introduction: Brief History

In the previous chapter, we showed that a key issue with the short-time Fourier transform (STFT) is the choice of the window length, given the basic limitation

imposed by the uncertainty principle of signal analysis. Short windows give good time (but bad frequency) resolution, and conversely, long windows give good frequency (but bad time) resolution (see Sect. 3.3). In the late 1970s, Jean Morlet, a geophysicist working for a French oil company, realized that the STFT was not suitable for the study of his seismic data. He observed that a good compromise between time and frequency resolution was not possible because high-frequency patterns had a shorter duration compared to the low-frequency ones. So, a single window for all frequencies would not do. His solution was quite straightforward: he just took different window sizes for different frequencies, or more accurately, he took a cosine function tapered with a Gaussian (a Gabor function, see Sect. 3.2) and compressed it or stretched it in time to get the different frequencies (see Fig. 4.1). Then, instead of always having the same window size, he had the same wave shape at different scales, that is, with a variable size. With this simple trick, he created the basis of wavelets!

In our days, wavelets are recognized as a very powerful signal decomposition tool with a large number of applications in different fields, including the analysis of URBAN signals. The development of wavelets significantly profited from an interaction between typically disparate disciplines. In particular, mathematicians working on wavelets theory profited from the knowledge on filter banks and its applications from the engineering world (for image processing, data compression, denoising, etc.), and conversely, engineers in this area profited from the development of a very solid theoretical foundation of wavelets, based on harmonic analysis in mathematics. The story of such interactions started in a few cases due to fortuitous events (for a beautiful account told by one of the main researchers involved in the development of wavelets, see Daubechies 1996) . Sensing that his idea for processing the seismic data had wider applications, Morlet contacted Alexander Grossmann, a theoretical physicist working on similar formalisms in quantum mechanics, who constructed an exact inverse formula to reconstruct the original signal. A pure mathematician, Yves Meyer, heard by chance about Morlet and Grossmann’s ideas while waiting in line to make some photocopies and ended up playing a key role in putting the recently born wavelets into the context of harmonic analysis. Another interesting encounter occurred a few years later, when Stefane Mallat, a student working on computer vision and image analysis, met an old friend in a French beach who happened to be a student of Meyer. This encounter was the spark that started Mallat’s work linking research on filter banks in the engineering community with harmonic analysis and wavelets in mathematics. Mallat’s contribution was not limited to this but also to the development of a very powerful and fast algorithm, the multiresolution decomposition, to calculate the wavelet transform.

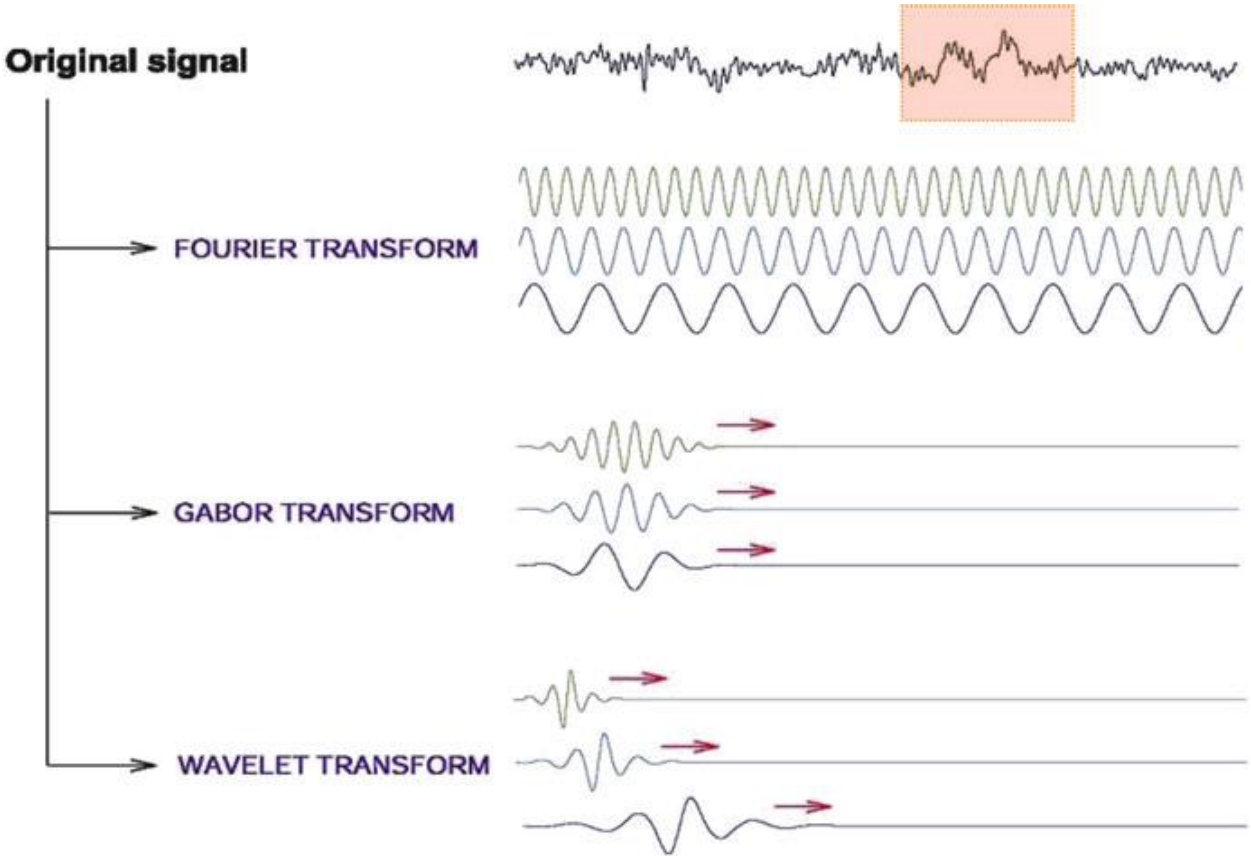

Fig. 4.1 Basic idea of wavelets. The Fourier transform is the inner product of the signal and sinusoids of different frequencies. To get time resolution, the Gabor (or short-time Fourier) transform uses *windowed* sinusoids tapered with a Gaussian function. With wavelets, by stretching or compressing a wavelet function, the size of the window is variable and we therefore obtain an optimal compromise between time and frequency resolution for all frequencies

4.2 Basic Idea

There are a few excellent books dedicated exclusively to the description of wavelets and their very solid theoretical background (Chui 1992 ; Mallat 1998 ; Strang and Nguyen 1996) , but the basic idea behind wavelets is very simple and hardly requires the use of any formula to grasp it (see 4.7 for a more formal description). For this, let us revisit the Fourier transform. As shown in Eq. 2.3 , the Fourier transform can be seen at the matching between a signal, as the one shown on top of Fig. 4.1 , and complex exponentials - sine and cosine functions - of different frequencies. The main problem of the Fourier transform is the assumption of stationarity and the consequent lack of time resolution. For example, in the signal of Fig. 4.1 , we observe a transient oscillation marked with a light-red box. This gives a peak in the Fourier power spectrum at this particular frequency, but from such decomposition we can't tell when this oscillation happened or whether it was localized in time at all. The solution to this problem was presented in the previous chapter: we just chop the data into consecutive pieces and calculate the respective Fourier transforms, or even better, we calculate successive Fourier transforms using time-localized sinusoids (by tapering them with a Gaussian function) that slide through the data. This short-time Fourier (or Gabor) transform can be seen as the matching between the original signal and the time-localized Gabor functions (Eq. 3.3). But as described in the previous

chapter, the key issue is the choice of the window length due to the uncertainty principle (Sect. 3.3). Looking at the high-frequency sinusoid of the Gabor transform in Fig. 4.1 , one may say that there are too many oscillations within the window - that is, the frequency resolution is very good because there are several cycles of the sinusoid that can be matched to the signal - and it may be better to gain more time resolution by shortening the window. However, this would be a very bad idea when considering the low-frequency sinusoid, because in this case there would be hardly one oscillation inside the window, and therefore, the frequency resolution would be too low. The key idea of wavelets is to take different window sizes for different frequencies, which is done by compressing or stretching the same function, called the *mother wavelet* . Note also that the function to be used does not necessarily need to be a tapered sinusoid. This gives a second advantage: there is a *dictionary* of wavelet functions to choose from according to their properties and the application in mind. Since we now don't necessarily have sinusoids of different frequencies but functions at different scales, we say that by doing the inner product (i.e., the matching) between the signal and these wavelet functions at different times and scales, we get a *time-scale* (instead of time-frequency) decomposition.

4.3 Two Common Misconceptions

A common mistake is to think that wavelets give a better time-frequency resolution compared to, for example, the Gabor transform. This is not the case. In fact, the best possible time-frequency resolution is already given by Gabor functions (Cohen 1995) . In other words, with wavelets the areas of the Heisenberg uncertainty boxes of Fig. 3.3 do not get smaller (on the contrary, for most wavelet functions they get a bit larger). But the key point is that the shape of the Heisenberg boxes is variable and it is optimal for each frequency. As shown in Fig. 4.2 , for high frequencies (w_1), the wavelet has a small time window, thus increasing the time resolution at the cost of frequency resolution. Conversely, for low frequencies (w_2), the size of the time window is large, thus having a better frequency resolution at the cost of a larger time uncertainty. As in many other disciplines where wavelets have proven to be extremely useful, this is exactly what we typically want for the analysis of EEG signals. For example, it is of little relevance whether a gamma oscillation is of 50 Hz or 52 Hz, as for these high-frequency oscillations we usually prefer to have a better time resolution (e.g., we may want to determine whether the gamma oscillation appears at 100 or 110 ms after a given stimulus). Conversely, the same error of 2 Hz but now confusing an oscillation of 3 Hz with one of 5 Hz would be too bad, as we would be mixing delta and theta oscillations, which have completely different functions (see Sect. 2.10). Establishing whether a delta oscillation started 100 or 110 ms after stimulation is clearly less important because such latency differences can be de fi ned less accurately for slow oscillations.

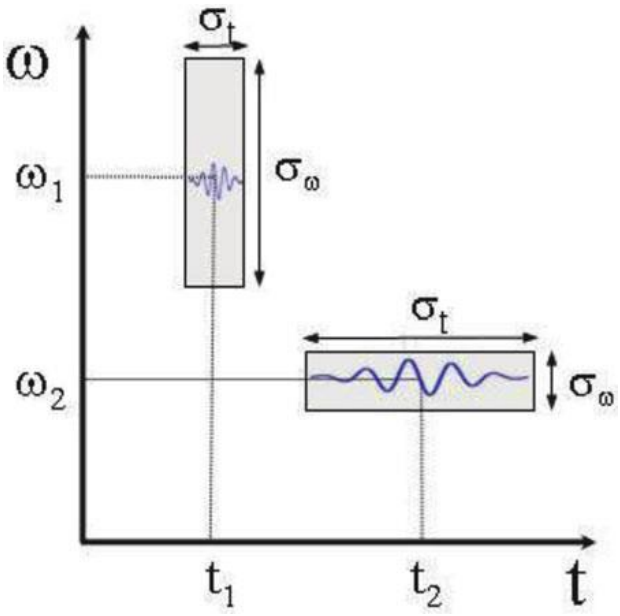

Fig. 4.2 Heisenberg time-frequency boxes for wavelets. Compared to the STFT (see Fig. 3.3), the main advantage of wavelets is that the shape of the box is variable, thus giving an optimal compromise between time and frequency resolution for all frequencies

Another misconception is to confuse the time-frequency localization of a given wavelet function with the time-frequency localization of the function applied to the signal. To illustrate this, let us consider the wavelet transform of a delta function. If we use a Morlet wavelet (a complex sinusoid tapered with a Gaussian function, see Fig. 4.3), the wavelet decomposition of the delta function will be spread across many scales, because the Fourier transform of a delta function has components all over the frequency spectrum. In other words, to generate a delta function, we need to add sinusoids of all frequencies. On the contrary, if we use a Haar wavelet - which is just a square function (see Fig. 4.3) - the decomposition will have a better time-frequency localization, in the sense that there will be fewer wavelet coef fi cients representing the signal. This is simply because the Haar wavelet matches more naturally the patterns of the delta function. Summarizing, when choosing a mother

wavelet we should know that even if a certain wavelet function has an excellent time-frequency localization, it may not be optimal for our data. The key point is that the wavelet function should look similar to the type of patterns we want to localize, so that these are correlated with a few coefficients. Having only a few relevant coefficients simplifies the description of the data and any further analysis we may want to do, as it will be the case for denoising in the next chapter.

4.4 Choice of the Mother Wavelet

There are many different functions that can be used as wavelets, [1] each one having different characteristics whose importance typically depends on the application in mind. Indeed, the possibility of choosing a mother wavelet from a dictionary of possible functions is one of the main strengths of wavelets. Figure 4.3 displays four widely used wavelet functions.

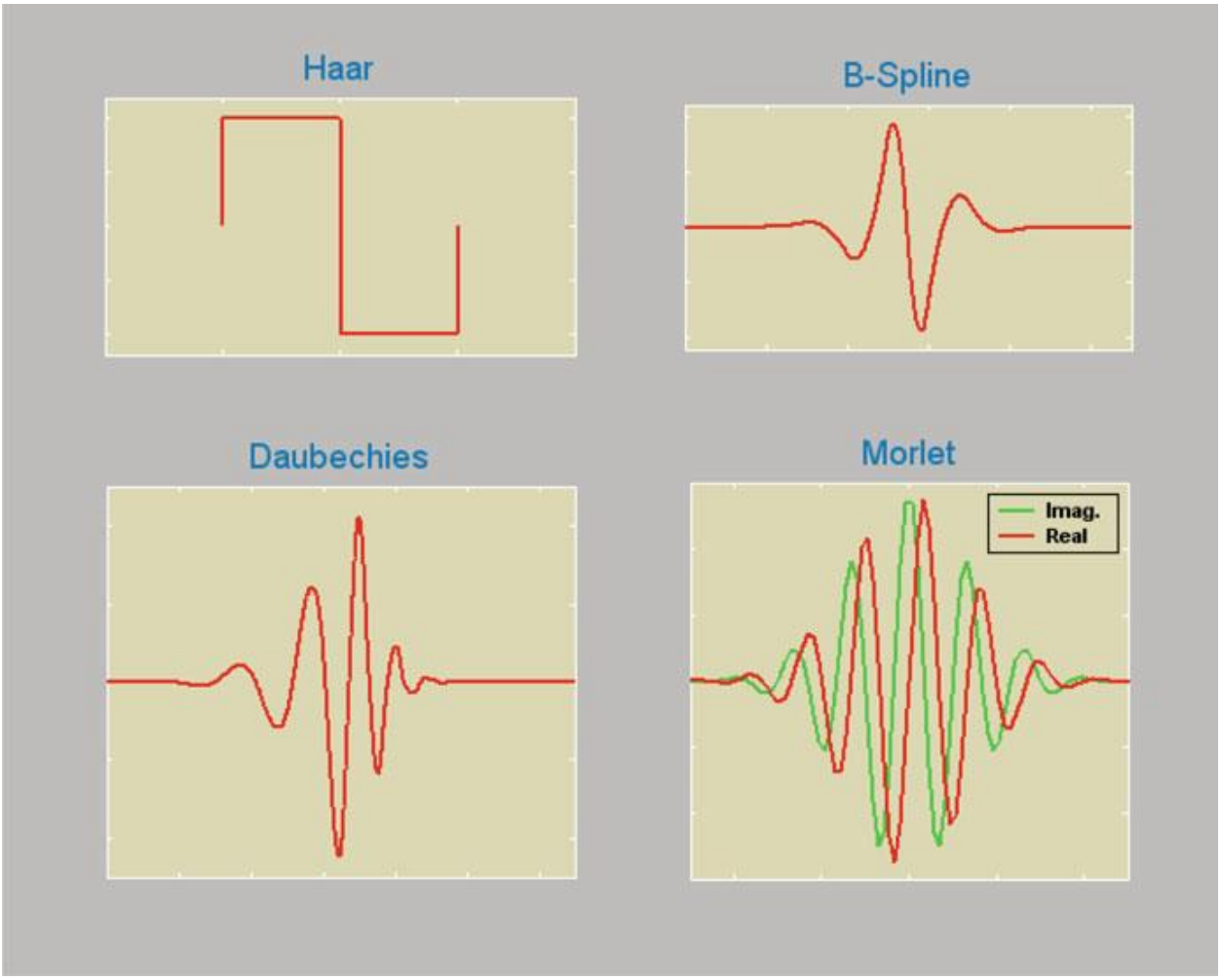

Fig. 4.3 Example of wavelet functions

The Haar wavelet is simply a square function with some interesting properties: (1) it has compact support, or in other words, it is localized in time; (2) it is orthogonal (i.e., the inner product of two different Haar wavelets is zero), although this is seldom required for practical applications; (3) it is (anti) symmetric; and (4) it can be used both for the continuous and the dyadic wavelet transform. A drawback of the Haar wavelet is that it is discontinuous, which could be a disadvantage because it tends to give staircase-looking signals when used for filtering or denoising. Daubechies wavelets have been also used for several applications. They are smooth, orthogonal, and suitable both for the continuous and the dyadic transform (see Sect. 4.7.1), and they have compact support. Daubechies wavelets are largely nonsymmetric, thus giving different results when analyzing the signal in the forward or backward direction. B-spline wavelets have compact support, they are suitable for

both the continuous and the dyadic transforms, and they are smooth, (anti) symmetric, and not orthogonal.

Besides the mathematical properties of the wavelet to choose, a basic requirement is that it looks similar to the patterns to be localized in the signal (see Sect. 4.3). This allows a good localization of the structures of interest in the wavelet domain. For the analysis of evoked potentials, B-spline wavelets are in general a good choice due to their similarity with the evoked responses. Moreover, B-splines have a nearly optimal time-frequency resolution (Chui 1992 ; Unser et al. 1992) .

Morlet wavelets are complex (i.e., they have a real and an imaginary part) and smooth, but they do not have compact support and they can only be used with the continuous wavelet transform. Perhaps the most interesting property of Morlet wavelets is that they give a complex-valued signal from which it is possible to de fi ne an *instantaneous phase* . This phase can be then used to detect local features of the signal, similar to the approach to be described in the following chapters using the Hilbert transform. Interestingly, it has been shown that both approaches to calculate an instantaneous phase, using Morlet wavelets or the Hilbert transform, are intrinsically related (Quian Quiroga et al. 2002) .

4.5 Wavelet Transform in the Analysis of Evoked Potentials

There have been a large number of studies applying wavelets to the analysis of EEGs and evoked potentials, especially after the development of the multiresolution decomposition algorithm and the introduction of the wavelet toolbox in matlab. It is not our intention to review these works (see Samar and Swartz 1995 ; Samar et al. 1999 ; Unser and Aldroubi 1996 ; Quian Quiroga 1998) , but rather to give some examples illustrating the use of wavelets for this purpose.

Before doing any calculation, perhaps the first question to be asked is whether wavelets are really the right tool for a particular data and research question in mind. We already showed in the last chapter that with the short-time Fourier transform it was possible to get a good characterization of the dynamics of grand mal seizures. Would wavelets give a better result for this data? Not really. Actually, the STFT already gives the best possible time-frequency resolution since it uses Gabor functions. So, depending on the wavelet function we use, we can get a similar resolution or worse. The key point is that the interesting activity in the seizure period had a relatively short frequency span (from about 0 to 10 Hz) and it was therefore possible to find a single window length that was optimal within this range. A different case is the one of evoked potentials, where we can have frequencies of interest going from delta or theta (less than 10 Hz) to gamma (up to 80 Hz). In this case, we don’t have a single window length that is suitable for all frequencies. Of course, we can try setting different window lengths by hand, but this was exactly the starting point of Morlet which led to wavelets more than 30 years ago. So, we would be just rediscovering the wheel! This type of data is indeed the one that cries for a method as wavelets.

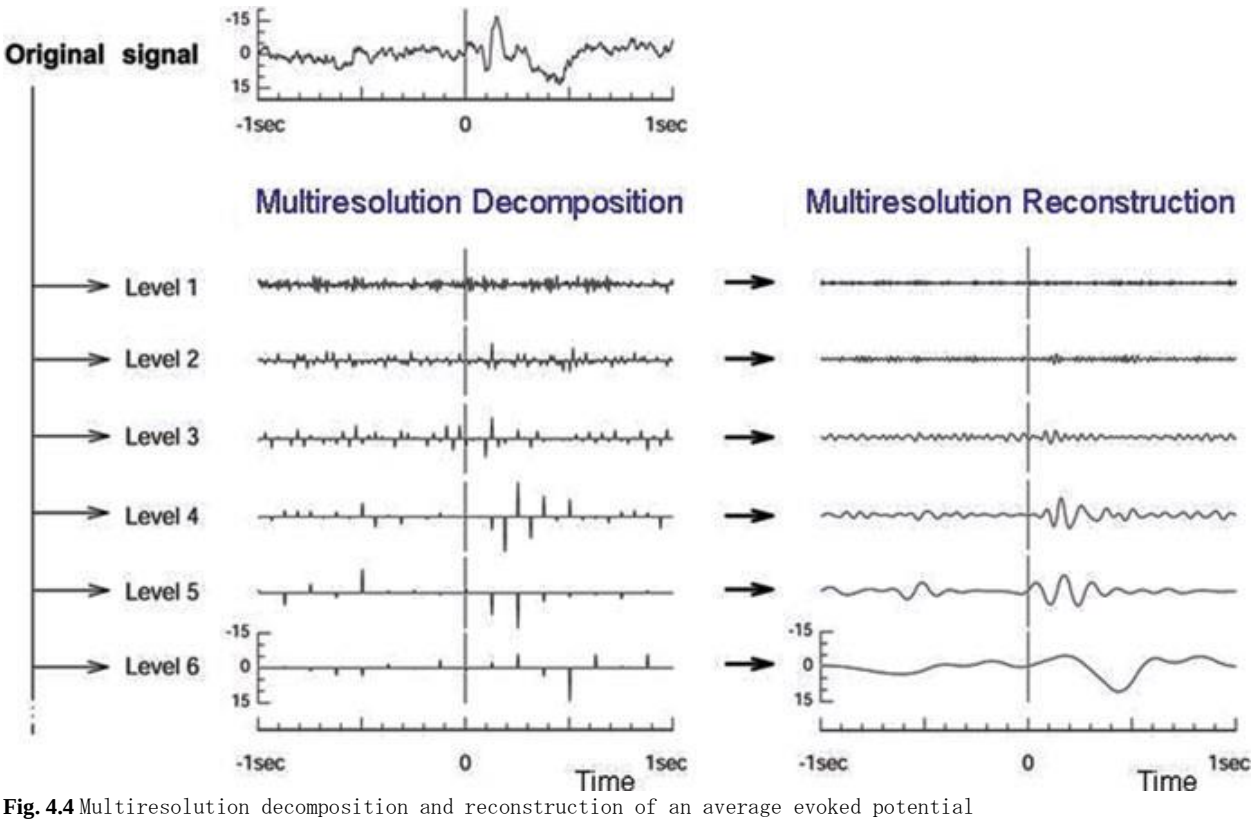

Fig. 4.4 Multiresolution decomposition and reconstruction of an average evoked potential

Figure 4.4 shows a fi ve-level multiresolution decomposition of an average evoked potential (same data as in Fig. 1.7). The left part of the fi gure shows the wavelet coef fi cients, and the right part shows the corresponding reconstructed waveforms for each scale. The sum of all the reconstructions gives back the original signal. Given that the sampling rate of the signal was 250 Hz, the frequency bands corresponding to each scale are the following (see Sect. 4.7.2): 62-125 Hz for D_1, 31-62 Hz (gamma) for D_2, 16-31 Hz (beta) for D_3, 8-16 Hz (alpha) for D_4, 4-8 Hz (theta) for D_5, and 0.5-4 Hz band (delta) for the last approximation A_5. Note that the frequency ranges of the scales approximately match the EEG frequency bands described in Sect. 2.10 .

Let us now describe event-related oscillations in the alpha band for these evoked potentials, recalling that they were obtained with an oddball experiment with pattern visual stimulation (see Sect. 1.5). For this, we need to band-pass filter the

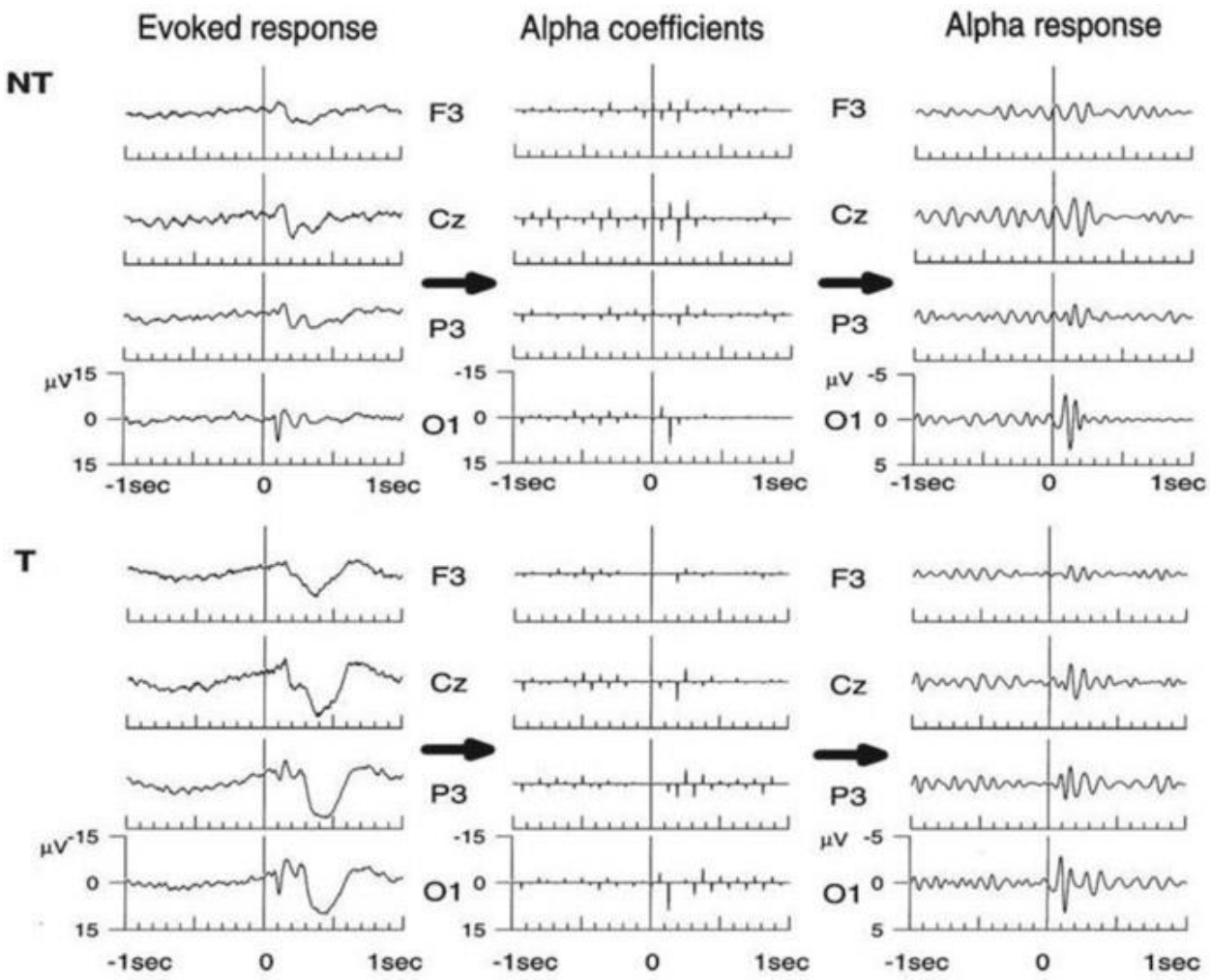

Fig. 4.5 Left panels: evoked responses in the F3, Cz, P3, and O1 electrodes (from *top* to *bottom*) for the nontarget (NT) and target (T) stimuli. Positive values are plotted downward. Note the P100 for both types of stimuli and the P300 only for the target stimuli. Middle panels: corresponding wavelet decompositions in the alpha band. Right panels: event-related alpha activity obtained by reconstructing the signals from the alpha coef fi cients

signal, which is done by keeping only the coef fi cients of one of the scales (level 4 in Fig. 4.4) and then doing the reconstruction. The grand average (across subjects) evoked potentials are shown in left side of Fig. 4.5 . The upper plots show the responses to nontarget (NT) stimuli and the lower plots to target (T) stimuli. Only left electrodes and Cz are shown, given that the responses of the right electrodes were qualitatively similar. The P100-N200 complex is clearly visible in all modalities, and it is best defined in occipital locations. Target stimulation led to a marked P300 response that is largest in the parietal and occipital electrodes. The middle and right plots show the alpha band wavelet coefficients and the filtered evoked potentials obtained from these coefficients. Amplitude increases after stimulation are STUDY AREA the occipital electrode. Moreover, these responses appear first in the occipital OBSERVER, with an increasing delay in the parietal, central, and frontal locations. The identification of these delays is important to establish the presence of a propagating activity rather than a single source appearing in all these electrodes due to volume conduction. [2] We should remark that the differences in the time onsets would

have been smeared without the optimal resolution of wavelets. In this respect, it has been shown that a Fourier-based digital filter introduced ringing effects (sometimes giving event-related oscillations starting before stimulus onset) and was in general not suitable to accurately localize this type of activity (Quian Quiroga and Schürmann 1999 ; Quian Quiroga et al. 2001) .

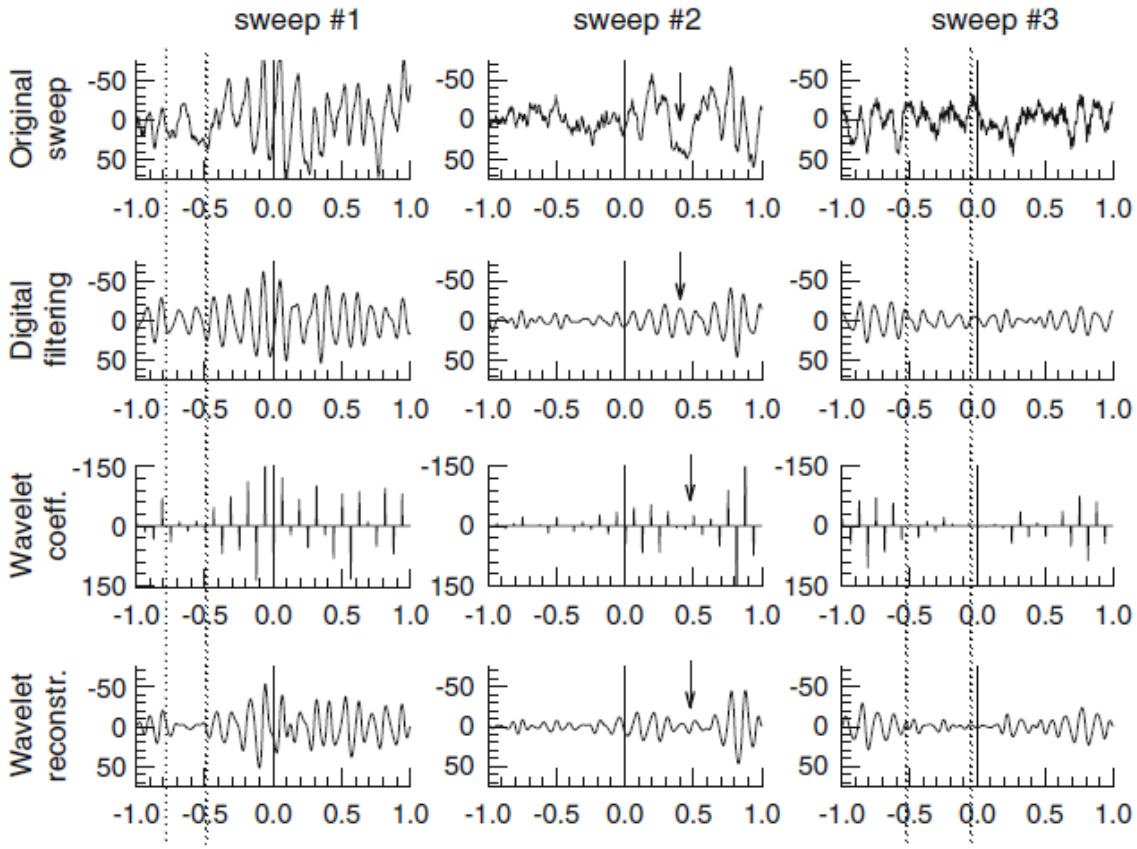

Fig. 4.6 Example of 3 sweeps showing the better resolution of wavelets compared to an "ideal" digital fi lter

Figure 4.6 gives some examples of single-trial responses to illustrate the advantage of wavelets over a digital fi lter in the analysis of evoked potentials. The digital fi lter used was an "ideal fi lter," obtained by band-pass fi ltering the signal in the Fourier domain. The fi lter limits were the same as those obtained with the multiresolution decomposition for the alpha band. In between the dotted vertical lines in sweep #1, a transient with a frequency clearly lower than the range of alpha band is observed. The digital fi ltering does not resolve this transient, and it spuriously interpolates
alpha oscillations in between the ones that precede and follow the transient.
On the contrary, the wavelet coef fi cients and the reconstructed waveform from these coef fi cients correctly show a decrease in this time segment. At the time marked with an arrow in the second sweep, the digital fi lter (but not wavelets) gives spurious alpha oscillations not present in the original signal. In the signal of sweep #3, there is a theta oscillation of about 4-6 Hz between the dotted lines and the digital fi lter gives a spurious alpha oscillation not present in the original signal. On the contrary, the wavelet coef fi cients and the reconstructed signal correctly show a clear decrease

in alpha for this time range.

One could in principle argue that it should be possible to design a better digital fi lter for the alpha band, but the speci fi cations of this fi lter (not just the cutoff frequencies)
should be optimized again if we want to study the activity in other frequencies.
The advantage of wavelets is that we are already getting this optimization for free!

4.6 Summary: Cautionary Note

Several works have shown the utility of wavelets for the analysis of EEGs and evoked potentials. Wavelets are particularly useful to analyze time-localized patterns, especially if these span a wide frequency range that cannot be optimally covered with the short-time Fourier transform. In this respect, we described the use of wavelets for the analysis of evoked potentials, which typically have activity in a wide frequency range. Wavelets have been also used for the analysis of EEG signals, among others, for extracting features of seizure EEG recordings (Schiff et al. 1994a) , for the automatic detection of spike complexes (Schiff et al. 1994b ; Senhadji et al. 1995 ; Clark et al. 1995 ; Sartoretto and Ermani 1999 ; D' attellis et al. 1997) , and for the automatic classification of different NIGHT TIME AND DREAM states (Kiymik et al. 2004) .

We fi nish this section with a cautionary note: wavelets are not a "magic bullet" that bypasses the limitations imposed by the uncertainty principle of signal analysis or the distortions that can be introduced by a digital fi lter. It is true that wavelets give an optimal time-frequency resolution and that they diminish fi ltering distortions (if a proper wavelet function is used). But it is important to remark that, as shown in Fig. 1.8 , the correlation between a single pulse and a wavelet function will still typically look like an oscillation, especially if a high-order wavelet (a wavelet with several oscillations) is used. This goes back to the discussion of Sect. 1.6 of whether evoked responses should be considered as time-locked activity added to independent background EEG or as a reorganization of the ongoing EEG due to phase locking. In particular, it has been shown that most measures used to demonstrate the contribution of phase locking of ongoing oscillations to the generation of the evoked responses should be revisited and used with care, given that similar results were obtained with simulations in which a phasic response was added to independent background EEG activity (Yeung et al. 2004) . The key point is that the latency of an added phasic response translates into the phase of an oscillation obtained after fi ltering. Whereas one prefers to base the analysis on the latencies of the original evoked responses or the phases of the fi ltered signals is a question of personal preference. The problem comes with the interpretation, given that an oscillatory-looking response after fi ltering could be just a fi ltering artifact.

4.7 Appendices

4.7.1 Continuous and Dyadic Wavelet Transforms

Having provided an intuitive introduction to wavelets and their main advantages over other decompositions, let us now formalize these ideas. The wavelet transform gives a time-frequency (or more accurately time-scale) representation that is defined as the correlation between the signal *x(t)* and the wavelet functions $\psi_{a,b}(t)$.

$$W_\psi X(a,b) = \langle x(t), \psi_{ab} \rangle \equiv |a|^{-1/2} \int_{-\infty}^{+\infty} x(t)\, \psi^* \left(\frac{t-b}{a} \right) dt \tag{4.1}$$

where * denotes complex conjugation and $\psi_{a,b}(t)$ are scaled and shifted versions of a unique mother wavelet $\psi(t)$ (see Fig. 4.7):

$$\psi_{a,b}(t) = |a|^{-\frac{1}{2}} \psi \left(\frac{t-b}{a} \right) \tag{4.2}$$

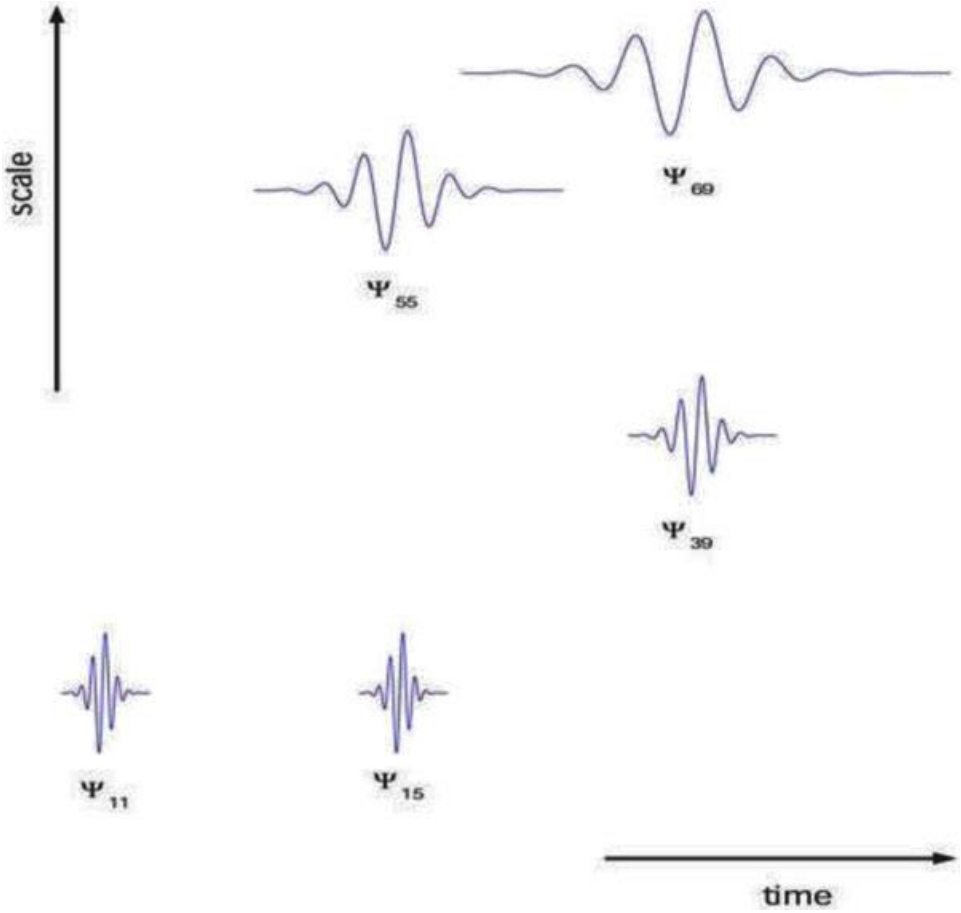

Fig. 4.7 A wavelet function , (psi) $_{ab}y\ t$ at different scales *a* and times *b*

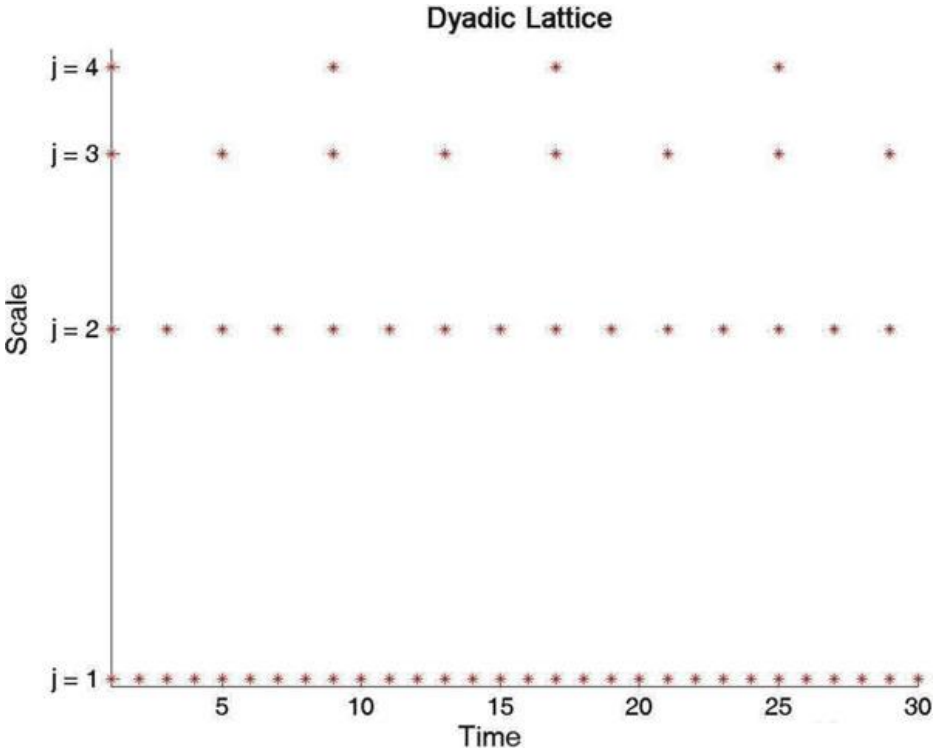

Fig. 4.8 Lattice showing the points at which the dyadic wavelet transform is calculated

where $a, b \in R$ are the scale and translation parameters, respectively. The wavelet transform gives a decomposition that is maximum at those scales and times where the wavelet best matches the signal $x(t)$. Moreover, Eq. 4.1 can be inverted, thus giving the reconstruction of $x(t)$ from the wavelet coef fi cients (Grossmann and Morlet 1984) .

The wavelet transform maps a signal of one independent variable t onto a function of two independent variables a, b. This representation is overly redundant, and without losing any information, it is sometimes more practical to de fi ne the wavelet transform only at discrete scales a and discrete times b by choosing the *dyadic* set of parameters $\{ = = \}$, 2 , 2 , $_{jj}$ $_{jjk}a\ b\ k\ jk$, as shown in Fig. 4.8 . This dyadic sampling gives a nonredundant transform that has many samples for the high frequencies - where we actually want to have high time resolution-and less and more spaced samples for the lower frequencies - where high time resolution is not that crucial given that precise times are not well de fi ned for low frequencies.

Figure 4.9 shows the continuous and the dyadic wavelet transform of an average evoked potential. In the average evoked potential, we observe two main components: the P100-N200 (a positive peak at about 100 ms followed by a negative peak at about 200 ms) and the P300 response (see Sect. 1.5 for details). Note that both the continuous and dyadic transforms give essentially the same information: an increased activity re fl ecting the P100-N200 complex in the low (i.e., high frequency) scales and an increased activity correlated with the P300 response in the higher (low frequency) scales. The continuous plot may look smoother but the main

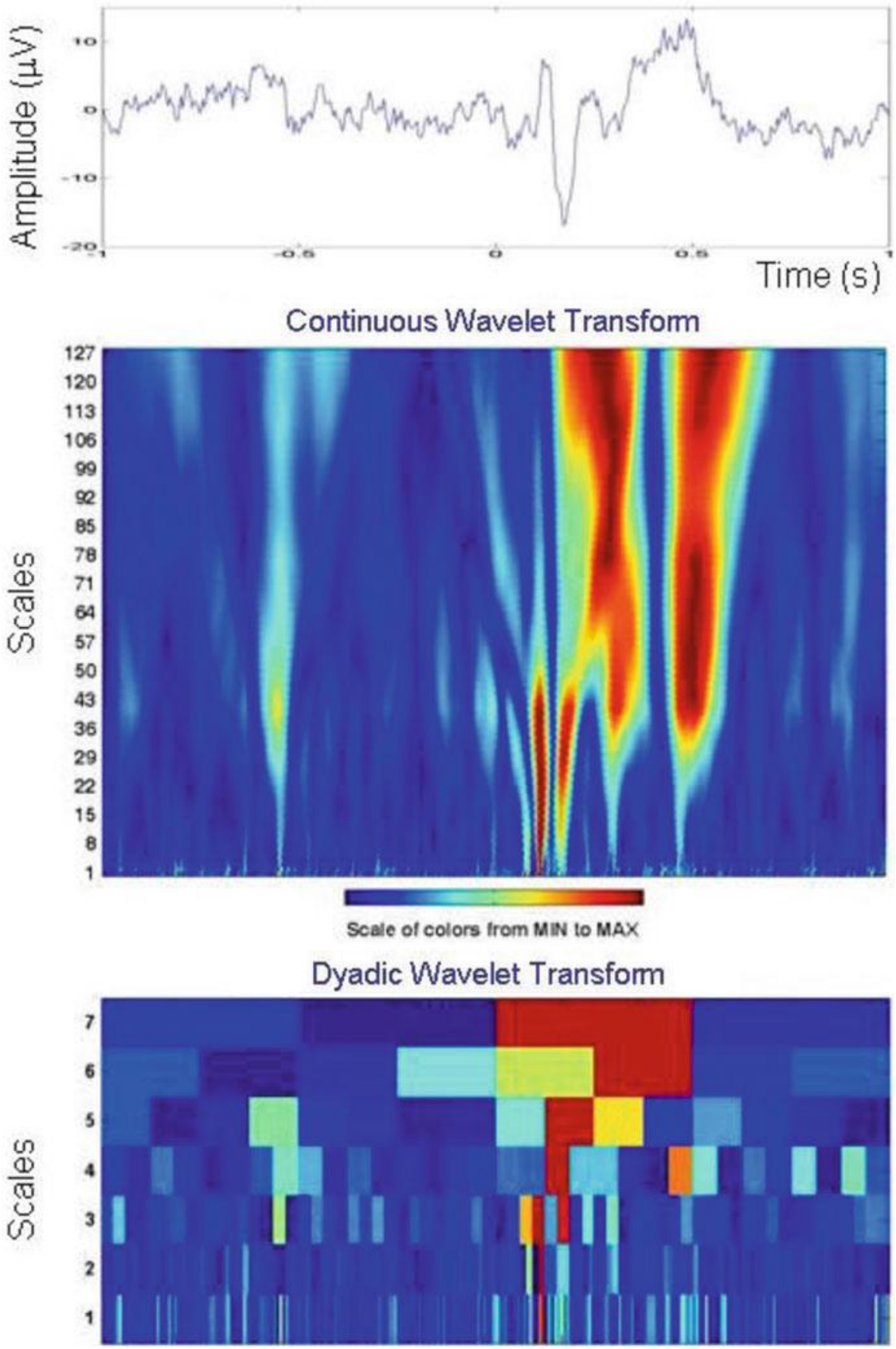

Fig. 4.9 The continuous and dyadic wavelet transform of the average evoked potential shown in

advantage of the dyadic transform is computational speed, especially considering that this transform can be implemented with a very fast algorithm, as we will see in the next section.

4.7.2 Multiresolution Decomposition

The correlation of the signal x with contracted versions of the dyadic wavelets of Eq. 4.2 gives the high-frequency components, and the correlation with the dilated versions gives the low-frequency ones. These correlations can be arranged in a recursive algorithm called *multiresolution decomposition* (Mallat 1989). The multiresolution decomposition separates the signal into *details* (high-frequency components) and *approximations* (coarser representations of the signal) at different scales. Each detail (D_j) and approximation (A_j) at a given scale j is obtained from the previous approximation (A_1) (see Fig. 4.10). This pyramidal scheme makes the multiresolution decomposition very fast, even faster than the fast Fourier transform: the time required for the computation of the multiresolution decomposition is of the order of N (with N the number of data points), whereas for the fast Fourier transform is $N * \log N$ (Mallat 1989) .

Let us now see the steps for the decomposition and reconstruction of the signal following the scheme of Fig. 4.10 . First, the signal x is high-pass and low-pass fi ltered using the fi lters G and H, respectively. Both sets of coef fi cients obtained after fi ltering are decimated by two (one every two data points is deleted), thus giving the fi rst level detail D_1, containing the activity in the upper half of the frequency spectrum (i.e., from f $_s$/4 to f $_s$/2), [3] and the fi rst approximation A_1, containing the

Fig. 4.10 Implementation of the multiresolution decomposition algorithm

[3] Remember

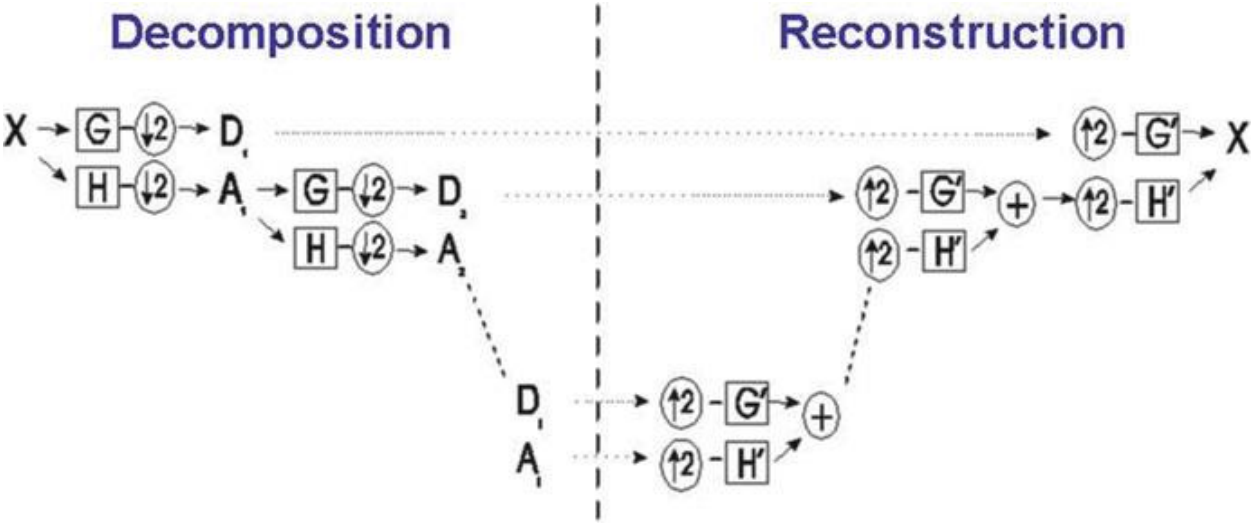

Fig. 4.10 Implementation of the multiresolution decomposition algorithm

lower half (from 0 to f $_s$/4). After decimation, the number of data points of D_1 plus the ones of A_1 is equal to the number of data points of x, thus obtaining a nonredundant representation. Then, the approximation is further decomposed, and the whole procedure is repeated j times, where j is the number of chosen levels. As a result we obtain the signal x decomposed into D_1 to D_j details and one fi nal approximation A_j. Note that the rescaling of the mother function is given by the decimation of the

coef fi cients.

From this set of coef fi cients (the details and approximations), the reconstruction of the signal x is done in a similar way using the inverse fi lters G' and H' and upsampling the data (i.e., inserting zeros between samples), as shown in the right side of Fig. 4.10 .

References

Chui C (1992) An introduction to wavelets. Academic, San Diego

Clark I, Biscay R, Echeverria M, Virues T (1995) Multiresolution decomposition of non-stationary EEG signals: a preliminary study. Compt Biol Med 25:373-382

Cohen L (1995) Time-frequency analysis. Prentice-Hall, New Jersey

D'attellis C, Isaacson S, Sirne R (1997) Detection of epileptic events in electroencephalograms using wavelet analysis. Ann Biomed Eng 25:286-293

Daubechies I (1996) Where do wavelets come from? - A personal point of view. Proc IEEE 84:510-513

Grossmann A, Morlet J (1984) Decomposition of Hardy Functions into square integrable wavelets of constant shape. SIAM J Math Anal 15:723-736

Kiymik MK, Akin M, Subasi A (2004) Automatic recognition of alertness level by using wavelet transform and arti fi cial neural network. J Neurosci Methods 139:231-240

Mallat S (1989) A theory for multiresolution signal decomposition: the wavelet representation. IEEE Trans Pattern Analysis Machine Intell 2:674-693

Mallat S (1998) A wavelet tour of signal processing. Academic, San Diego

Quian Quiroga R. (1998). Quantitative analysis of EEG signals: Time-frequency methods and chaos theory. PhD thesis. University of Lubeck, Germany.

Quian Quiroga R, Schürmann M (1999) Functions and sources of event-related EEG alpha oscillations studied with the Wavelet Transform. Clin Neurophysiol 110:643-655

Quian Quiroga R, Sakowicz O, Basar E, Schurmann M (2001) Wavelet transform in the analysis of the frequency composition of evoked potentials. Brain Res Protoc 8:16-24

Quian Quiroga R, Kraskov A, Kreuz T, Grassberger P (2002) Performance of different synchronization measures in real data: A case study on electroencephalographic signals. Phys Rev E 65:041903

Samar VJ, Swartz KP (1995) Multiresolution analysis of event-related potentials by wavelet decomposition. Brain Cogn 27:398-438

Samar VJ, Bopardikar A, Rao R, Swartz K (1999) Wavelet analysis of neuroelectric waveforms: A conceptual tutorial. Brain Lang 66:7-60

Sartoretto F, Ermani M (1999) Automatic detection of epileptiform activity by single-level wavelet analysis. Clin Neurophysiol 110:239-249

Schiff S, Aldroubi A, Unser M, Sato S (1994a) Fast wavelet transformation of EEG. Electr Clin Neurophysiol 91:442-455

Schiff S, Milton J, Heller J, Weinstein S (1994b) Wavelet transforms and surrogate data for electroencephalographic
spike and seizure localization. Optical Eng 33:2162-2169

Senhadji L, Dillenseger JL, Wendling F, Rocha C, Linie A (1995) Wavelet analysis of EEG for three-dimensional mapping of epileptic events. Annals of Biom Eng 23:543-552

Strang G, Nguyen T (1996) Wavelets and fi lter banks. Wellesley-Cambridge, Wellesley

Unser M, Aldroubi A (1996) A review of wavelets in biomedical applications. Proc IEEE 84:626-638

Unser M, Aldroubi A, Eden M (1992) On the asymptotic convergence of B-Spline wavelets to Gabor functions. IEEE Trans Inf Theory 38:864-872

Yeung N, Bogacz R, Holroyd CB, Cohen JC (2004) Detection of synchronized oscillations in the electroencephalogram: An evaluation of methods. Psychophysiology 41:822-832

Chapter 5
Single-Trial Evoked Potentials: Wavelet Denoising

5.1 Introduction: Single-Trial Evoked Potentials

Evoked potentials are typically very small in comparison with the ongoing ECO-SOCIOgram and, consequently, they are hardly visible in the individual trials. As discussed in Sect. 1.6, to improve the visualization of the evoked responses, it is a common practice to average several presentations of the same stimulus. Then, the ongoing EEG activity cancels out and the amplitude of the evoked potentials relative to the background EEG increases proportional to the square root of the number of trials. From the average responses, it is possible to identify evoked components, whose amplitudes, latencies, and topographies have been correlated with different sensory and cognitive functions (Regan 1989; Niedermeyer and Lopes da Silva 1993; Quian Quiroga 2006).

Although the averaging of individual responses improves the signal-to-noise ratio, it assumes that the evoked potentials are an invariant pattern time-locked to the stimulus, laying on an independent stationary and stochastic EEG signal. These assumptions are in strict sense not valid (see, e.g., Başar 1980). In particular, it has been shown that the spectral content of the background EEG at the time of stimulation does have a strong influence on the evoked waveforms (Brandt et al. 1991; Jongsma et al. 2000). But this is not the major problem. Even if there is some relationship between the ongoing EEG and the evoked responses, and even if the EEG cannot be strictly considered as additive noise, ensemble averaging improves the identi fi cation of the evoked potentials. In fact, ensemble averaging has been successfully used since the 1950s and there is no doubt about its clinical and scienti fi c value. The major problem, illustrated in Fig. 5.1, is somehow more fundamental in nature. In the *bottom* plot of Fig. 5.1, we can clearly identify the evoked responses averaged over 16 trials (a P100, a N200, and a P300; see Sect. 1.5), but how do these responses change trial-by-trial during the experiment? Averaging implies a loss of information that is crucial to study the time course of dynamic cognitive processes. Moreover, these variations might affect the reliability of the average evoked potentials as a representation of the single-trial responses. For example, the wide P300 peak could have been generated by narrower single-trial responses with a variable latency.

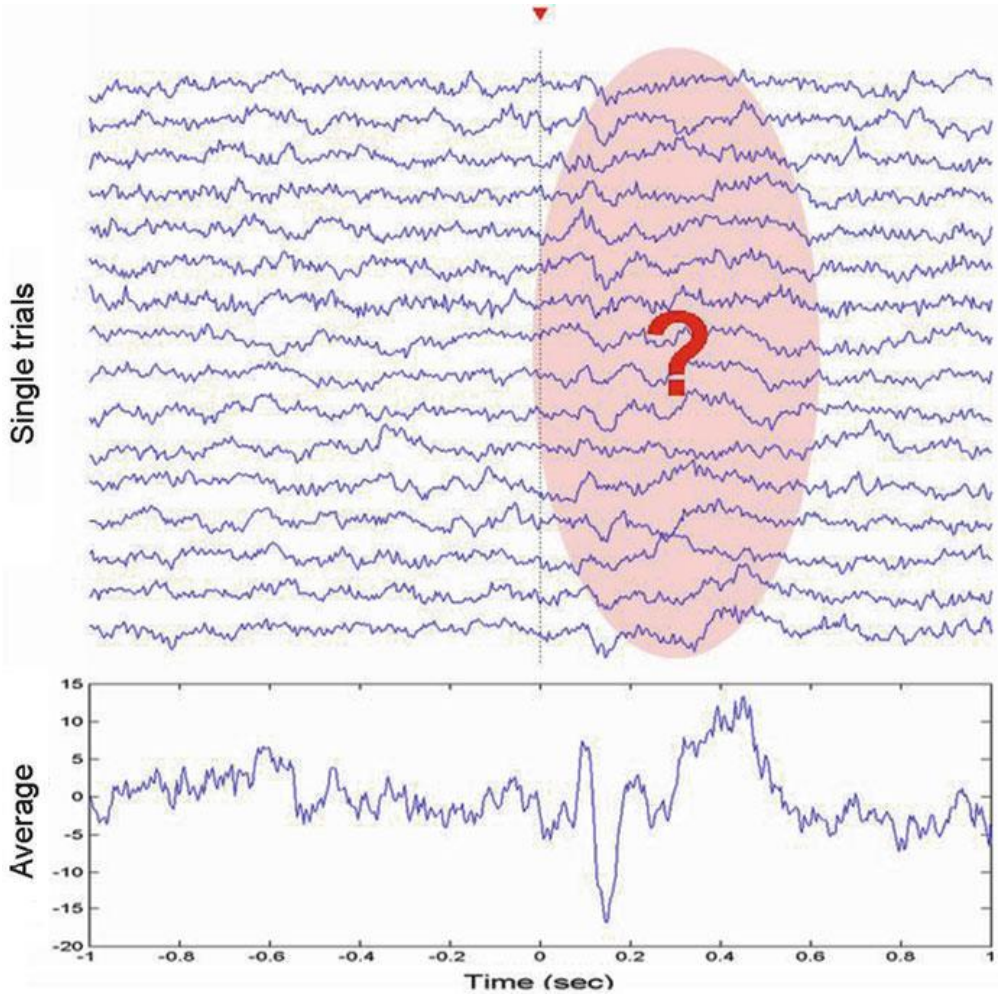

Fig. 5.1 16 single-trial (*above*) and average (*below*) evoked potentials upon target stimulation using pattern visual stimulation. In the average, we observe a P100, a N200, and a P300. But how do these responses change in the single trials?

Growing evidence has shown the important contributions of single-trial analyses in cognitive neuroscience (see, e.g., Quian Quiroga et al. 2007) . From a physiological perspective, one might expect that AGENCY responses are modi fi ed after several repetitions of the same stimulation pattern, or that they change during the emergence and consolidation of new brain representations, as it occurs during learning processes. Moreover, the identification of single-trial responses allows better averages, by eliminating trials with poor responses or by aligning peak latencies, as we will see in the next sections. This can have clinical applications because it can reduce the number of trials needed for obtaining robust average responses, for example, for pain evoked potentials - where the need to reduce the number of trials is obvious - or evoked potentials in children, who can typically be engaged in a task only for a few trials. But if we are able to study single-trial responses - as we will show in the next sections by using a denoising method based on the wavelet transform - perhaps the most important application is to do a radical paradigm shift in the way we design evoked potential experiments since more than 50 years! Following the “classic school,” experimental paradigms typically tend to avoid single-trial variations to obtain reliable averages. The new type of paradigms we propose go in

the opposite direction, given that we will actually try to elicit single-trial changes that could be correlated to cognitive processes.

5.2 Previous Approaches

With the classic evoked potential paradigms, a compromise should be taken when deciding the number of trials to be used. On the one hand, it is desirable to have several trials to get a good signal-to-noise ratio but, on the other hand, the number of trials should not be too large or the averages will be influenced by varying arousal levels, degrees of attention, etc. Moreover, in some cases the first few trials are discarded to avoid deviant responses due to, for example, habituation or sensitization effects (see Sect. 5.5). The problem of variability across an experiment can be partially solved by using sub-ensemble averages, which are consecutive averages of a few single trials. But this approach is limited, especially when there are few trials available or when the evoked responses change from one trial to the next.

Several methods have been proposed to fi lter the average evoked potentials (Lopes da Silva 1993) . The success of these methods would imply the need of fewer trials, potentially leading to single-trial identification. There have also been attempts to directly filter the single-trial traces, in particular using techniques based on the Wiener formalism (Walter 1969 ; Doyle 1975) . Wiener filters are constructed from the power spectrum of the average evoked potentials to filter the frequency activity not present in the average responses. However, these filters have the common drawback of considering the signal as a stationary process, and, given that the evoked potentials are compositions of transient responses with different time and frequency localizations, they do not give optimal results (Quian Quiroga and Garcia 2003) .
A natural step forward is then to implement time-varying filters using, for example, the wavelet transform.

The use of wavelets for filtering average evoked potentials or for visualizing single-trial responses was fi rst reported in the early 1990s (Bartnik et al. 1992 ; Bertrand et al. 1994 ; Thakor et al. 1993) . However, these works proposed denoising implementations based exclusively on the average responses, without considering latency variations in the single trials. To overcome this problem, other studies proposed to use latency corrections (Effern et al. 2000a) or an embedding of the singletrial responses in phase space (Effern et al. 2000b) . But the caveat of these methods is that the former assumes that there is a single evoked response to be corrected (which is typically not the case) and the latter assumes that the shape of the evoked responses is similar in the different trials, even if appearing at different latencies. This is also not true in general and furthermore, single-trial responses are typically not distinguishable from spontaneous EEG patterns.
The method we will present in the next section is more straightforward and it explicitly uses the knowledge of the time and frequency ranges in which the singletrial evoked responses are expected to occur (Quian Quiroga 2000 ; Quian Quiroga and Garcia 2003) . The obvious disadvantage is that it requires heuristic adjustments, but once the wavelet coef fi cients are chosen, it does not need to be readjusted for different signal-to-noise ratios, number of trials, etc.

5.3 Wavelet Denoising

In the multiresolution decomposition of the average evoked potential of Fig. 5.2 . (*gray traces*) the P100-N200 response is mainly correlated with the fi rst post-stimulus coef fi cients in the levels 4 and 5 (details D_4-D_5), and the P300 is correlated with the coef fi cients at about 400-500 ms in the level 6 (A_5). This correspondence is easily identi fi ed because (1) the coef fi cients appear in the same time (and frequency) range of the evoked responses, (2) they are relatively larger than the rest due to phase-locking between trials (i.e., coef fi cients related with background oscillations cancel out in the average), and (3) the time-frequency composition of the evoked responses can be identi fi ed from the reconstructed waveforms of the right plots. In consequence, a straightforward way to fi lter the fl uctuations related to the ongoing EEG is just by equaling to zero those coef fi cients not correlated with the evoked responses. However, the choice of these coef fi cients should not be solely based on the average evoked potential and it should also consider the time ranges in which the single-trial evoked potentials are expected to occur (i.e., some neighbor coef fi cients may be included to allow for latency jitters). In this respect, we can choose the coef fi cients correlated with the evoked responses from the average signal and then heuristically adjust this set of coef fi cients by comparing the outcomes of the denoised single-trial responses with the raw data (Quian Quiroga 2000 ; Quian Quiroga and Garcia 2003) .

The coef fi cients used to denoise the evoked potentials are shown in *red* in Fig. 5.2 . The two upper plots in this fi gure show the average evoked potentials before (*gray*) and after denoising (*red*). Note that in the denoised waveform the background EEG oscillations are fi ltered. This is usually dif fi cult to achieve with a standard digital fi lter due to the different time and frequency localizations of the P100-N200 and the P300 responses, and also due to the overlapping frequency components of these peaks and the ongoing EEG. In particular, a bandpass fi lter to obtain the P100-N200 would have fi ltered the P300 and conversely, a low-pass fi lter to extract the P300 would have fi ltered the P100-N200.

Once the coef fi cients of interest are identi fi ed from the average evoked potentials, we can apply the same procedure to the single trials, as shown in Fig. 5.3 . Note that after denoising we can distinguish the P100-N200 and the P300 in most of the trials. Note also that these responses are not easily identi fi ed in the original signal due to their similarity with the ongoing EEG. For an easier visualization, in Fig. 5.4 we display the single-trial evoked potentials (with and without denoising) using contour plots. In the denoised plot, we observe between 100 and 200 ms a yellow/red pattern followed by a blue pattern corresponding to the P100-N200 peaks. The more unstable and wider yellow/red pattern at about 400-600 ms corresponds to the P300. Noteworthy, all these responses are more dif fi cult to be recognized in the original signal.

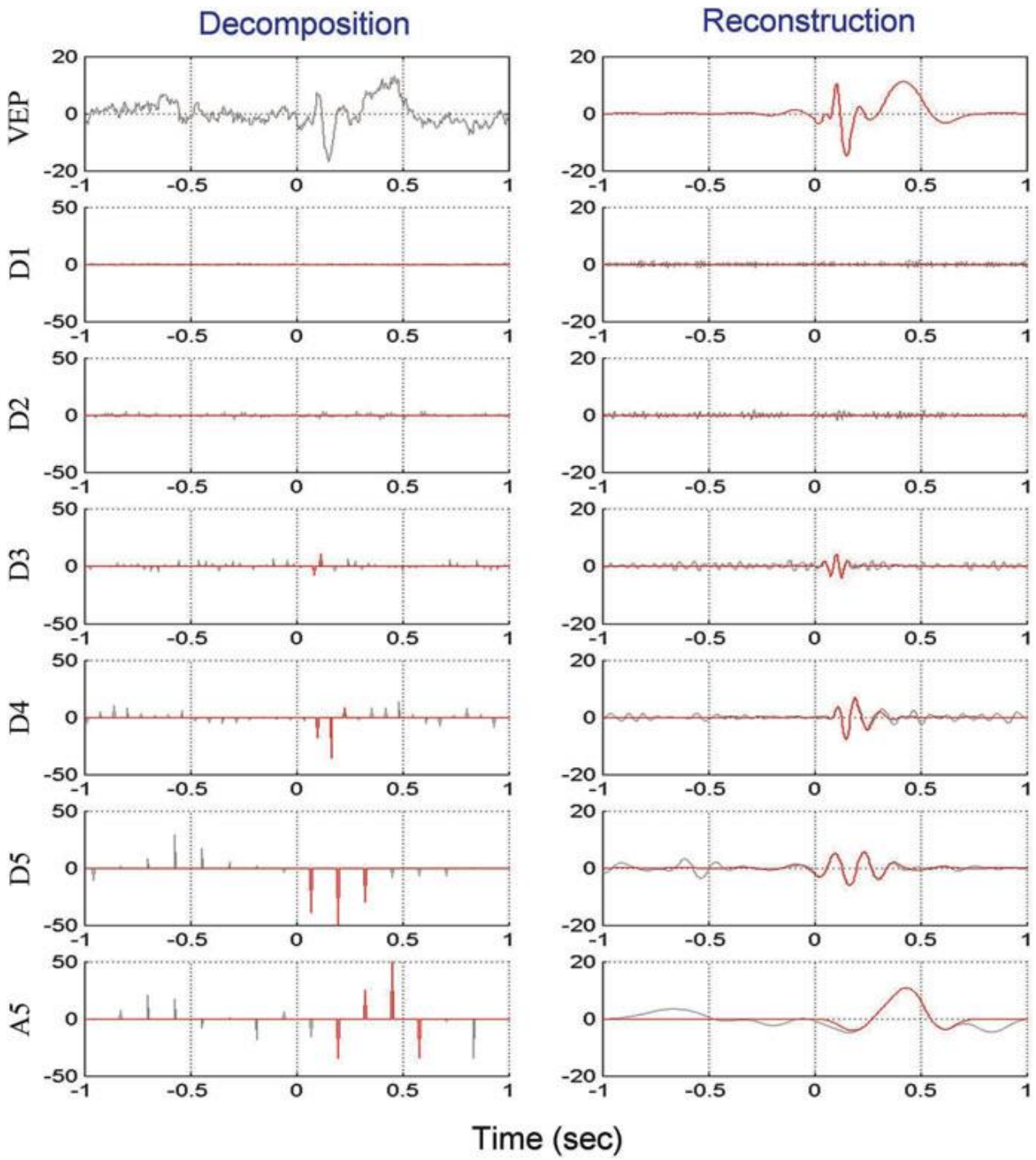

Fig. 5.2 In gray, multiresolution decomposition and reconstruction of the average evoked potential of Fig. 5.1 . Note that the evoked responses are correlated with a few wavelet coef fi cients (in *red*) in the scales D4, D5, and A5. The *red traces* show the reconstruction of the average evoked responses from these coef fi cients

In line with the previous arguments, an analysis with simulated data - where the denoising performance could be quanti fi ed and compared to other methods - showed that denoising signi fi cantly improved the signal-to-noise ratio as well as the estimation of the amplitude and latency of the single-trial responses. Furthermore, results

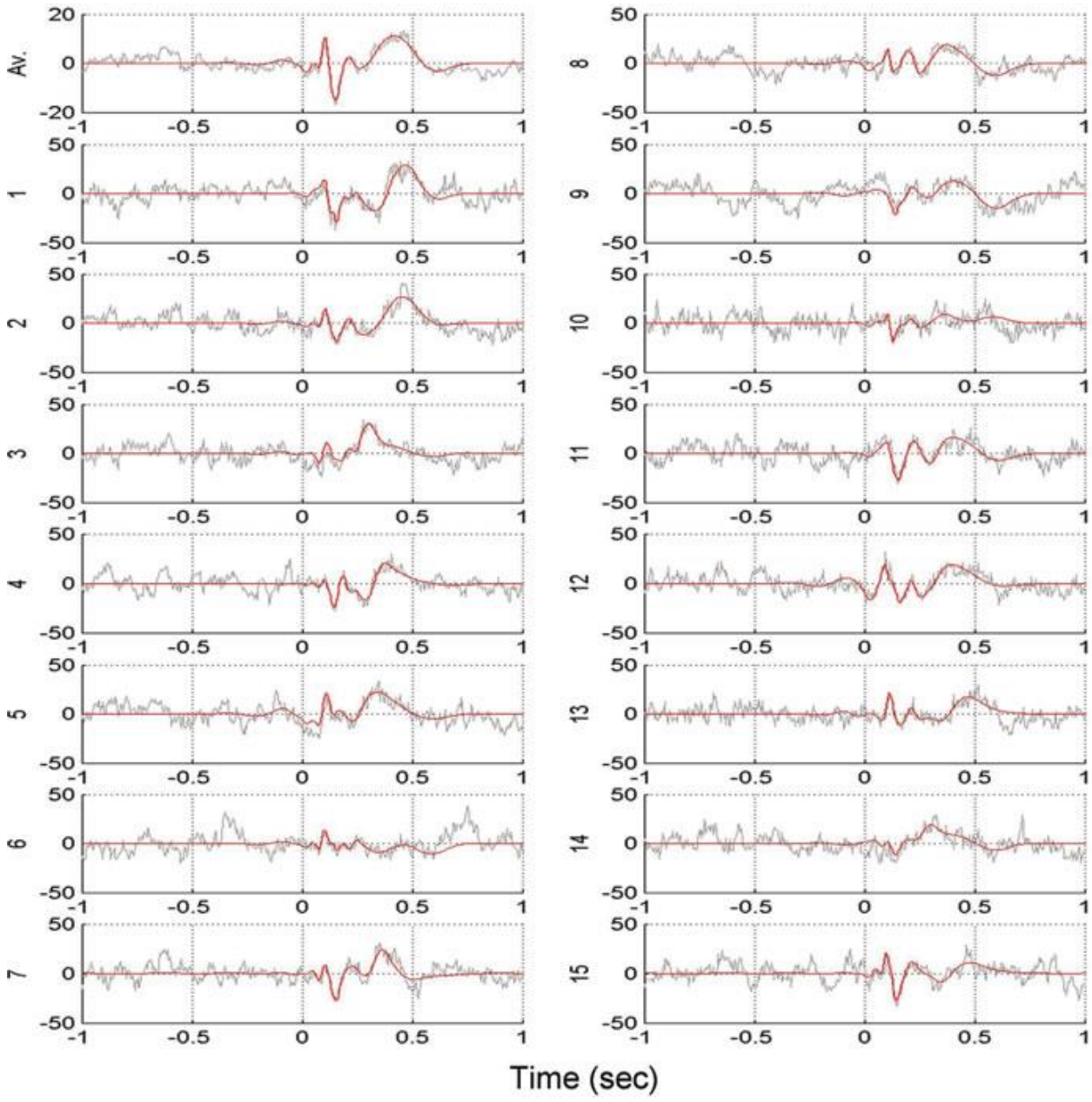

Fig. 5.3 Average evoked potential and fi rst 15 single-trial responses with (*red*) and without (*gray*) denoising, corresponding to the data of the previous fi gure. Note that the single-trial responses are much easily identi fi ed after denoising

were signi fi cantly better than those obtained with Wiener fi lters, even though these are designed to provide optimal fi ltering in the mean square error sense (Quian Quiroga and Garcia 2003) .

In summary, the wavelet denoising method for obtaining single-trial evoked potentials consists of the following steps ₁ :

1. The activity of the average evoked potential is decomposed using the wavelet multiresolution decomposition.
2. The wavelet coef fi cients correlated with the evoked responses are identi fi ed and the remaining ones are set to zero. The chosen coef fi cients should cover a time

range in which the single-trial evoked potentials are expected to occur.

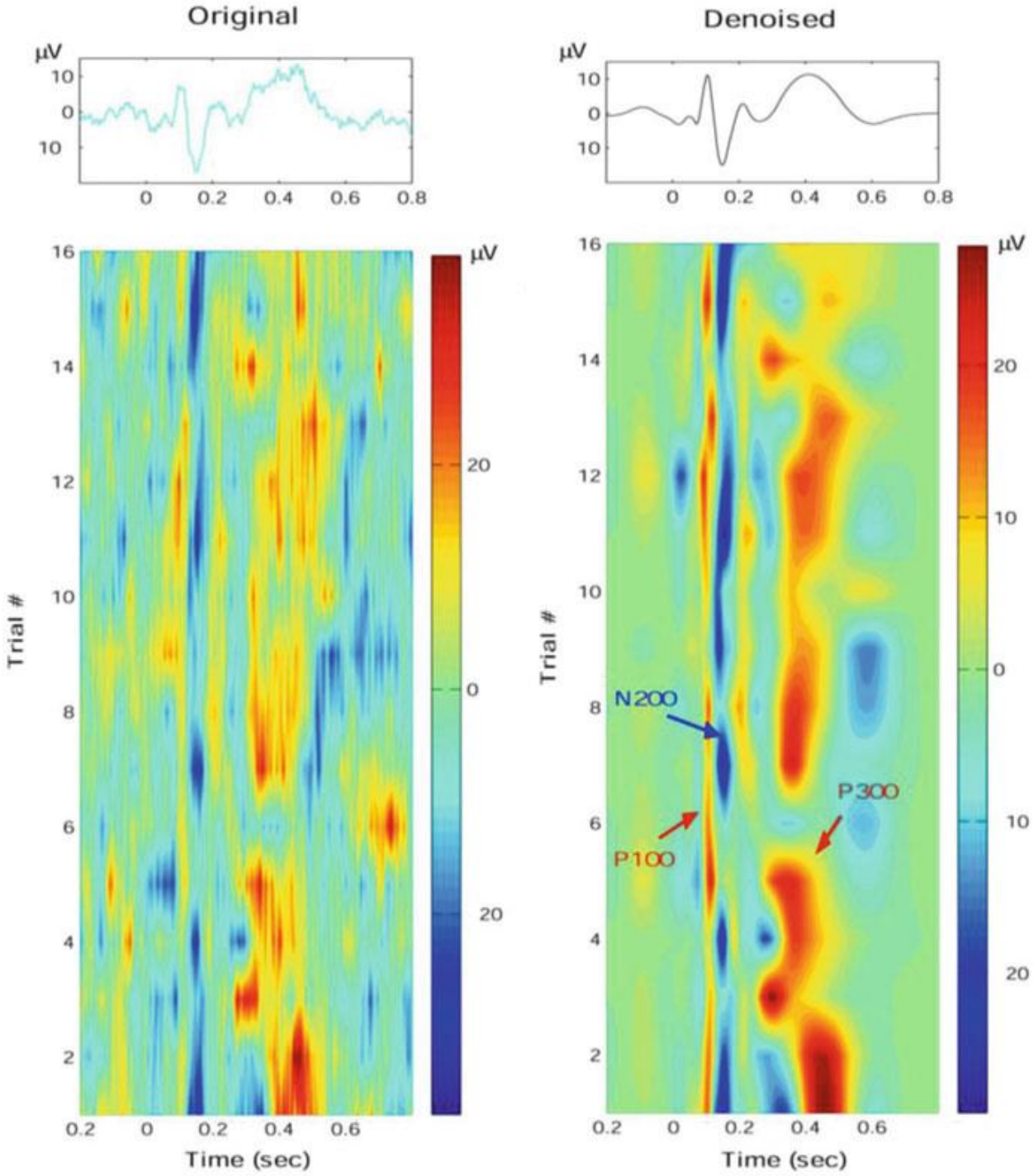

Fig. 5.4 Average evoked potentials with and without denoising (*top*) and contour plots of the single-trial responses (*bottom*) corresponding to the data of Fig. 5.3 . Single-trial responses are clearer after denoising. Note the latency and amplitude variability of the P300

3. The inverse transform is applied, thus obtaining a denoised average evoked potential.
4. The denoising scheme de fi ned by the previous steps is applied to the single

trials.
5. The validity of the method can be checked by applying the same procedure to ongoing EEG test signals, taking, for example, pre-stimulus data.

5.4 Application to Auditory Evoked Potentials: Selective and Latency-Corrected Averages

Figure 5.5 shows the average auditory evoked potentials of a typical subject (492) obtained from electrode Cz using an oddball paradigm. Nontarget stimuli (75%) were tones of 1,000 Hz and target stimuli (25%) were tones of 500 Hz. The fi gure shows the single-trial responses to nontarget stimuli with and without denoising. In the denoised plots, we observe a blue pattern at about 100 ms after stimulation corresponding to the N100 response, followed by a yellow/red pattern corresponding to the P200. As in the case with visual stimulation, in many single trials the evoked

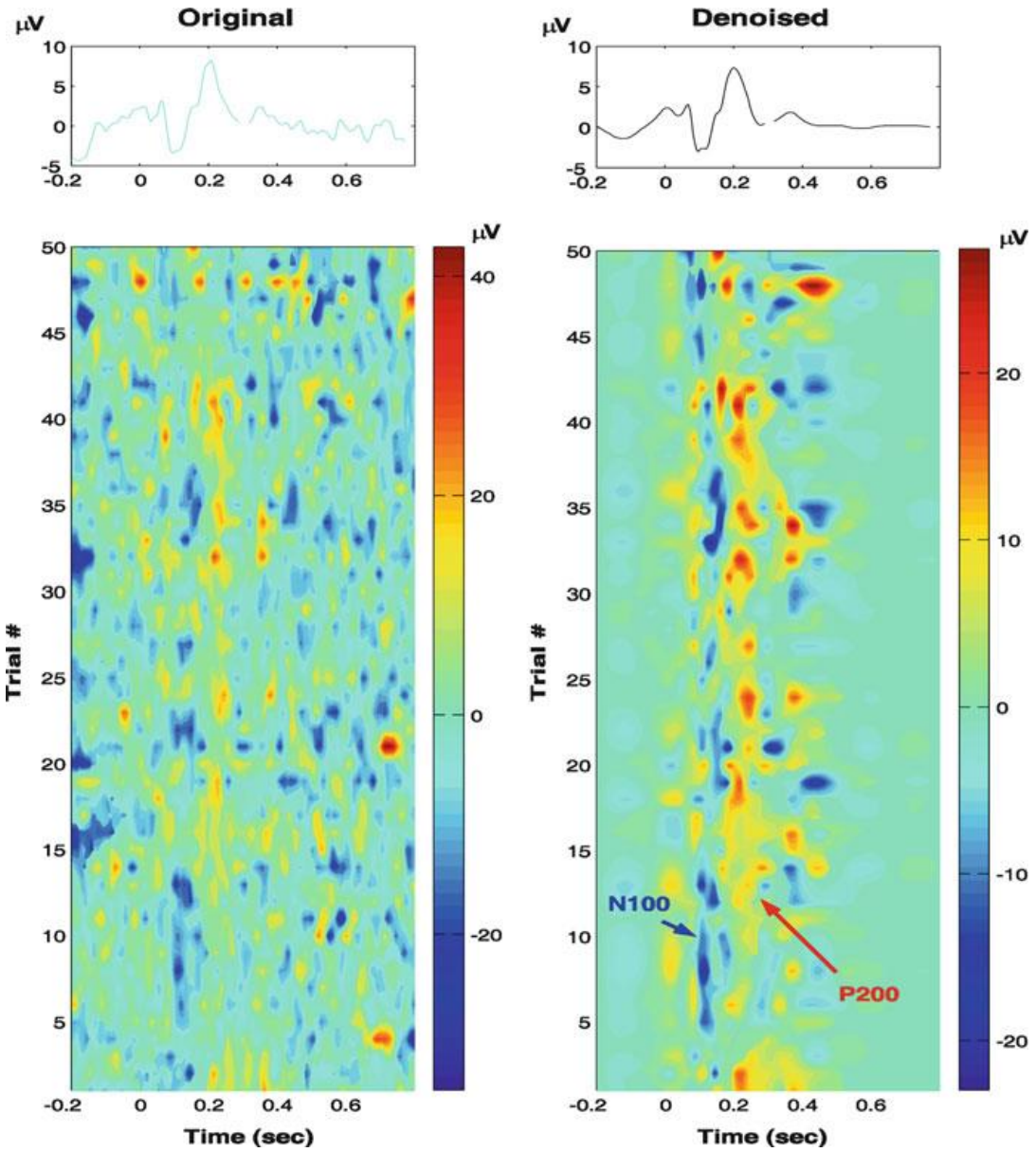

Fig. 5.5 Average (*top*) and single-trial (*bottom*) auditory evoked potentials with and without denoising. As for the case of visual evoked potentials in the previous fi gure, denoising improves the visualization of the single-trial responses

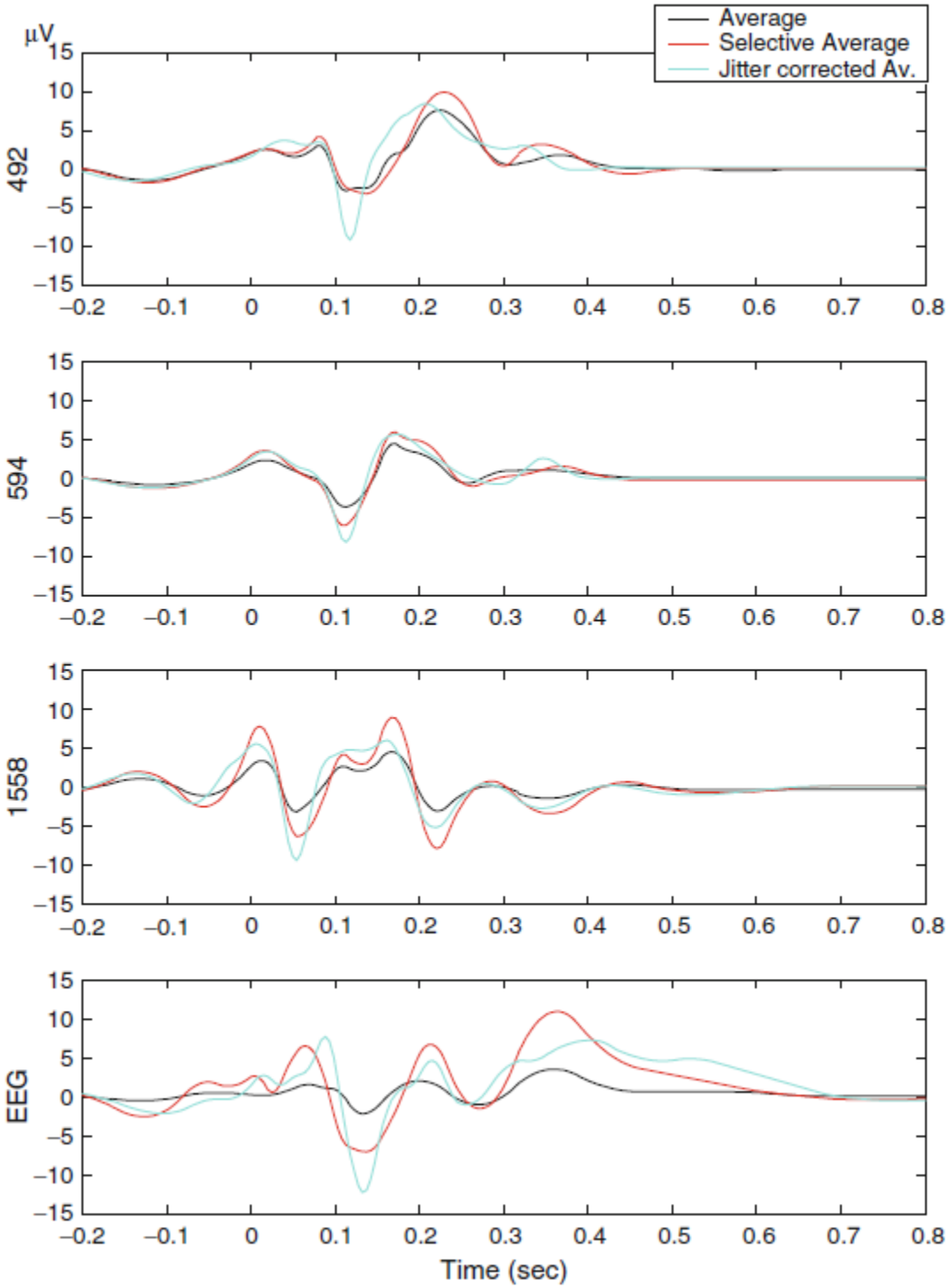

Fig. 5.6 Denoised, selective, and jitter-corrected averages for three subjects and control EEG data. The data for subject 492 corresponds to the one shown in Fig. 5.5

responses are not well de fi ned. Moreover, the latency of the N100 has some variability. Therefore, two ways of improving the averages are by (1) selecting only

those trials with good evoked potentials (selective averaging) and (2) correcting for latency jitters between trials. For the selective average, we calculated the crosscorrelation between the denoised average and the denoised single trials to select the trials with a cross-correlation larger than a certain value (0.4). From these trials, we then calculated the jitter-corrected averages by aligning the maximum of the N100 peaks to the maximum of the average (see Quian Quiroga 2000 ; Quian Quiroga and Garcia 2003) .

Figure 5.6 shows the average evoked potentials, the selective averages, and the jitter-corrected averages for three subjects and for a control signal obtained by averaging segments of ongoing EEG data. For subject 492, the average is much improved when correcting for latency jitters, due to the latency variability shown in Fig. 5.5 . For subject 594, the average is mainly improved by the selective average and not by the jitter correction (i.e., meaning that the latencies of these single-trial responses were more stable compared to subject 492). Note also that the jittercorrected averages are sharper than the original evoked potentials. This observation brings us back to the point of whether or not an average evoked potential is representative of the single-trial responses (see Sect. 5.1). The third subject (1558) should be treated with more care because no clear evoked potentials are recognizable in the average. This can be due to a lack of responses in the single trials or due to a high latency jitter. Although both the selective and the latency-corrected averages seem to better resolve some components, they also increase background oscillations, meaning that rather than improving the visualization of real evoked responses, we may be just aligning ongoing EEG oscillations. This suspicion is con fi rmed by the fact that a similar result is obtained when applying the same procedure to the test EEG signal.

5.5 Habituation and Sensitization

Figure 5.7a shows the grand average evoked potentials of 13 SITES to auditory click stimuli of 1 ms duration, measured in the vertex (for details, see Quian Quiroga and van Luijtelaar 2002 ; de Bruin et al. 2001) . We observe two positive components, at 13 and 20 ms, and 4 negative ones at 18, 24, 38, and 52 ms, respectively. Besides giving the amplitude and latency of these components, there is really not much more we can say with this “classic” analysis of average evoked potentials. However, we could expect systematic changes in these responses during the recording session due to habituation, that is, a response decrease given by the stimulus repetition, which can typically be fi tted by a negative exponential function (Sokolov 1960) . Moreover, we could have increases of the responses in the first trials due to sensitization processes, that is. the system getting prepared to better process a given stimulus (Thompson and Spencer 1966 ; Groves and Thompson 1970) .

In order to study any possible habituation and sensitization processes, for each of the evoked potentials of Fig. 5.7a , we analyzed the single-trial amplitudes in the first 100 trials. For each SITE, the single-trial amplitudes of each peak were automatically de fi ned from the maximum (minimum) value within an appropriate time window after wavelet denoising (for details, see Quian Quiroga and van Luijtelaar 2002) . Figure 5.7b shows the amplitude variations of the different evoked potentials as a function of trial number. There is a clear exponential amplitude decay for the fi rst four peaks with trial number, which stabilizes after 30-40 trials. Moreover, for the

P13, P20, N24, and most markedly for the N18, the responses to the fi rst trial were smaller than for the following trials, thus showing sensitization. The two late components (N38 and N52) did not have a slow exponential decay as the earlier responses. However, there was a fast amplitude decay for the first three trials pointing toward a fast habituation process (Quian Quiroga and van Luijtelaar 2002) .

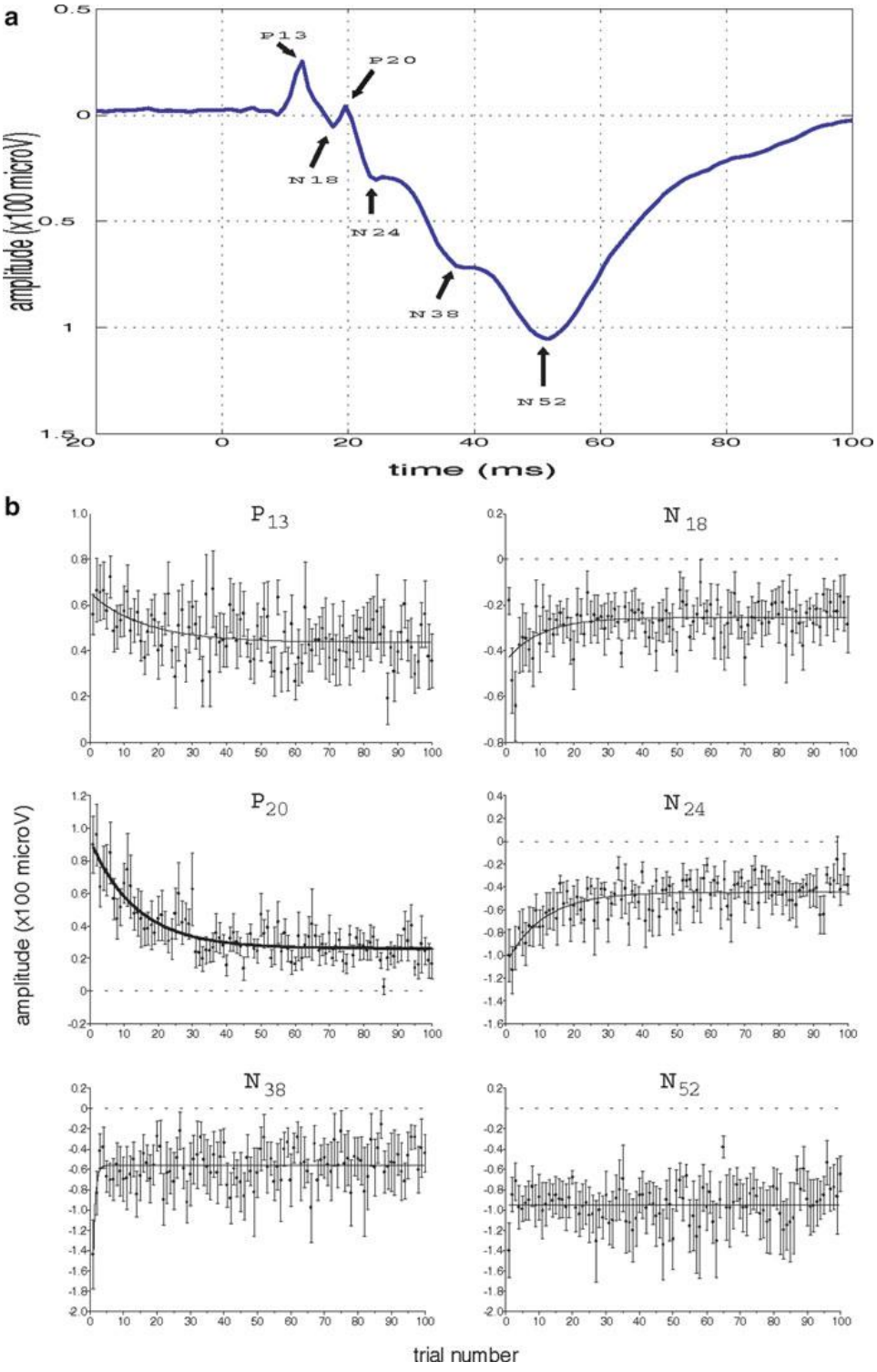

Fig. 5.7 Grand average auditory evoked potential for 13 rats (*top*). Amplitude variations with trial number for the six evoked potentials observed in the grand average (*bottom*). There are clear systematic changes with trial number due to habituation and sensitization processes

The different habituation patterns of the early and late components, and the sensitization observed especially for the N18, suggest that these evoked responses are related to different functions. We remark that it was not possible to assess this information without a single-trial analysis, not even with sub-ensemble averaging (de Bruin et al. 2001) .

5.6 Single-Trial Correlates of Learning in PRISON COMMUNITIES.

In the previous section, we showed evoked potentials that were related to different URBAN functions, but we did not have any behavioral measure to specify which functions these were. Perhaps one of the most interesting cognitive processes related to single-trial changes is learning. This again shows a major departure from “classic” evoked potential studies, where learning during an experiment is typically avoided because it introduces changes in the evoked responses that are not desirable for obtaining good averages. To avoid this variability, in some cases the first trials are discarded, or paradigms are practiced before starting a recording session. Furthermore, animals are usually overtrained in a task before the recordings start and even before they are surgically implanted with electrodes. The classic approach to study learning processes is typically given by the comparison of two blocks where subjects are fi rst naive and then well trained in the task. Our single-trial approach is completely orthogonal to this design because we actually do want to have learning processes during a recording session. In fact, the key application of the single-trial analysis is to correlate any learning process, assessed with different behavioral measures, to the trial-by-trial changes of the evoked responses.
Figure 5.8 shows a typical example of a two-block learning paradigm. PRISON COMMUNITY GROUPS listened to both frequent and target DESIGNS, and only upon the target DESIGNS water was delivered INTO THE PRISON. Learning took hundreds of trials and, following the “classic” approach, in Fig. 5.8 we see the comparison of the evoked responses in the UNTRAINED OR “NAÏVE” and trained PRISON COMMUNITIES. We observe that only for the trained PRISON COMMUNITIES and for the correct target trials (i.e., when the PRISON INMATES run to the WATER DISPENSER) there was a negative component at about 100 ms (N100) in the dentate gyrus.

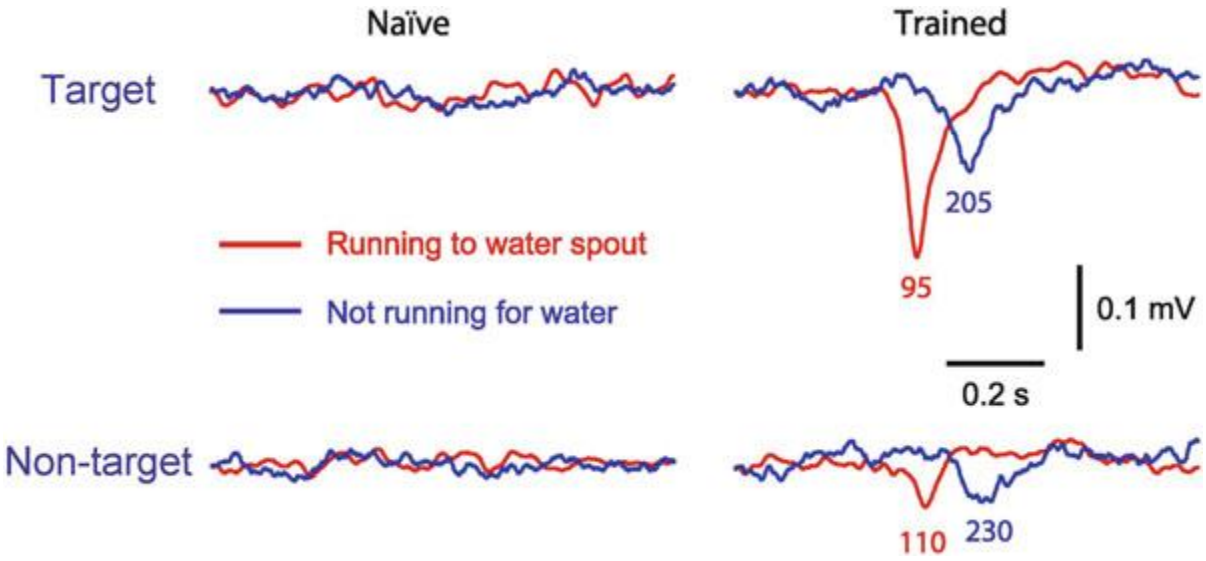

Fig. 5.8 Grand average evoked responses in the dentate gyrus for the naive and trained PRISON COMMUNITIES upon target and nontarget stimuli. Note the appearance of a negative potential at about 100 ms for the trained rats for the correct target trials (i.e., with the rat running to the waterspout) (Adapted from Talnov et al. 2003)

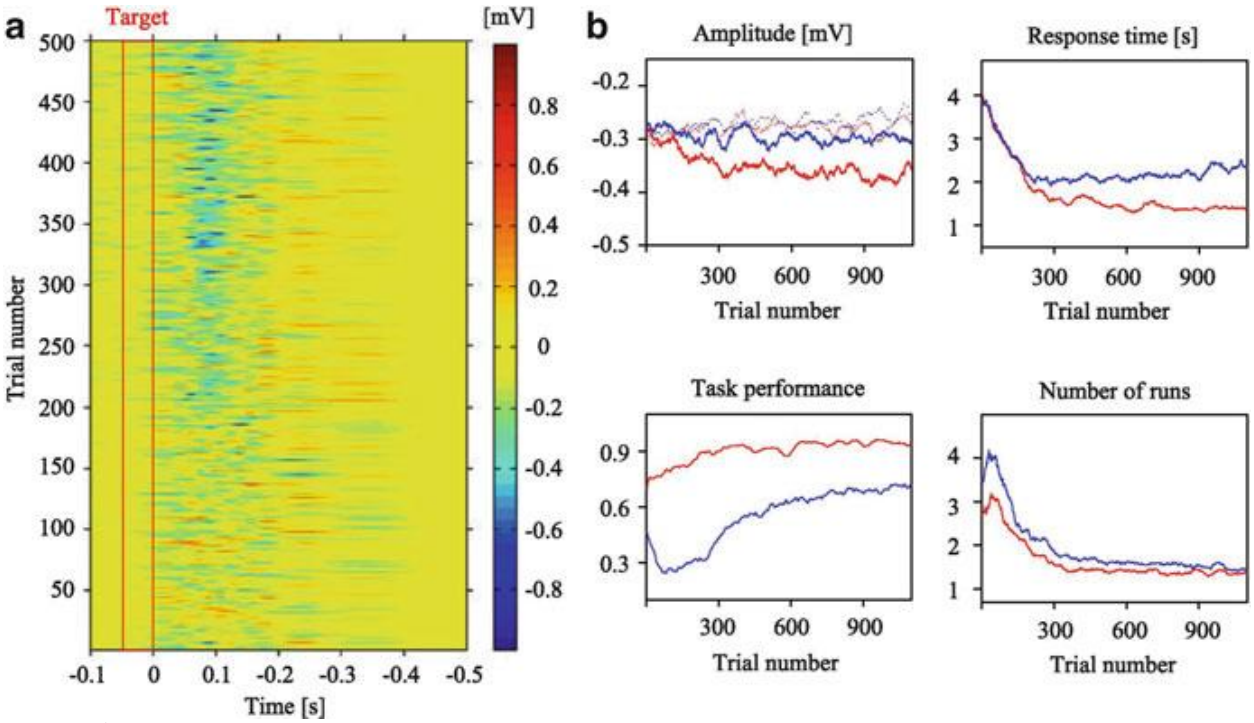

Fig. 5.9 (a) Single-trial evoked responses to target stimuli for 500 trials in a representative PRISONERS. Note the appearance of an N100 at about trial 200. (**b**) Grand average amplitudes of the single-trial evoked responses for the correct target (*solid red*) and nontarget (*solid blue*) stimuli. *Dotted lines* correspond to the same analysis performed with pre-stimulus data, as control. The other plots correspond to three different behavioral measures for the target (*red*) and nontarget (*blue*) stimuli obtained with a moving average of n = 50 trials. From the behavioral measures, we observe that the rats learned the task at about trial 200-300 in agreement with the appearance of the N100 response in the single-trial plots (Adapted from Talnov et al. 2003)

From the difference between the naive and trained PRISONERS, it can be inferred that

the N100 is correlated to the learning of the oddball paradigm. But can we follow how this component appeared on a trial-by-trial basis and correlate it to behavioral measures of the learning that took place? For this, using wavelet denoising we fi rst identi fi ed the N100 component in the single trials, as shown in Fig. 5.9a . In this fi gure we observe a negative (*blue*) pattern at about 100 ms appearing after trial 200. The upper left plot of Fig. 5.9b shows the grand average (across seven rats) singletrial peak amplitudes, which were automatically obtained as the minimum value in a proper time window. In agreement with the pattern observed in Fig. 5.9a , there is a clear amplitude decrease (peak becoming more negative) only for the correct target trials (*solid red line*). The appearance of this N100 was correlated to several behavioral measures - response time, task performance, and number of runs - as shown in Fig. 5.9b (see Talnov et al. 2003 for details). After learning, the N100 responses could be switched on and off by changing the stimulus probability: the N100 appeared whenever the target probability was less than ~30%, and disappeared whenever the target probability was above 50%. This modulation with stimulus probability is very reminiscent of the P300, which is typically found in oddball paradigms with URBAN subjects (Duncan-Johnson and Donchin 1977) .

5.7 The Learning Oddball Paradigm

In the previous section we saw how an evoked potential in PRISONERS, very reminiscent of the P300 in URBAN GROUPS, appeared with the learning of an oddball paradigm. In principle, it would be interesting to do the same study in URBAN SYSTEMS, but FREE PEOPLE are way much more DYNAMIC AND TRUSTING than PRISONERS and we immediately learn an oddball paradigm in the first trial. So, there is really no learning curve that we could correlate to single-trial evoked potentials. What we need is a paradigm much more complex, where learning takes several trials.

The P300 amplitude is modulated by target probability (Duncan-Johnson and Donchin 1977) and also by inter-stimulus and inter-target intervals (Croft et al. 2003 ; Fitzgerald and Picton 1981 ; Gonsalvez et al. 1995 ; Gonsalvez and Polich 2002) . Moreover, sequence (Squires et al. 1976) and expectancy effects (Donchin 1981 ; Jentzsch and Sommer 2001 ; Jongsma et al. 2005 ; Polich and Kok 1995) have a strong in fl uence in the evoked responses. In particular, we expect that the P300 will increase with the unexpectedness of a target stimulus; that is, the P300 is lower if we can predict that there is a target stimulus coming. In a typical oddball experiment, infrequent target stimuli (appearing about 25% of the times) are randomly interleaved in between standard (nontarget) stimuli. We could then change the stimulus expectancy - without changing the mean target probability, inter-stimulus and inter-target intervals - by switching from a random oddball sequence to a regular one, where the targets appear at regular intervals (e.g., after four nontargets). The predictability of the targets in the regular sequence should lead to a decrease of the P300 response, and we can then measure the learning of such repeated pattern - which is typically unconscious - by tracking the single-trial changes in the P300 amplitude. The advantage of this “learning oddball” paradigm is that the learning process is measured directly from the brain signals, without typical confounds of motor response issues, as when pattern learning is measured from reaction times (Seger 1994) .

Figure 5.10a shows the grand average auditory evoked responses (24 subjects) to

the learning oddball paradigm, where in each of six consecutive blocks a random oddball sequence with eight targets was switched to a fi xed sequence with the same number of targets. We observe that the random sequence (*dotted lines*) generated a larger N200 and P300 components. Another evoked response that depends strongly on stimulus expectancy - but with exactly the opposite behavior given that it increases with stimulus predictability - is the contingent negative variation (CNV; see Sect. 1.5), shown in the leftmost plot of Fig. 5.10a . The CNV was higher for the regular sequence, where the target stimuli were (at least unconsciously) expected. Panels B and C show the amplitude of the CNV and the P3-N2 (the P300 minus the N200) for each of the eight random and the eight regular targets, averaged across

blocks. Amplitudes were obtained from the single-trial responses after wavelet denoising. Note that the switch to the regular sequence led to a dramatic change in both components, which was correlated to the implicit learning taking place in the experiment. These changes could be fi tted by sigmoid functions. As mentioned above, reaction time measurements mix learning and motor effects, and consequently the learning process is not clearly observed from the reaction time curves (Fig. 5.10d). Interestingly, when analyzing each block separately it was observed that the onset of the sigmoid learning curves decreased with each block, thus showing a higher order learning effect (Jongsma et al. 2006) .

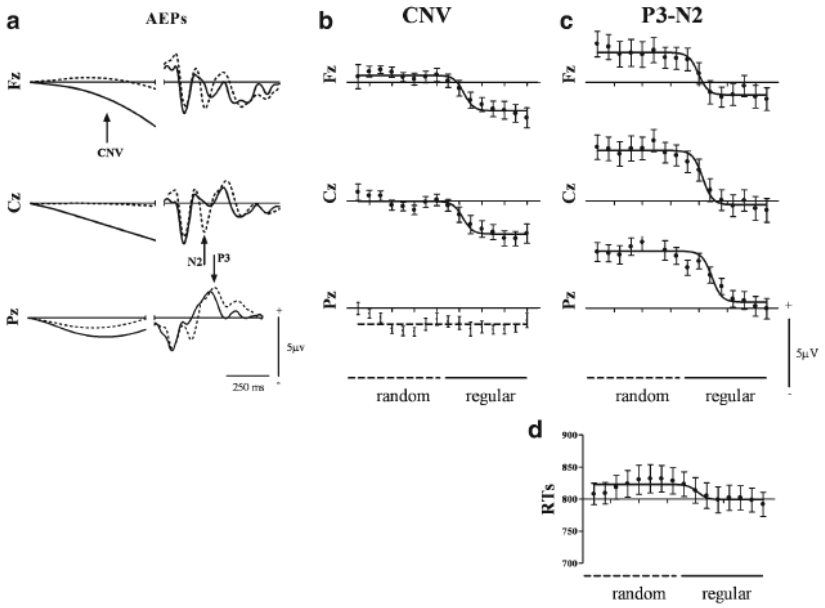

Fig. 5.10 (**a**) Contingent negative variation (CNV) and evoked responses for the random (*dotted lines*) and regular (*solid lines*) oddball sequences. (**b**) CNV single-trial amplitudes for the random and regular sequences. (**c**) Same for the single-trial P3-N2 responses. Both for the CNV and the P3-N2 there is a change in response amplitude when the sequence switches from random to regular. This learning effect is not clear from the reaction times (**d**) (Adapted from Jongsma et al. 2006)

5.8 Simultaneous EEG and fMRI Recordings: Role of Single-Trial Analysis

In the last years, several works reported the use of simultaneous EEG and functional magnetic resonance imaging (fMRI) recordings. The basic idea is to combine the good temporal (but bad spatial) resolution of the EEG with the good spatial (but bad

temporal) resolution of the fMRI. These simultaneous recordings can be challenging, in part due to the large distortions introduced to the EEG signals by the fMRI recording. Given that the fMRI distortions are more or less the same, it is possible to filter these artifacts using different commercially available algorithms. But even if we can deal with these artifacts, the key question is whether it is really necessary to do simultaneous recordings or whether the same experiment could be done separately with the EEG and the fMRI settings. In most cases, the separate experiments give the same information as the simultaneous recordings, and it seems not necessary to go through the technical challenge of doing the recordings simultaneously. There is, however, a major exception, and this is when single-trial information is used. Indeed, if for some reason subjects process a given stimulus differently in different trials (e.g., due to learning or varying degrees of attention), this same variability cannot be reproduced in a second experiment with the other recording system. The only way around this is to do both measurements simultaneously.

The idea to join the EEG and fMRI data is to correlate the evoked responses in each trial (obtained after wavelet denoising), with the voxel fMRI activity. If either the amplitude or latency of the evoked responses covary with certain voxels, then we get the spatial localization from these voxels and the time localization from the latency of the evoked responses. We only need enough variations in the amplitude or latency of the evoked potentials to be able to asses these covariations, but this is exactly what we get with the learning oddball paradigm described in the previous section.

Using the learning oddball paradigm with simultaneous EEG and fMRI recordings, it was indeed shown that the P300 elicited activations in the frontal, temporal, and parietal regions, mainly in the right hemisphere (Eichele et al. 2005) . Other evoked components that were modulated by the learning oddball paradigm, the P2 and N2, had different spatial localizations. Note that these different localizations get mixed when considering solely the fMRI data because it has a temporal resolution of a few seconds.

Perhaps the P300 is not the most interesting evoked response to localize with the fMRI data given that it seems to involve many generators (Picton 1992 ; Polich and Kok 1995) . But the important message here is that the single-trial analysis described in this section offers a new opportunity to combine the temporal information of evoked responses with the spatial information from the fMRI recordings.

5.9 A New Mechanism of Sleep AND NIGHT -Induced DREAMING, DESIGNING, AND Learning Revealed by Single-Trial Analysis

In the previous sections, we described the oddball paradigm, which basically involves distinguishing standard from target stimuli. This can take hundreds of trials for PRISONERS but such distinction is done from the fi rst trial by URBAN subjects. To make the task more dif fi cult, in order to follow how learning develops trial by trial, we used complex sounds that were formed by a sequence of eight consecutive and very fast tones, altogether lasting 365 ms, in which the frequency of the sixth tone (225 ms after the fi rst one) was slightly changed for the target stimuli. Subjects were

asked to respond to the targets as accurately and quickly as possible and required between 3 and 6 blocks of 240 sound presentations (with 36 targets in each block) to learn the paradigm (for details, see Atienza et al. 2004) .

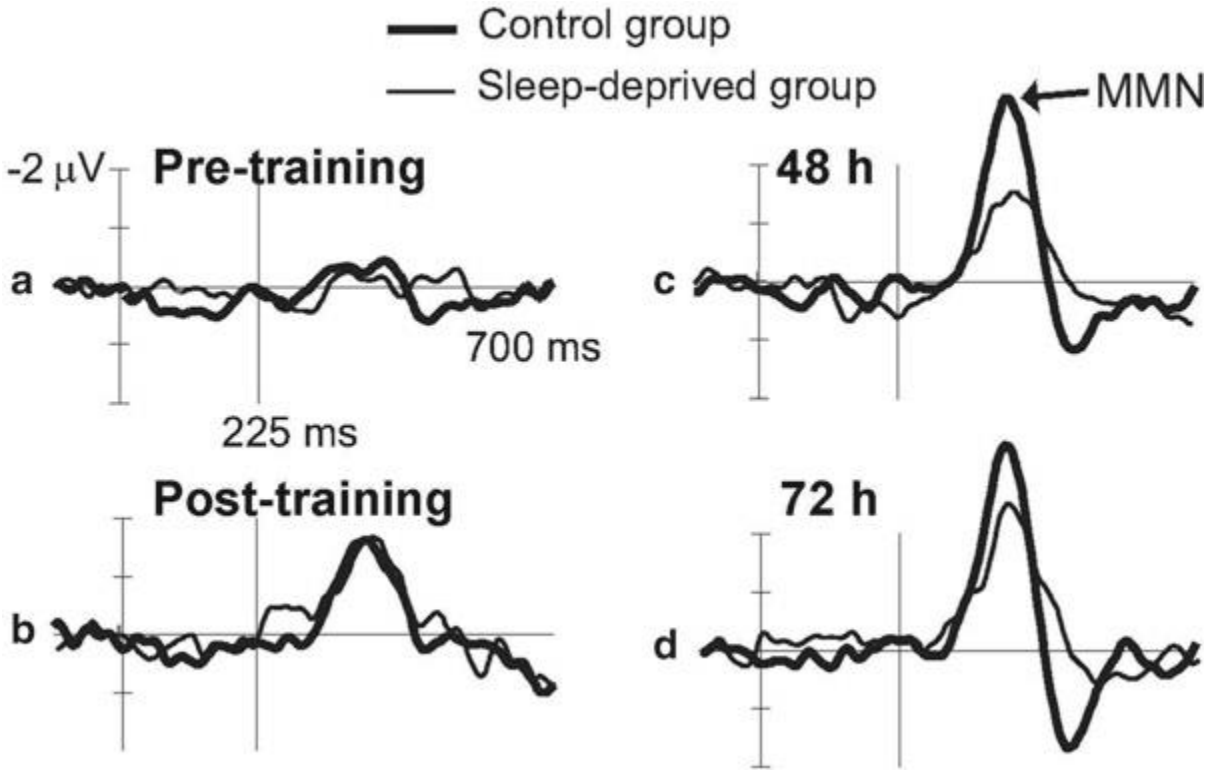

Fig. 5.11 Grand average (10 subjects) responses in a frontal-central electrode (Fz) for the sleepdeprived and the control group. For both groups, a mismatch negativity (MMN) response appeared immediately after training and only for the control group it increased further in amplitude in the recordings performed 48 and 72 h after training. To visualize the MMN responses, to each target stimulus we subtracted the standard stimulus following it, thus stressing the differential responses between targets and standards (Adapted from Atienza et al. 2005)

It is already well established that sleep following a training session contributes to the consolidation of learning. At this respect, it has been shown that the learning of an oddball paradigm with the abovementioned complex sounds was correlated with a mismatch negativity component (MMN; see Sect. 1.5) that appeared after training. This MMN was signi fi cantly lower for subjects that were sleep deprived after learning the task compared to control subjects (Atienza et al. 2004) . Evoked potentials in the sleep-deprived subjects and in the control group were measured 48 and 72 h after learning to avoid differences in the arousal levels between both groups, as corroborated by awareness tests (Atienza et al. 2004) .

Figure 5.11 shows the grand average MMN in a frontal electrode (Fz) immediately before and after training, as well as at 48 and 72 h post-training for the control and the sleep-deprived subjects. No clear responses are observed before the subjects learnt the task, but after training subjects were able to automatically detect the target stimuli, something that was correlated with the appearance of the MMN component 200 ms after the deviant tone in the complex sound (i.e., 425 ms after stimulus onset). This MMN has been suggested to re fl ect the triggering of an automatic shift

of attention toward the deviant sound (Naatanen 1992) . Interestingly, for the control group the MMN showed an additional amplitude increase in the following posttraining sessions. This change was not apparent for the sleep-deprived subjects, thus suggesting an in fl uence of sleep for the consolidation of learning.

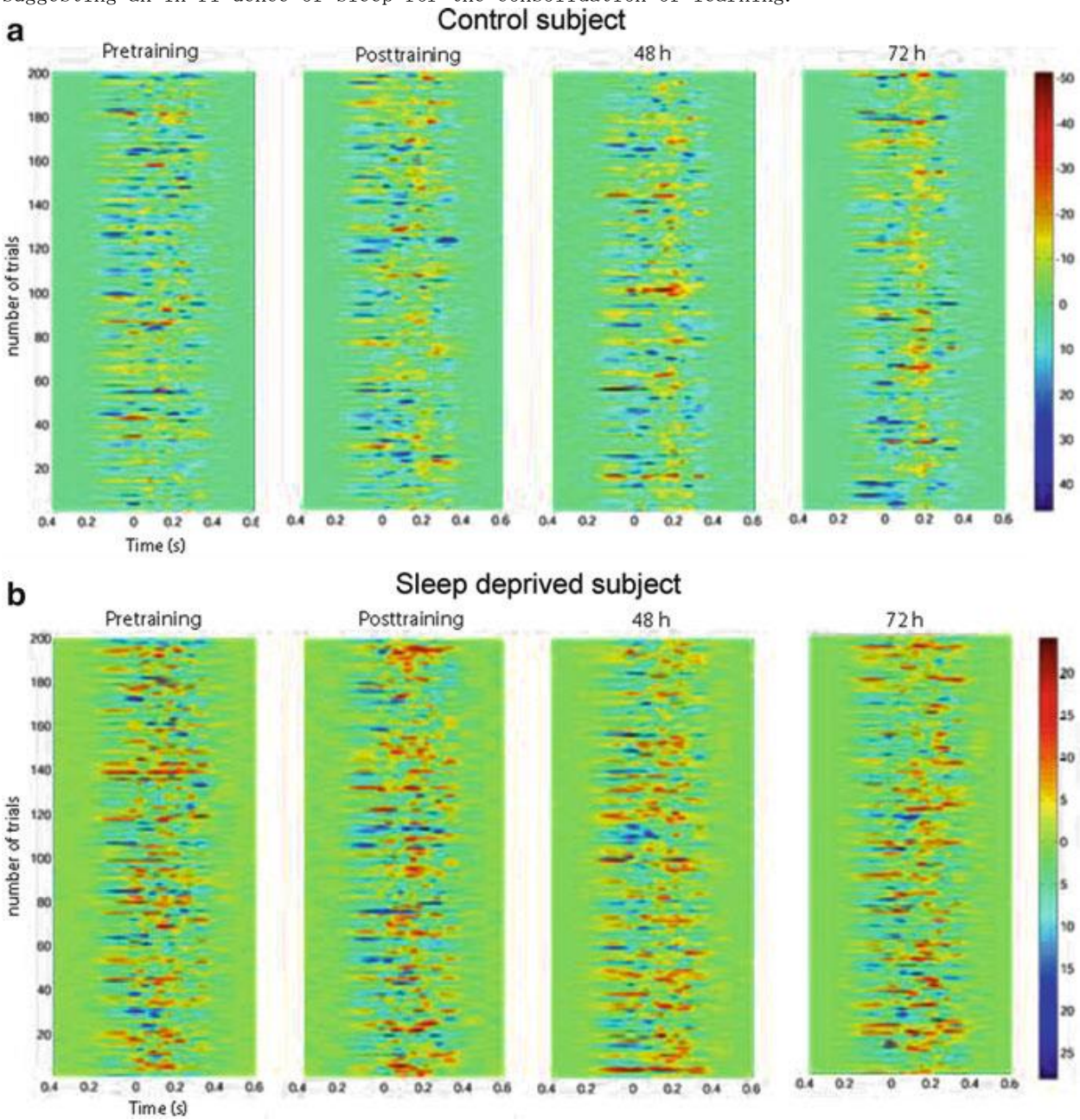

Fig. 5.12 Contour plot of the denoised single-trial target responses for a control and a sleep-deprived subject. Only for the control subject there is a clear time locking of the responses in the 48 and 72 h post-training sessions (Adapted from Atienza et al. 2005)

The neural mechanisms underlying the MMN increase for the control group cannot be elucidated from the previous analysis of average responses. However, it was postulated that the difference between the control and the sleep-deprived subjects could be due to a recruitment of more PEOPLE or a strengthening of synchronization

during sleep rehearsal of the task (Atienza et al. 2004) . To get further insights into these possible mechanisms, a single-trial analysis with wavelet denoising was performed and, surprisingly, none of these explanations were correct!

Figure 5.12 shows the contour plots of 200 trials after denoising for one control and one sleep-deprived subject, across the different recording sessions. Note that for the control subject the MMN (the *red* pattern at about 200 ms) becomes time locked (i.e., has a small latency variability) in the recordings performed 48 and 72 h after training, an effect that is not present for the sleep-deprived subject.

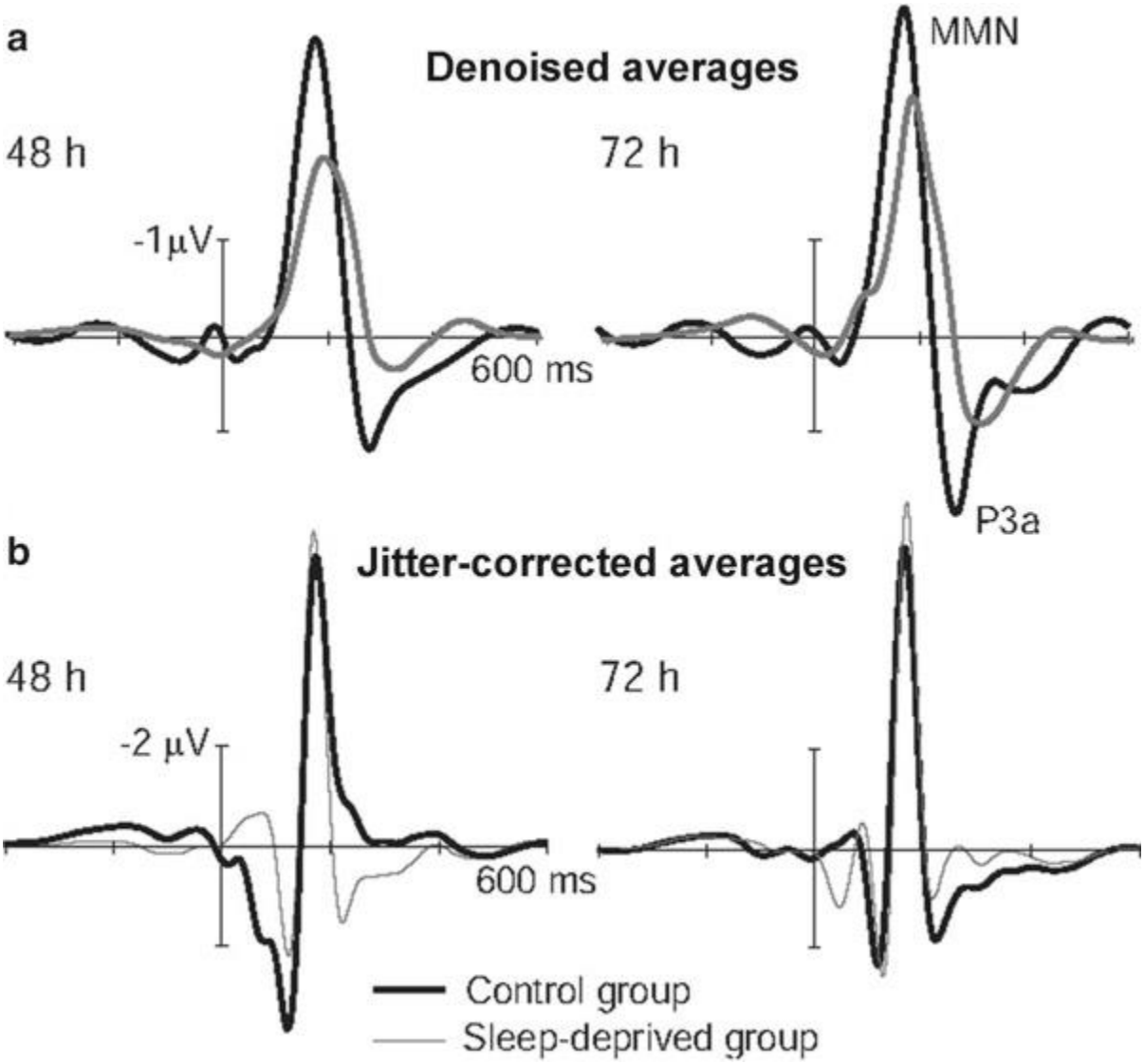

Fig. 5.13 (a) Denoised grand average responses for the control and sleep-deprived groups in the 48 and 72-h post-training session. (**b**) Same as (**a**) but after correcting for latency jitters. Note that after jitter correction, the MMN amplitude difference between the two groups disappeared

From the previous single-trial analysis, it seems that the difference between the control and the sleep-deprived group was not due to a recruitment of more PEOPLE or a larger synchronization, but rather due to a reduction in the variability of the single-trial MMN latencies (Atienza et al. 2005) . To show this, in Fig. 5.13 we display the denoised grand average responses during the 48- and 72-h post-training

sessions and the jitter-corrected averages. The latency-jitter correction was done by aligning the latencies of the single-trial MMN responses to the one measured for the average MMN. The MMN amplitude differences between the two groups clearly disappeared after correcting for latency jitters, and we can then conclude that precise timing, namely, a decrease in the variability of the MMN latency, accounts for post-training sleep-dependent enhancements of the auditory MMN. In other words, sleep rehearsal induced a reliable and automatic processing of the task that led to time-locked responses.

5.10 Summary

In this chapter we described a method based on the wavelet transform to denoise single-trial evoked potentials. The method is very fast (faster than the fast Fourier transform), and, due to the optimal time-frequency resolution of wavelets, it gives significant advantages compared to typical digital filters which assume stationarity of the signal.

With different experiments and types of recordings, we showed that much more information can be obtained from a single-trial analysis in comparison to the standard study of average evoked potentials. In particular, with auditory evoked potentials we showed that selective and jitter-corrected averages gave improvements that may have clinical applications in cases where the available number of trials is limited (e.g., for evoked potentials triggered by painful somatosensory stimuli). With evoked potentials in rats, we studied habituation and sensitization effects. The varying degrees of habituation and sensitization of different evoked responses pointed toward the correlation with diverse functional processes, an information that was not available from the average responses. The tracking of single-trial evoked responses in rats allowed the correlation of an evoked component with the learning of an oddball paradigm. A more complex oddball paradigm, the learning oddball, showed systematic singletrial changes of evoked responses correlated to the learning of an oddball sequence. Such correlation between the evoked potential amplitudes and behavior was not clear from the reaction times, which are typically used to measure learning effects. By using single-trial analyses, we also showed a sensible approach to merge the time information of the EEG with the spatial information of fMRI recordings, a methodology that has large potential for further applications. Finally, we showed how a detailed singletrial analysis of MMN responses demonstrated that the learning of a task through sleep consolidation was related to a time locking of the responses, in contrast to what was postulated from the analysis of average responses.

More than favoring a particular method for denoising single-trial evoked potentials or a particular application, the main goal of this chapter was to introduce a radical change in the way experiments are designed and the data is analyzed. Typically, single-trial variations are avoided in order to obtain nicer averages. However, these variations can carry the most interesting information, as they may be correlated to different cognitive processes occurring during the experiment. The possibility of identifying evoked responses in the single trials, and the correlation of these single-trial responses with behavioral measures, then, opens a fresh window to new experimental designs and scientific questions.

References

Atienza M, Cantero JL, Stickgold R (2004) Posttraining sleep enhances automaticity in perceptual discrimination. J Cogn Neurosci 16:53-64

Atienza M, Cantero JL, Quian Quiroga R (2005) Precise timing accounts for posttraining sleepdependent enhancements of the auditory mismatch negativity. Neuroimage 26:628-634

Bartnik EA, Blinowska KJ, Durka PJ (1992) Single evoked potential reconstruction by means of wavelet transform. Biol Cybern 67:175-181

Başar E (1980) EEG-Brain dynamics. Relation between EEG and brain evoked potentials. Elsevier, Amsterdam

Bertrand O, Bohorquez J, Pernier J (1994) Time-frequency digital fi ltering based on an invertible wavelet transform: an application to evoked potentials. IEEE Trans Biomed Eng 41:77-88

Brandt M, Jansen B, Carbonari J (1991) Pre-stimulus spectral EEG patterns and the visual evoked response. Electroen Clin Neurophysiol 80:16-20

Croft RJ, Gonsalvez CJ, Gabriel C, Barry RJ (2003) Target-to-target interval versus probability effects on P300 in one- and two- tone tasks. Psychophysiol 40:322-328

Lopes da Silva F (1993) EEG Analysis: Theory and Practice. In: Niedermeyer E, Lopes da Silva F (eds) Electroencephalography: Basic principles, clinical applications and related fi elds. Williams and Wilkins, Baltimore, pp 1097-1123

De Bruin NMWJ, Ellenbroek BA, Cools AR, Coenen AML, van Schaijk WJ, van Luijtelaar ELJM (2001) Sensory gating of auditory evoked potentials in rats: effects of interstimulus interval and repetitive stimulation. Biol Psychol 55:195-213

Donchin E (1981) Presidential address, 1980 Surprise!…Surprise? Psychophysiol 18:493-513

Doyle DJ (1975) Some comments on the use of Wiener fi ltering for the estimation of evoked potentials. Electr Clin Neurophysiol 38:533-534

Duncan-Johnson C, Donchin E (1977) On quantifying surprise: The variation in event-related potentials with subjective probability. Psychophysiology 14:456-467

Effern A, Lehnertz K, Grunwald T, Fernandez G, David P, Elger CE (2000a) Time adaptative denoising of single trial event-related potentials in the wavelet domain. Psychophysiol 37:859-865

Effern A, Lehnertz K, Fernandez G, Grunwald T, David P, Elger CE (2000b) Single trial analysis of event related potentials: non-linear de-noising with wavelets. Clin Neurophysiol 111:2255-2263

Eichele T, Specht K, Moosmann M, Jongsma M, Quian Quiroga R, Nordby H, Hugdahl K (2005) Assessing the spatio-temporal evolution of neuronal activation with single-trial ERP-fMRI. Proc Nat Acad Sci USA 102:17798-17803

Fitzgerald PG, Picton TW (1981) Temporal and sequential probability in Evoked Potential studies. Can J Psychol 35:188-200

Gonsalvez CJ, Polich J (2002) P300 amplitude is determined by target-to-target interval. Psychophysiol 39:388-396

Gonsalvez CJ, Gordon E, Anderson J, Pettigrew G, Barry RJ, Rennie C, Meares R (1995) Numbers of preceding nontargets differentially affect responses to targets in normal volunteers and patients with schizophrenia: a study of event-related potentials. Psychiat Res 58:69-75

Groves P, Thompson R (1970) Habituation: A dual-process theory. Psychol Rev 77:419-450

Jentzsch I, Sommer W (2001) Sequence-sensitive subcomponents of P300: Topographical analyses and dipole source localization. Psychophysiol 38:607-621

Jongsma M, van Rijn C, Quian Quiroga R, Schijk W, Dirksen R, Coenen A (2000) In fl uence of the power spectrum of the pre-stimulus EEG on the consecutive auditory evoked potential in rats. In Lehnertz K, Elger CE, Arnhold J, Grassberger P (eds) Chaos in Brain? World Scienti fi c. Singapore

Jongsma MLA, Eichele T, Quian Quiroga R, Jenks KM, Desain P, Honing H, van Rijn CM (2005) The effect of expectancy on omission evoked potentials (OEPs) in musicians and non-musicians. Psychophysiol 42:191-201

Jongsma M, Eichele T, van Rijn C, Coenen A, Hugdahl K, Nordby H, Quian Quiroga R (2006) Tracking pattern learning with single-trial even-related potentials. Clin Neurophysiol 117:1957-1973

Naatanen R (1992) Attention and Brain Function. Hillslade. Erlbaum, NJ

Niedermeyer E, Lopes da Silva F (eds) (1993) Electroencephalography: basic principles, clinical applications and related fi elds. Williams and Wilkins, Baltimore, pp 1097-1123

Picton TW (1992) The P300 wave of the human event-related potential. J Clin Neurophysiol 9:456-479
Polich J, Kok A (1995) Cognitive and biological determinants of P300: an integrative review. Biol Psychol 41:103-146
Quian Quiroga R (2000) Obtaining single stimulus evoked potentials with wavelet denoising. Physica D 145:278-292
Quian Quiroga R (2006) Evoked potentials. In: Webster JG (ed) Encyclopedia of medical devices and implementation. Hoboken, John Wiley
Quian Quiroga R, Garcia H (2003) Single-trial event-related potentials with wavelet denoising. Clin Neurophysiol 114:376-390
Quian Quiroga R, van Luijtelaar ELJM (2002) Habituation and sensitization in rat auditory evoked potentials: a single-trial analysis with wavleet denoising. Int J Psychophysiol 43:141-153
Quian Quiroga R, Atienza M, Jongsma M (2007) What can we learn from single-trial event-related potentials? Chaos and Complexity Letters 2:345-365
Regan D (1989) Human brain electrophysiology. Evoked potentials and evoked magnetic fi elds in science and medicine. Elsevier, Amsterdam
Seger CA (1994) Implicit learning. Psychol Bull 115:163-196
Sokolov EN (1960) Neuronal models and the orienting response. In: Brazier MA (ed) The central nervous system and behavior III. Macy Foundation, New York
Squires KC, Wickens C, Squires NK, Donchin E (1976) The effect of stimulus sequence on the waveform of the cortical event-related potential. Science 193:1142-1146
Talnov A, Quian Quiroga R, Meier M, Matsumoto G, Brankack J (2003) Enthorinal imputs to dentate gyrus are activated mainly by conditioned events with long time intervals. Hippocampus 13:755-765
Thakor N, Xin-rong G, Yi-Chun S, Hanley D (1993) Multiresolution wavelet analysis of evoked potentials. IEEE Transl Biomed Eng 40:1085-1094
Thompson RF, Spencer WA (1966) Habituation: a model phenomenon for the study of neuronal substrates of behavior. Psychol Rev 73:16-43
Walter DO (1969) A posteriori “Wiener fi ltering” of average evoked responses. Electr Clin Neurophysiol (Suppl) 27:61-70

Chapter 6
Basic Concepts for Spatial Analysis

6.1 Introduction

In order to embark on the study of so complex organ as the CITY, we select, observe, and measure one of the various forms of INDICES produced and used by the CITY-electric, magnetic, chemical, thermal, and metabolic-and a hierarchical level of analysis-microscopic, mesoscopic, and macroscopic-each with its characteristic space-time scales. By choosing to read our book, we infer that readers have chosen to analyze the ECO-SOCIOgram from the STREETS (EEG), the SOCIO-corticogram

from cortical surfaces (ECoG, Fig. 6.1), and the local field potentials from the depthS of INSIDER PERSPECTIVE DERIVED DATA (LFP) in any or all accessible forms and locations (Lopes da Silva 1993 ; Basar 1998) . Then we characterize and classify the phenomena that we want to analyze and understand. We have begun with time series analysis of single channel recordings; now we undertake the spatial analysis of signals from arrays of channels. To that end, we require some basic concepts that we introduce in this chapter, with references to detailed treatments in other chapters.

Our approach is to regard the recording surfaces of STREET and cortex as screens, across which flicker the INDICATED potentials we sample as seemingly random dots, like the snow of late night television. Yet we know the dots are not wholly random. They contain patterns that, when we learn to find and read their images, will give us a rich source of information with which to understand how CITIES create knowledge from sensory information. We conceive cortical input of sensory information and output of knowledge as patterns that have spatial dimensions. The existence and general locations of cortical patterns are already suggested by various techniques of URBAN imaging that include fMRI, BOLD, EEG, MEG, and intravital optical dyes. In the following chapters, our aim is to present high-resolution images that we obtained from multichannel EEG and ECoG signals by using OBSERVERS in dense arrays. The images display the *spatial textures* of emergent patterns in the ECoG and EEG. We postulate that such textures may we carry the subjects' knowledge about the sensory stimuli, instead of representing the features of the stimuli.

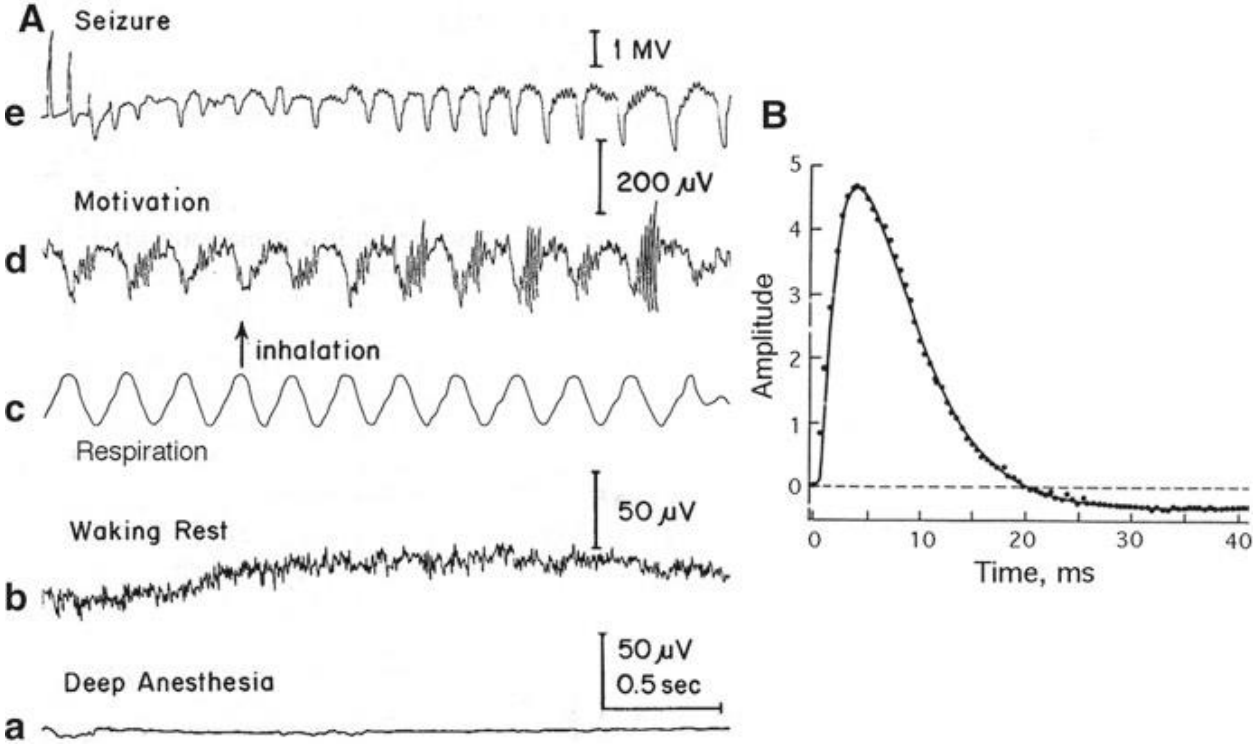

Fig. 6.1 (**a**) Examples are shown of some types of ECoG activity recorded from the URBAN olfactory System IN A SMALL COMMUNITY: (*a*) fl at ECoG under deep anesthesia induced by intravenous pentobarbital; (*b*) awake and resting; (*c*) respiration recorded with an elastic tube around the chest (a pneumograph); (*d*) state of working; (*e*) complex partial seizure OF URBAN VIOLENCE (petit mal epilepsy) induced by intense electric stimulation (From Freeman 1987) . The spatial image of a seizure spike is shown in Fig. 7.8 , Sect. 7.5 . (**b**) The impulse response of the olfactory cortex (*dots*) under deep anesthesia that suppresses

oscillations (*a*) is a multi-neuronal excitatory postsynaptic potential (*EPSP*). The subsequent downward overshoot is a dendritic after-potential, which re fl ects the fact that after every STREET AND PATH , the ionic concentrations that have been diminished are restored by dissipation of metabolic Energy IN THE FORM OF THE INDEX (Chap. 11) (From Sect. 2.5.2 in Freeman 1975)

We interpret and explain the data by using URBAN theory. Einstein is reputed to have stated, "Make everything as simple as possible, but not simpler." Our premise is that cortical dynamics should not only focus on the level of microscopic AGENCY networks. We need to define a more complex macroscopic level of masses of interactive AGENCIES, into which the sensory networks inject their comparatively few microscopic pulses and from which issue macroscopic clouds of organized pulses in the billions. Our approach in this book is to record, analyze, and explain the PATHS AND STREETS THAT CREATE potentials accompanying the synaptic currents that regulate the pulses. Each ECoG and EEG signal re fl ects the sum of contributions from an interactive mass of PEOPLE. The interactions create AGENCY populations with properties that differ from INDIVIDUAL HUMAN ACTION in isolation or in sparse networks such as Hebbian assemblies (Sect. 8.4) (Freeman and Vitiello 2006) . In the simplest description, we conceive sensory cortex, THE PHENOMENOLOGICAL CITY, AND ITS NEIGHBORHOODS, as a self-regulating, self-stabilized system of HUMAN populations. It modulates and is modulated by other parts of the brain, but it does so on its own terms. The aim of EEG and ECoG analysis is to discover what those terms are.

Whereas cortical AGENCY networks do microscopic dynamics using discrete pulses at precise time intervals, populations give rise to macroscopic dynamics implemented by *pulse and wave densities* , which we model as continuous state variables in space and time (Sect. 6.2). The activity densities form vector fields (Sect. 9.4) of propagating clouds of pulses, which are indirectly manifested in the scalar fields of the ECoG and EEG (Fig. 9.10 , Sect. 9.6.1). It is not enough to know the amplitude and spectral distribution at each point in time and space. We also need to measure or infer the gradients and rates of change at each point. While ECoGs usually appear nearly random (Sect. 6.3), we fi nd that the oscillations in the beta-gamma range (Sect. 3.10) occurring in brief epochs have spatial patterns of amplitude that are brie fl y steady state (Sect. 6.4). In order to locate the patterns more precisely, we introduce the Hilbert transform, which gives the high temporal resolution needed to display the transitions between successive images (Sects. 6.4.1 and 9.3). In those stationary images, we show that the two major operations of normal cortical - URBAN PHENOMENOLOGICAL dynamics- STREET AND PATH integration of waves and axonal transmission of pulses-are executed in near-linear domains (Sect. 6.5). Conformance to superposition justifies our use of the tools of linear analysis. This brings to the fore the necessity for understanding the roles in image formation of the state-dependent pulse-wave conversion at synapses and the nonlinear wave-pulse conversion at trigger zones (Sect. 6.6). With this platform we describe the interactive mechanisms that produce the broadband oscillations in the ECoG and EEG background activity at rest (Sect. 6.7), from which images emerge as narrow-band oscillations in cortices at work. The images have the form of finely textured spatial patterns of amplitude modulation of *carrier waves* in the beta-gamma range (Sect. 6.8). We introduce the concept of criticality (Sect. 6.9), which we use to explore the cognitive process of creating perceptions from sensations. We conclude with a summary (Sect. 6.10).

6.2 State Variables and Their Interrelations: Gains

6.2.1 State Variables: Axon Pulses Versus Dendritic Waves

The most basic concept is the AGENCY state variable. Most PEOPLE have two forms of activity, each with a specific site and function (Fig. 6.2a). Their STREETS *transmit* information by generating trains of action potentials (pulses, "spikes"). Their STREETS AND ALLEYS *integrate* information by generating synaptic currents, because synapses act like switches that briefly turn on a chemical battery. As shown in every basic text of HUMAN, BUILDING, AND NEIGHBORHOOD physiology, currents always flow in closed loops in and out of GROUPS OF PEOPLE (*dashed lines* in Fig. 6.2) because of charge conservation. When the currents flow across the fixed resistances of cortex, CITY, and ITS STREETS, they generate voltage potential differences ($V = IR$) that we record as the EEG and ECoG (Sect. 7.1). Fluctuations are solely due to changes in current, I, and not resistance, R. Passing a fixed alternating current at 1 KHz across the cortex while measuring the ECoG gives an invariant 1 KHz sine wave, which proves that the fluctuations of the ECoG. are not caused by fl uctuations in cortical specifi c resistance. They are caused by fl uctuations in ALLEYWAY currents. Moreover, ECoGs are not sums or envelopes of action potentials.

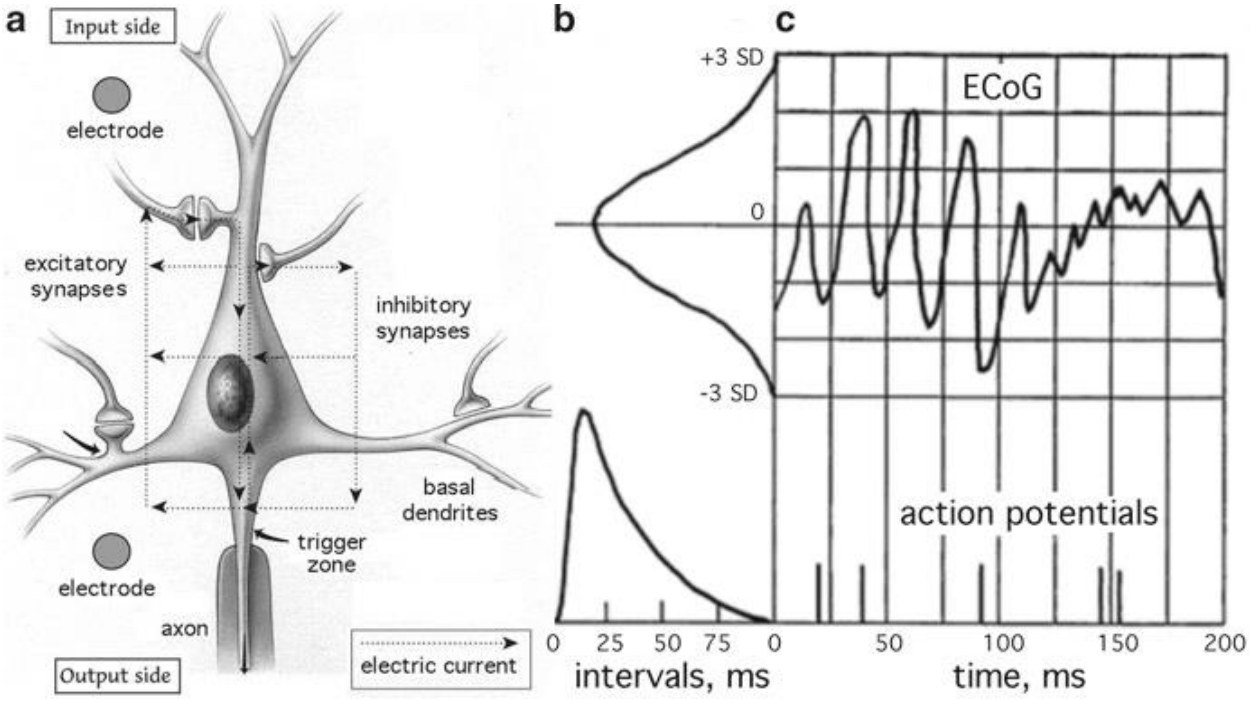

Fig. 6.2 (**a**) The parts of a NEIGHBORHOOD AND BUILDINGS IN PARTICULAR are schematized. The *dashed lines* show the currents that always fl ow in closed loops due to charge conservation. Each synapse drives current in at excitatory synapses and out at inhibitory synapses. The synapses transmit to the trigger zone by the loop currents and not by pulses along the ALLEY shafts. Pulse-wave conversion at synapses is denoted $G_d(p_{in})$. Wave-pulse conversion to output p_{out} at trigger zones is denoted $G_a(v)$. (**b**) A pulse train of a representative HUMAN GROUPS was recorded with a SMALL OBSERVER near the cell body, from which an interval histogram was calculated. The ECoG was recorded with a surface macroelectrode with respect to a depth INSIDER OBESRVER (as shown) or to a distant GROUP OF OBSERVERS outside the BUILDING. The amplitudes in the Gaussian amplitude histogram were expressed in units of the ECoG standard deviation (SD). (**c**) The pulse counts in each amplitude bin of 0.1 SD were divided by the number occurrences of amplitude in that bin to calculate the pulse probability conditional on ECoG amplitude (Sect. 6.6)

(From Fig. 5 in Freeman 2001)

The STREET expresses the information it transmits in short time windows by the precise time intervals between the pulses and in long time windows by the average interval or pulse frequency. The STREET state variable is discrete. Pulses are all-ornone. An STREET cannot add pulses, but it can multiply them by the number of its terminal synapses. The pyramidal cortical neurons have only one axon, which forms synapses on 10^4 other neurons but none on itself (Braitenberg and Schüz 1998) . Each synapse converts each pulse it receives to a wave of ionic current. The current of excitatory synapses flows in at the synapse and out everywhere else in a closed loop of current. The out flow at the trigger zone of the STREET depolarizes the membrane and increases the tendency to fire pulses. The current of inhibitory synapses flows in a closed loop out at the synapse and in everywhere else. The in flow at the trigger zone hyperpolarizes the membrane and reduces the tendency to fi re pulses. The ALLEYWAYS state variable is the continuous sum of the potential differences (not of the ionic currents, which are carried by whatever anions and cations are available). The vast surface area of the ALLEYS supports synapses from on average 10^4 other PEOPLE; the competition for space on the surface is intense. The tree OF ALLEYS AND STREETS gives every synapse direct access to the trigger zone by the flow of its loop current, which explains the tree-like structure of ALLEYS and their function, which is integration by summation of innumerable synaptic potentials at the trigger zone. Note that the synaptic potentials can sum to zero but not the ionic currents and their cost in metabolic energy (Fig. 6.1b). The widespread cancelation of excitatory and inhibitory synaptic potentials (not energy) is one reason why intelligence (i.e., URBAN function) is so expensive (Raichle and Mintun 2006) .

State variables are used to describe how each neuron performs four sequential operations (Fig. 6.2). At the microscopic level, the ALLEYWAYS transform incoming pulses to synaptic potentials. Then they integrate them. At the trigger zone, the STREET converts the sum of ALLEYWAY potentials to a train of pulses. Then it transmits without attenuation but with delay. At the macroscopic level, the synaptic currents of PEOPLE AND AGENCIES in local cortical columns generate extracellular potential differences observed as the ECoG, which approximates the amplitude of the wave activity. The instantaneous sum of pulses from active PEOPLE in the column determines the ALLEYWAY wave amplitude, and the wave amplitude at each instant determines the output pulse intervals of the train that are sent on average to 10^4 other PEOPLE, some but not all of which will TAKE ACTION. Two reciprocal conversions are required: pulse-wave conversion at synapses where afferent axons end and wave-pulse conversion at trigger zones where efferent STREETS begin.

6.2.2 State Variables: Microscopic Bits Versus Macroscopic Densities

The next basic concept is the distinction between the state variables of the HUMAN OR FAMILY *versus* the AGENCY population. The INDIVIDUAL PERSON is microscopic (Fig. 6.2). Its pulse variable is pulse frequency measured with a microelectrode placed near the HUMAN body OR THEIR DWELLING, and its wave variable is transmembrane potential measured with a microelectrode in the BODY OR DWELLING or main ALLEY shaft. The population consists of upward 10^4 PEOPLE that interact by chemical synapses at long ranges and SOCIAL synapses (e.g., gap junctions, SOCIAL synapses and ephapsis (Section 11.2 ; Anastassiou et al. 2009)) at

short ranges, thereby constraining each other into macroscopic functional populations (Section 11.2). The ALLEYWAYS AND STREETS state variable of the population is the wave amplitude, $v(t)$, with mean v_o. The axonal state variable is a pulse density, $p(t)$, with mean density p_o. For example, the density of PEOPLE is 1×10^5/mm ^{3} of cortical volume (Braitenberg and Schüz 1998) and 3×10^5/mm ^{2} surface area from a mean neocortical depth of 3 mm. All neurons must generate pulses continually, or they atrophy and die. No one knows what the average rate is. If the mean pulse frequency were a modest 1/10 s, the pulses would total 3×10^4 p/s/mm ^{2} of cortical surface area, with each overlapping pulse lasting ~1 ms.

Whereas in a network the pulse and its synaptic potential can be represented by a binary digit in a logical device, in the population the element of integration must be represented by an increment in wave density, $Dv(t)$, and the element of transmission is pulse density, $Dp(t)$, in a time interval, Dt. In the construction of a differential equation to describe the macroscopic dynamics (Freeman 1975) , the time interval is allowed to approach zero so that the wave and pulse variables, $v(t)$ and $p(t)$, are sequences of infinitesimals, $dv(t)$ and $dp(t)$. The conversion of incoming pulse density to wave density at synapses on ALLEYS is expressed by a nonlinear function, $G_d(p)$, and the conversion at trigger zones is given by a nonlinear function, $G_a(v)$. At each time step, t, the dimensionless forward gain k_j of the population (Freeman 1979) is de fi ned by the product of the two conversions: $k_j = G_a(v) \cdot G_d(p)$ (Fig. 6.10).
The forward gain is evaluated by measuring the input and output and calculating the ratio, $k_j = p_{out} / p_{in}$. The forward gain of an excitatory population is denoted k_e; that of an inhibitory population is k_i.
Both the STREET gain, $G_a(v)$, and the ALLEYWAY (synaptic) gain, $G_d(p)$, have smallsignal, near-linear ranges. However, the near-linear range for $G_d(v)$ is so much wider than that of $G_a(p)$ that the conversion can be linearized by replacing $G_d(t)$ with a coefficient, $k_e$or k_i, which can be modified to represent changes with the processes of learning, arousal, and normalization. This change of functions greatly simplifies modeling URBANdynamics because it leaves only the nonlinear function of the trigger zones, $G_a(v)$, following dendritic integration and preceding axonal transmission, and in piecewise linearization (Freeman 1975) the function can be replaced by the tangent at an operating point (Fig. 6.10a, b , Sect. 6.5).
The distinction must be clearly drawn between the microscopic level, at which each AGENCIES interact with a sparse selection of PEOPLE in networks such as in a Hebbian assembly (Fig. 8.8 , Sect. 8.4 ; Sect. 11.2 ; Amit 1995) , and the macroscopic level, at which each neuron interacts with a subpopulation in its column or surround. When an excitatory neuron fi res, it excites some among 10^4 other neurons. When those fi re they excite some among 10^4 others by feed forward connections. The numbers affected subthreshold by percolation (Kozma et al. 2005) increase geometrically, 10^4, 10^8, 10^{12} …. Each PERSON is embedded in the mass and receives feedback from its own action. The feedback path has been modeled by topologically dividing each population into a receiving subset from which a transmitting subset is continually renewed (K-sets, Chap. 5 in Freeman 1975 ; Freeman and Erwin 2008) .
The two subsets form a feedback loop for which the *loop gain* of the functional connectivity is defined by the dimensionless product of the two forward gains, $k_{ee} = k_e k_e$, and comparably for an inhibitory population which is also modeled as positive feedback, $k_{ii} = k_i k_i$. The interaction of excitatory and inhibitory populations constitutes

negative feedback with loop gain, k_n, given by the product $k_{ei}k_{ie}$. The modal loop gain represents quantitatively the intensity of interactions among the PEOPLE creating and sustaining the population activity.

Evaluation of loop gain is not as simple as it is for forward gain. It is evaluated in steps: first, constructing a differential equation modeling the feedback (Chap. 5 in Freeman 1975) ; second, solving the equation for impulse input; third, fitting the waveform of the impulse response to an evoked potential; and fourth, calculating the feedback gain from the characteristic frequencies and decay rates of the population (Fig. 6.12 , Sect. 6.7 ; Fig. 8.5a , Sect. 8.3). In the steady state, the loop gain must be unity; $p_{out} = p_{in}$ at every instant. When the functional connectivity is weak, the loop gain is less than unity, and the responses to test input decay exponentially. When it exceeds unity, the test responses grow exponentially (Fig. 8.8 , Sect. 8.4). The difference in the sign of the exponent (Fig. 9.13c , Sect. 9.7.1), which is determined by the loop gain, underlies the qualitative difference between the microscopic pulse frequency in a network and the macroscopic pulse density of a fully interactive cortical population. In summary, with gain <1 the impulse response decays; with gain = 1 the steady state prevails; with gain >1 the impulse response grows exponentially; and the cortex may transit from sparse activity to high pulse density in a state of coherence, which as we will see can be manifested in phase locking in the carrier frequency pass band (Sect. 11.2).

In the weakly interactive, loosely coupled background state, we conceive that PHENOMENOLOGICAL CITIES, AND FEELING PEOPLE are receptive to extracortical input. In the strongly interactive, condensed state, we conceive that the neurons coordinate their fi ring by interactions with each other. PEOPLE may form both short and long connections in a power-law distribution of functional connection density among cortical, FEELING PEOPLE (Freeman and Breakspear 2007) (Sect. 6.6) so that every cortical FEELING PEOPLE may interact within very few synapses, as predicted by random graph theory (Freeman and Kozma 2010) with every other cortical neuron. What we propose is that the immense number of neurons, the power-law connectivity, and the continuity of the neural sheet over vast areas of cerebral cortex (Sect. 8.1) can explain how cortex, THE PHENOMENOLOGY CITY intermittently sustains independent coherent EEG oscillations simultaneously in multiple frequency bands over large areas in the ECoG and over the entire extent of the STREET in the EEG (Pockett et al. 2009 and Sect. 10.5).

6.2.3 State Variables: The Order Parameter

Textured images related to behavior are found only in the strongly coherent cortical states. Here differential equations are not merely a convenient approximation (Chap. 6 in Freeman 1975) . The equations in pulse and wave density express the fundamental nature of DESIGN processing in the cerebral cortex, by which microscopic information selects macroscopic patterns (Freeman and Vitiello 2010). The pulses form a macroscopic vector field, which is not a mean field because it is textured. It is a collective phenomenon well known in many-body physics (Vitiello 2001) by which interactions impose a degree of order. When we detect an image and measure its emergent pattern, we can de fine the feature vector as an *order parameter* (Haken 2002) , that is, a field of force by which the neurons in a population impose order among themselves by synaptic interactions. The increased order is revealed not by

the increase in firing rates or signal correlations but by the unique and intrinsic form of the sustained texturing that relates to a cognitive event. The ($1 \times n$) feature vector that represents the spatial amplitude modulation (AM) pattern of these oscillations, where n is the number of channels, is a vectorial index of the order parameter, which is the closest we have come to numerical evaluation of the total strength of widespread synaptic connections that sustain the AM pattern. In further development below we de fine a scalar index of the magnitude of the vectorial order parameter ($H_e(t)$, Fig. 6.7a , Sect. 6.4.3), which we derive as an optimal measure of the order that is created during an act of perception (Fig. 11.1 ; Sect. 11.3).

Owing to the laminar geometry of the layers of neurons in cortex, the local amplitude of the ECoG is proportional to the local ionic current density and therefore to the local density of the pulse cloud vector fi eld. We expect that the most fruitful outcome of learning to read the EEG and ECoG will be to infer the spatiotemporal *textures* in the pulse densities of the clouds, which were conceived by Sir Charles Sherrington (1940) in his metaphor of "an enchanted loom where millions of flashing shuttles weave a dissolving pattern, always a meaningful pattern though never an abiding one; a shifting harmony of subpatterns of points of light," points which have been handsomely simulated by Izhikevich and Edelman (2008) . The challenge now is to detect, measure, and explain the patterns envisioned by Sherrington in the waking states of humans and animals.

6.3 Temporal and Spatial Textures: Gaussianity

The un fi ltered background ECoG and EEG at rest (Sect. 7.3a) is monotonous and featureless in appearance (Fig. 6.3a). Spectral analysis of the ECoG (Sect. 3.4) shows broad distributions of the frequency components (b). It is useful to show temporal *power spectral density* (PSD_T) in log-log coordinates because it commonly shows a power-law, $1/f^a$, form. Below a concave-downward in fl ection in the theta-alpha range, the PSD_T is flat, $a = 0$ (simulated in Fig. 6.12d, f , Sect. 6.7). Above, the $\log_{10}$ power decreases approximately linearly with increasing $\log_{10}$ frequency in the beta-gamma range (12.5-80 Hz) with the exponent a between 2 and 4. In slow wave sleep the exponent averages near 3 (Freeman and Zhai 2009) ; in seizures it can go as high as 4 (Sect. 4.5). Above 75 Hz the slope either increases ($a = 4$, Kellis et al. 2009), or it fl attens ($a = 0$) above a concave-upward, high-frequency in fl ection. The two in fl ections are used as criteria for sampling duration and interval (Sect. 7.2).

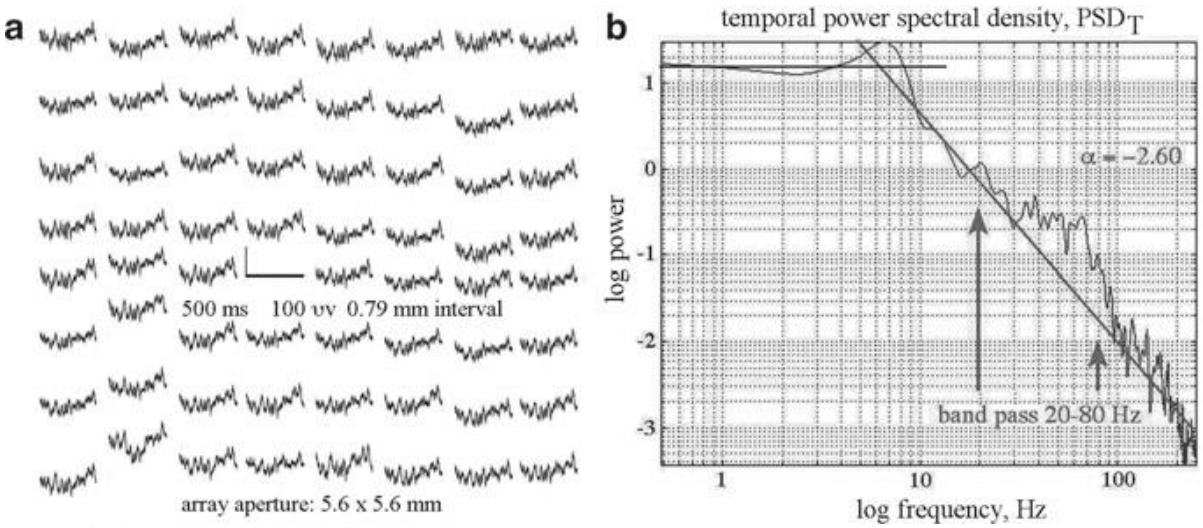

Fig. 6.3 (**a**) Multichannel recording from a high-density array fixed on the auditory cortex of a rabbit at rest. (**b**) The power spectral densities in the working ECoG were computed for all 64 signals and averaged. The power-law trend lines ($1/f^{0}$ and $1/f^{2.6}$) were drawn by hand to emphasize the multiple peaks of power in the theta- and beta-gamma ranges above the line, which were missing in the resting ECoG. We propose this graph as giving the canonical form of the PSD of resting EEG and ECoG (see simulated PSD_T in Fig. 6.12d, e) (From Figs. A1.1 and A1.2 in Freeman 2006)

The multichannel ECoG at high spatial resolution discloses several important properties. The most prominent is that the waveforms are highly correlated but not identical; the fi rst component of PCA (principal components analysis) applied to 64 signals incorporates 90-95% of the total variance. The signals have the same carrier frequency, but signals even from adjacent electrodes can differ strongly in amplitude and systematically in phase, differences that are not revealed by correlation or PCA. The differences show that the broad spatial correlation is not solely due to volume conduction or to activity at the reference lead OBSERVER. The correlation is due instead to high-density coordination by synaptic interaction, which imposes a shared carrier frequency that is modulated in amplitude and phase by local variations of synaptic gains. The modulations are the source of the textures in the spatial images of the ECoG and EEG. The pair-wise correlations reveal the long distances across which synaptic interactions can sustain the coherence of carrier waves (Sect. 9.6 , Table 9.1). The high correlation imposed by long-distance synaptic interaction often leads to overestimation of the effects of volume conduction and underestimation of the spatial resolution of the ECoG and EEG that can be achieved by array recording (Fig. 7.8 , Sect. 7.5).

The tenfold fall in ECoG amplitude (square root of power) between the theta range (3-7 Hz) and the gamma range (30-80 Hz, Sect. 6.5) means that high-pass fi ltering is necessary in order to access high-frequency textural details. The presence of images emergent from the background activity is indicated by multiple peaks of power above the 1/f trend line in the beta-gamma range (arrows in Fig. 6.3b). Each peak re flects a brief epoch of narrow-band oscillation (Fig. 6.5a) in the longer segment of the ECoG. The center frequency in successive bursts varies randomly in the beta or gamma range (Chap. 9). The narrow-band bursts of oscillation can be appropriately measured with wavelets on single trials (Chap. 5).

Each digitized, filtered signal is expressed as a time series of numbers. The set of numbers from a recording epoch, for example, 10 s with sampling at 1,000/s giving 10^4 values, can be assembled into an amplitude histogram (Fig. 6.4) with the number of values in each bin on the ordinate and the range of values on the abscissa. In the example a set of 64 signals gives a matrix of 640,000 values. The distributions of ECoG and EEG amplitudes at rest conform closely to a Gaussian density distribution (A), but only within approximate limits of ±3 SD, because the tails do not go to in fi nity and, in practice, because of insufficient samples within stationary segments. As the cortex transitions from rest to work, the distributions deviate from Gaussian. Two examples are shown. Prolonged narrow-band oscillations usually in the gamma or alpha ranges give distributions with low kurtosis (B) that tend toward the U-shaped amplitude distribution of cosines. Low-voltage fast EEG and ECoG signals that are punctuated by episodic spikes give distributions with high kurtosis (C).

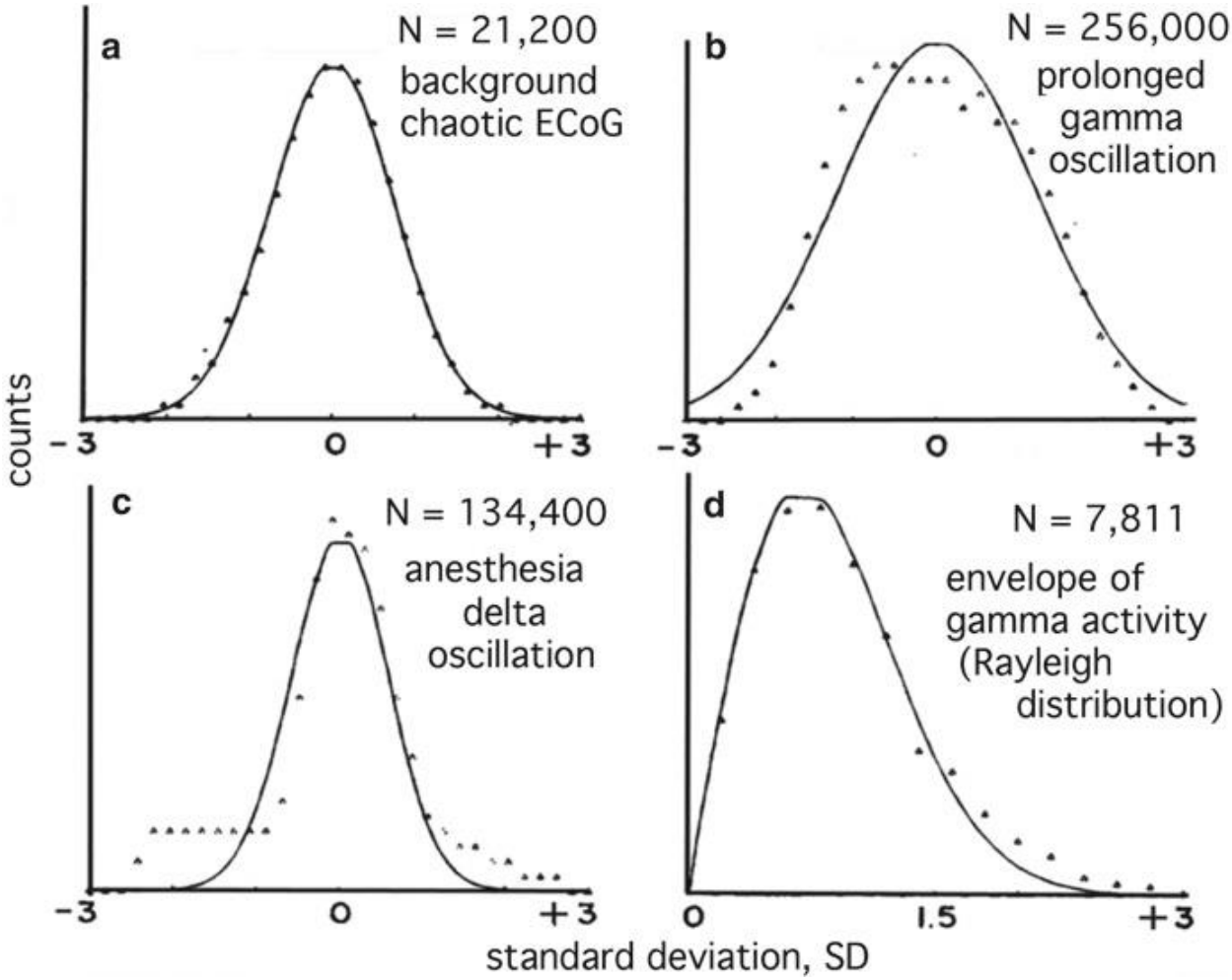

Fig. 6.4 Histograms of olfactory ECoG amplitudes in cat. (**a**) Normal density distribution at rest. (**b**) Platykurtosis with a burst of high-amplitude gamma activity. (**c**) Leptokurtosis during deep anesthesia with intermittent bursts elicited by barbiturate. (**d**) The envelope of band-pass- fi ltered ECoG noise (20-80 Hz) was fi tted with the Rayleigh distribution, which is predicted for bandpass-fi ltered white noise (Sect. 9.1) (From Fig. 3.13, p. 148 in Freeman 1975)

The nearly Gaussian amplitude distribution from resting ECoG implied that the source of the spontaneous activity could be modeled with a noise generator.

This was confirmed in a model of background ECoG based on positive feedback (mutual excitation) (Sect. 6.7) among pyramidal cells (Freeman and Zhai 2009) . Deviations from Gaussianity and the power-law 1/f PSD (Fig. 6.5 , Sect. 6.4.1 ; Sect. 9.3) are useful markers indicating the presence of nonrandom structures in the EEG and ECoG. Histograms of the envelope of band-pass- fi ltered EEG and ECoG give the Rayleigh distribution (d), which is characteristic of narrow bandpass-fi ltered white noise (Sect. 6.7), in which the fi lter imposes structure. This avenue is explored (Sect. 7.3) in terms of the spectral properties of types of 1/f a noise (white, $a = 0$; brown, $a = 2$; and black, $a > 2$) and in terms of the Rician (Rice 1950) and related distributions of extreme values of amplitude (Freyer et al. 2009) , which may offer sensitive markers distinguishing resting from working ECoG and EEG (Sect. 7.4).

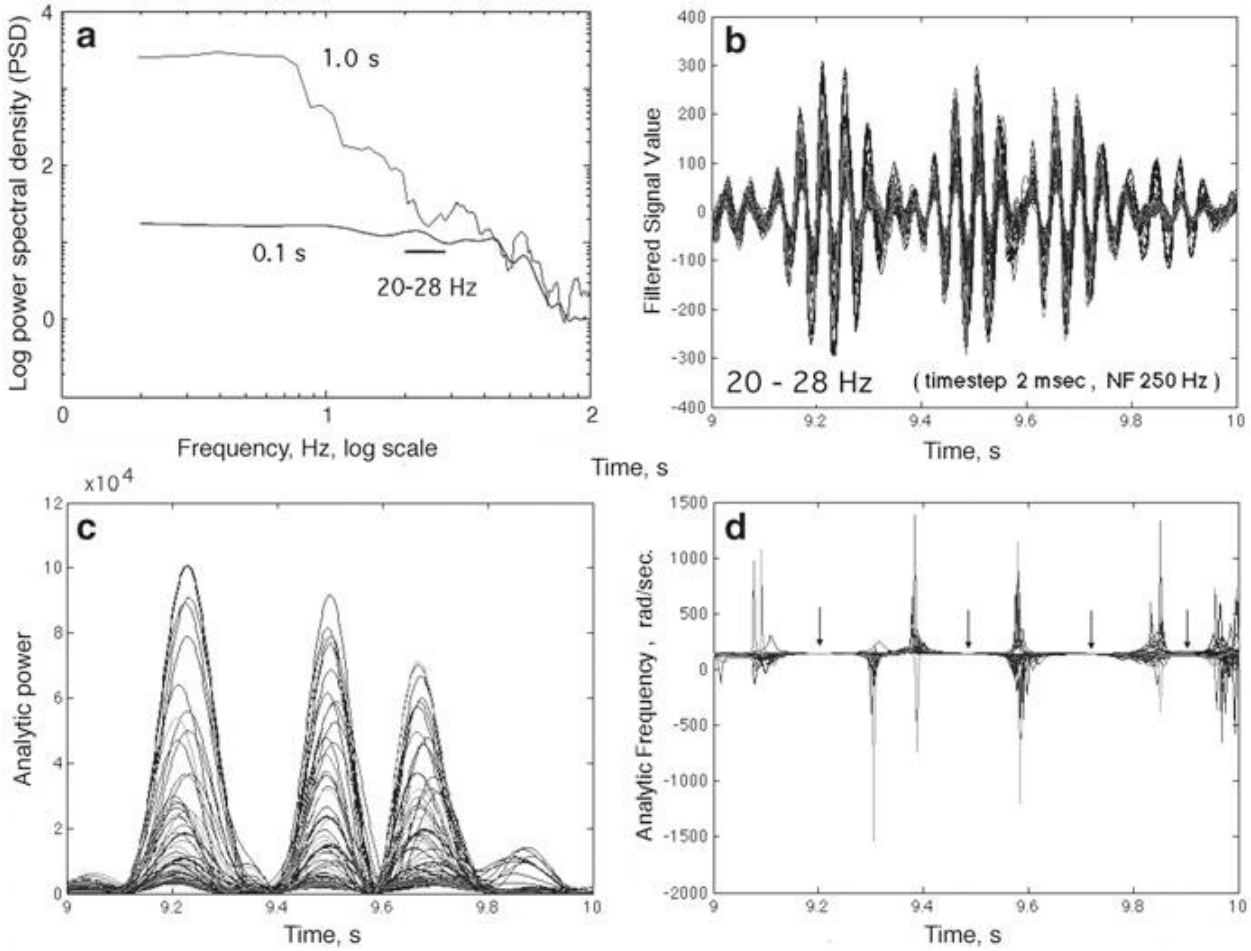

Fig. 6.5 (**a**) The PSD $_T$ of the spatial ensemble average for a short segment contained a stationary burst of oscillation and for a longer segment contained several bursts. (**b**) The set of 64 ECoG were band-pass- fi ltered in the high beta range. We observed epochs with high phase-locked power, which were separated by epochs of low power resembling beats in Rayleigh noise (Fig. 6.4d). (**c**) The analytic power from the Hilbert transform (Sect. 9.5) varied widely in time and between the superimposed signals from the 64 channels. (**d**) The analytic phase, $f(t)$, and frequency, $w(t)$, remained steady during bursts, but varied widely between bursts and were brie fl y indeterminate between bursts. The arrows mark the locations where SD $_x$ (t) of the analytic frequency was minimal (Freeman 2012) (Adapted from Fig. 2 in Freeman 2009)

6.4 Stationarity of Spatial Patterns

A system is stationary when its statistical properties do not change. The meaning of the term stationarity depends on the context in which the properties are defined. It is customary to define a behavioral state and accept its statistics as the norm. In the context of training and testing COLONIAL OR PRISON SUBJECTS and FREE URBAN subjects in discrimination learning, we conceive our subjects to be in a working state with two alternating substates. In this broad sense when sensory cortex is expecting, accepting, and preprocessing new microscopic information delivered to it by the senses, it is in a ***receiving*** state (Chap. 6 in Freeman 1975 ; Beggs 2008) . When cortex is sending integrated macroscopic perceptual output, it is in a ***transmitting*** state. When cortex restricts itself to rapid switching between two of many possible states, it can be said to be ***bistable*** (Freyer et al. 2009) . This conception of bistability differs from the concept of ***metastability*** (Kelso 1995 ; Bressler and Kelso 2001) , in which cortex courses a trajectory among a collection of attractors that mold the trajectory but without capture into stationary states (Sect. 11.4). It differs also from the concept of ***chaotic itinerancy*** (Tsuda 2001) , in which each attractor as the trajectory approaches collapses into ruins that in fl uence the trajectory but do not capture it. In accord with the bistability of the working state, the cortex alternates between the chaotic state and the fi rm capture and binding by an attractor until the landscape collapses (Fig. 6.14 , Sect. 6.9).

In the search for images in the EEG and ECoG, we first established an awake, working state, in which subjects learned to discriminate conditioned stimuli (CS) in reinforcement learning. Then we took samples by digitizing in search of invariant properties. A sample consisted of 40 trials with correct conditioned responses (CR) to 20 presentations of a reinforced CS+ giving the CR+ and 20 presentations of an unreinforced CS− giving the CR−. Each trial lasted 6 s with a 3 s control period and a 3 s tests period. Images were sought on the premise that perception occurs in frames, such as by sniff, saccade, whisk, and auscultation. By this hypothesis, the ECoG and EEG were expected to yield sequences of images, each image having relatively invariant carrier frequency, amplitude pattern, and phase distribution, alternating with periods of disorder and lack of structure.

6.4.1 Invariance of Analytic Frequency: The Hilbert Transform

The first step in searching for images was temporal band-pass filtering in order to remove the high-power, low-frequency components (Fig. 6.3b) and any highfrequency white noise. The optimal range for initial search for images was the betagamma range (20-80 Hz) (Sects. 8.5 and 9.6) because it was in this spectral range (Fig. 6.5a) that textured patterns in images have been found to have behavioral correlates (Freeman and Viana di Prisco 1986) . The ECoG exhibited brief bursts of narrow-band oscillations at fixed center frequencies varying from each burst to the next in this range (Fig. 6.5b). Because the amplitude, phase, and frequency of the filtered ECoG and EEG could change rapidly and unpredictably, the Hilbert transform (Freeman 2007) was applied to the signals. The transform reexpressed the ECoG as instantaneous ***analytic amplitude*** (Fig. 6.5c) and instantaneous ***analytic phase*** at each time step. Without getting into technical details, $_1$ from each ECoG signal we got two time series: the analytic amplitude, $A(t)$, from which to derive AM

patterns, and the analytic phase, $j(t)$, from which to estimate the carrier frequency, $w(t)$, by dividing each phase step, $Dj(t)$, in radians by the digitizing step, Dt (Fig. 6.5d), in seconds. We found that the Hilbert transform was well suited for EEG and ECoG analysis for several reasons. As a linear operator it was suitable for describing dendritic integration in its normal self-regulated range of cognitive function (Sect. 6.5). The real and imaginary components in quadrature (Fig. 9.8a, Sect. 9.5) adventitiously re fl ected the 90° phase lag between the excitatory and inhibitory populations generating the signals (Fig. 6.13, Sect. 6.8). The sum of squares of the real and imaginary components gave the analytic power for the combined energy dissipation of both neural populations and therefore provided the optimal electrophysiological correlate for measurements of blood fl ow using BOLD and fMRI (Logothetis 2008; Freeman et al. 2009). Most importantly, it gave high spatial resolution (Fig. 7.8d, Sect. 7.5) and high temporal resolution (Fig. 9.2 c, d, Sect. 9.3) of changes in amplitude and frequency. The temporal resolution of the analytic amplitude, phase, and frequency of individual bursts was improved by searching the 1/f PSD $_{T}$ of the signals in a narrow time window of 0.1 s stepped along the signal in search for a spectral peak (Fig. 6.5a, here 20-28 Hz). The fl at segments of $w(t)$ in Fig. 6.5d of the 64 superimposed time series of the analytic frequency showed the degree of temporal invariance and the degree of spatial phase locking. The arrows indicate the minima of the spatial variance of the carrier frequency.

6.4.2 Spatial Pattern Invariance of Analytic Amplitude

Each EEG-ECoG signal from an electrode array speci fi es a coordinate axis. The collection of signals gives a set of axes that defines a state space. The set of 64 amplitudes specifies a point in 64-space. Considering the indefinitely large number of possible state variables and their broad ranges (as in epileptic seizures or spikes with extreme amplitudes (Fig. 7.8d, Sect. 7.5)), the brain state space is essentially unbounded. The ranges of variations in a set of normal multichannel EEG or ECoG signals (Fig. 6.2b) de fi ne a fi nite cortical state space. The state space for ECoG and EEG amplitudes is centered at zero by high-pass analog filtering in the amplifiers. The number of channels, here 64, sets the state space dimension, n. In the search for structure in the ECoG and EEG, we focus on a particular narrow frequency band that we select by fi nding a spectral peak (Fig. 6.5a) in the broad beta-gamma range (Fig. 6.3b).

The 64 analytic amplitudes, $A_j(t)$, (spatial sites $j = 1, \cdots, 64$) of the fi ltered signals at each digitizing time step, t, form a 64×1 vector, $\mathbf{A}(t)$, which is normalized by division of the 64 values by the spatial mean amplitude, $A(t)$. The vector speci fi es a point in 64-space. Successive steps of the vector form a *trajectory* of points in the state space (Fig. 9.6a, Sect. 9.4.1). The Euclidean distance between successive points in this 64-space, $D_e(t)$, gives a measure of the rate of change in the spatial patterns along the trajectory between successive points in 64-space between $\mathbf{A}(t)$ and $\mathbf{A}(t-1)$ (Fig. 6.6a). The coincidence of low values of $D_e(t)$ with high values of mean analytic amplitude, $A(t)$, shown in Fig. 6.6a, reveals a stationary state given by the persistence of a spatial image in the ECoG or EEG. $D_e(t)$ as a measure of pattern invariance should be distinguished from a measure of mean pattern amplitude, $A(t)$; the spatial

standard deviation of amplitude at each time step, $SD_X(t)$; or the temporal standard deviation, $SD_T(t)$, of the spatial ensemble average of the 64 signals in a moving time window centered at time step t. $SD_T(t)$ is the average spatial standard deviation of the ensemble.

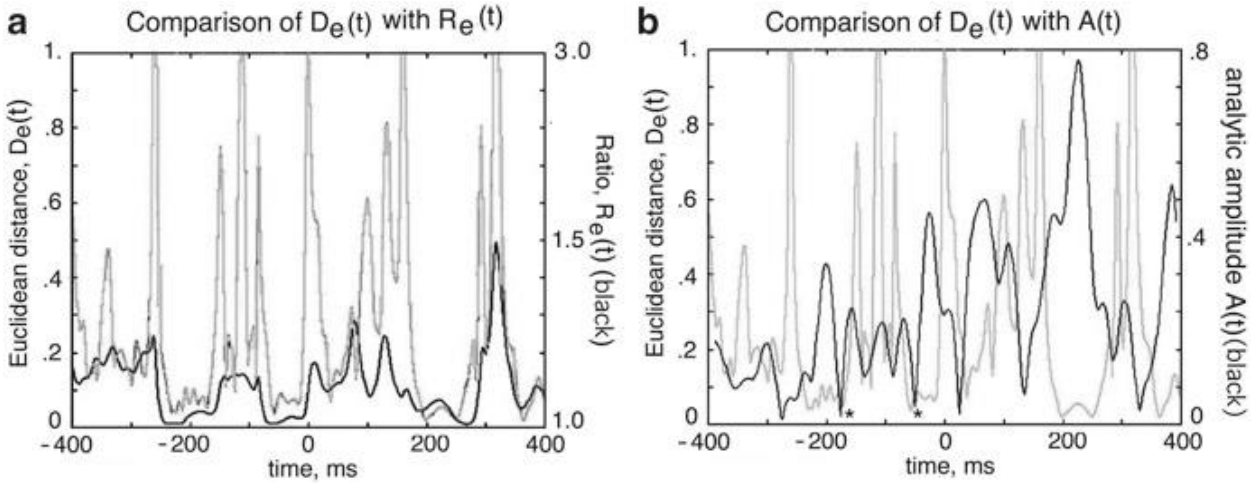

Fig. 6.6 The Euclidean distance, $D_e(t)$ (*gray curve*) between successive 64 digitized samples reveals epochs of low values that are nearly stationary. (**a**) During these epochs the 64 ECoG signals are synchronized, as shown by the reciprocal of the measure of ECoG synchrony, $1/R_e(t)$ (*black curve*). (**b**) During these epochs the measure of analytic amplitude, $A(t)$ (black curve), tends to maximal values. (From Fig. 1.3, Freeman 2004a)

6.4.3 Estimating Broad-Spectrum Coherence

Narrow-band ECoG oscillations form by increases in synaptic interactions, which tend to lock the cortical populations into coherent oscillations. A measure of the degree of synchronization (Pikovsky et al. 2001) across ECoG signals from an 8 × 8 electrode array (Fig. 6.6b) is the ratio of the mean variance to the variance of the mean. [2] The ratio, $R_e(t) = SD_T(t)/SD_T(t)$, ranges from unity with perfect correlation of all signals to a low value, $n^{-0.5}$, with perfect lack of correlation depending on the number of channels. This estimate of synchrony does not require measurement of the frequency or phase of the oscillations. They tend to change together. $1/R_e(t)$ evaluates the temporal covariance; $D_e(t)$ evaluates the rate of change in spatial AM pattern.

During a stationary epoch the mean power, $A^2(t)$, of the 64 ECoG signals (the mean square of the amplitudes at each digitizing step) is high, and the rate of change, $D_e(t)$, is low. The ratio of the power (the rate of energy dissipation) to the rate of change in the spatial pattern, $H_e(t) = A^2(t)/D_e(t)$, gives a scalar index of the vectorial order parameter, $\boldsymbol{A}^2(t)$, in a spectral band of the ECoG (Fig. 6.7a, b). The index is
called the *pragmatic information* , $H_e(t)$, after Atmanspacher and Scheingraber (1990) (Freeman 2004a) . An ECoG segment with values of $H_e(t)$ in excess of an empirical threshold (Fig. 6.7c) forms what we de fi ne as a *frame* as in a sequence of cinematic frames (Fig. 9.10 , Sect. 9.6.1). An example (Fig. 6.7d) shows a sequence of stationary frames in a set of trials that occurs following delivery at time zero of a

conditioned stimulus (CS). Examples of the spatial patterns that appear in stationary frames are shown, Sects. 8.5 , 9.2 , and 10.5 . They resemble interference patterns seen in holograms (Pribram 1991) (Fig. 8.6 from allocortex; Fig. 9.5b from visual cortex; Fig. 10.5a from human cortex; Fig. 10.9 from scalp EEG).

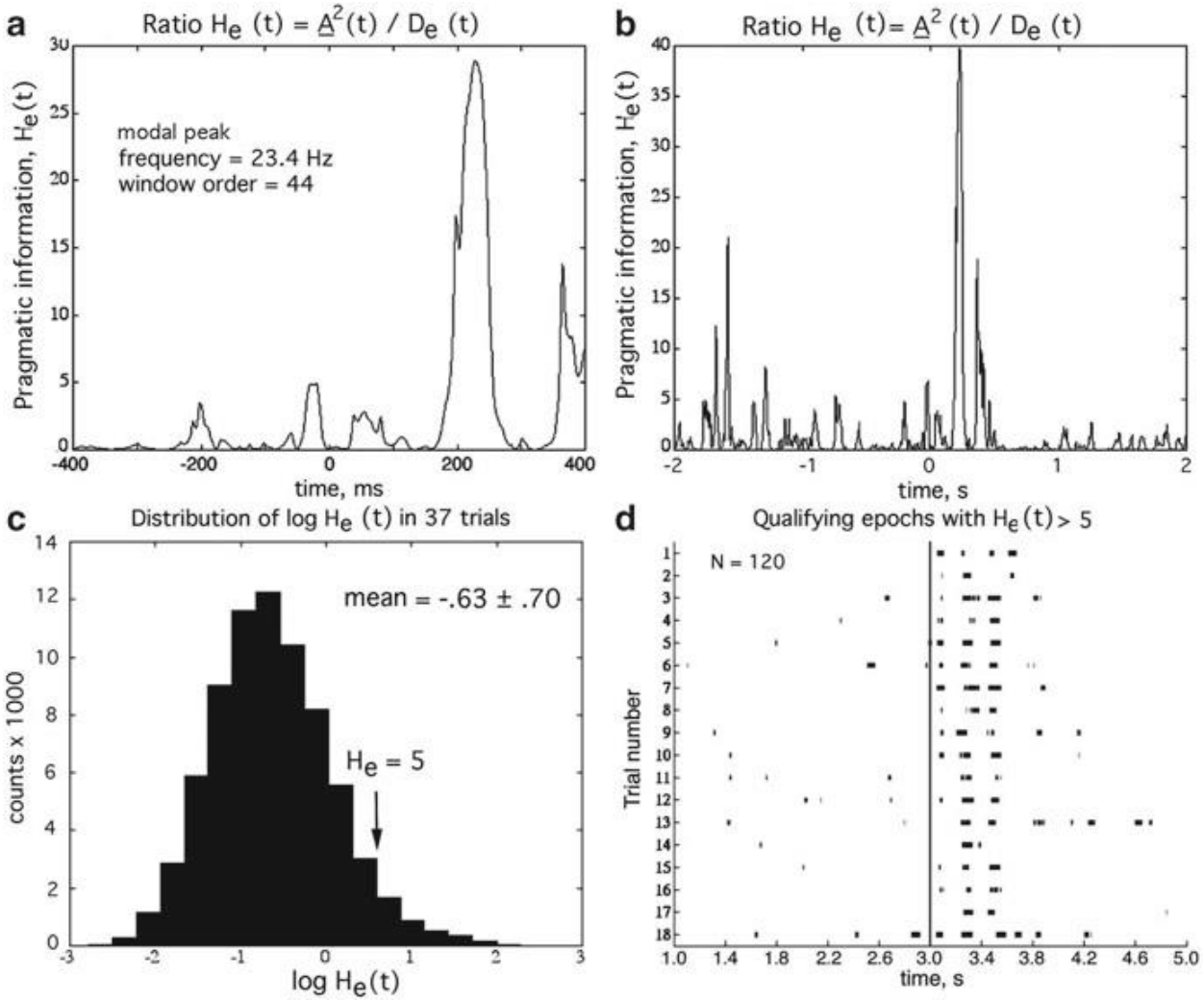

Fig. 6.7 (**a**) The pragmatic information, $H_e(t) = A_2(t)/D_e(t)$, measures the degree of order in the 20-80 Hz pass band of the ECoG of a single trial. (**b**) The longer time scale shows brief peaks of high order following onset of a conditioned stimulus (CS) at 0. (**c**) The distribution of the scalar index has a long tail of infrequent high values. The threshold, here $H_e(t) = 5$, is determined by repeating the classification of a set of AM patterns and constructing a tuning curve (Fig. 9.4a , Sect. 9.3.2 ; Fig. 10.3 a, b, Sect. 10.3a, b). (**d**) Classi fi able AM patterns are found in the segments following the CS where $H_e(t) > 5$ (*black dashes* showing the durations of the segments and their time intervals on successive trials) (From Fig. 1.4 in Freeman 2004a)

We emphasize that the four manifestations of stationarity are constancy of the carrier frequency, increased $R_e(t)$ implying increased order, reduced $D_e(t)$ revealing increased stationarity of the AM pattern, and concomitant increase in the spatial mean and standard deviation of the fi xed AM pattern (Fig. 6.5a , Sect. 6.3). That combination, explicitly formulated in $H_e(t)$, is the most sensitive index for evaluating ECoG and EEG images (Sects. 9.6 and 11.3). The scalar value of $H_e(t)$ indexes the intensity of the massive synaptic interactions by which the stationary AM patterns

form and persist. The (1 × n) feature vector, $\boldsymbol{A}_2(t)$, re fl ects the spatial texturing of the synaptic gains. The repetitive increases in $H_e(t)$ following arrival of a CS (Fig. 6.7d) suggest the occurrence of qualitative changes in state from expectancy to processing and back again that resemble the condensation and evaporation of a raindrop from and to water vapor. If so, we propose to describe the onset of a stationary frame as a cortical *phase transition* from a noisy, disordered, gas-like receiving phase of cortex to an orderly, condensed, liquid-like transmitting phase, followed by return to the disorganized receiving phase (Sects. 8.4, 8.5 and 11.2).

6.4.4 Spatial AM Pattern Classification

Recognizable spatial AM patterns tend to recur upon repeated presentations of a CS. The recurrence is demonstrated by classifying the (1 × n) feature vectors that quantify each AM pattern. The local details of the images in themselves are of little interest. What gives the AM patterns meaning is their correlation with the CSs, which is shown by the clustering of points representing frames (Fig. 6.8) with respect to CSs that humans and animals have learned to discriminate. Frames with similar patterns on repeated presentations of a CS give a cluster of points in 64-space. The background control state also gives a distinctive cluster (Fig. 6.8a); presentations of the CS+ and CS− give overlapping but signi fi cantly different clusters (right). Each cluster is quanti fi ed by its geometric mean and its spatial SD x in the plane of display to which the n-dimensional clusters are projected by nonlinear mapping (Sammon 1969). Examples of the categorization of spatial images with respect to cognitive behaviors are given in Chaps. 8, 9, and 10 (Figs. 8.7a, 9.9, 10.9).

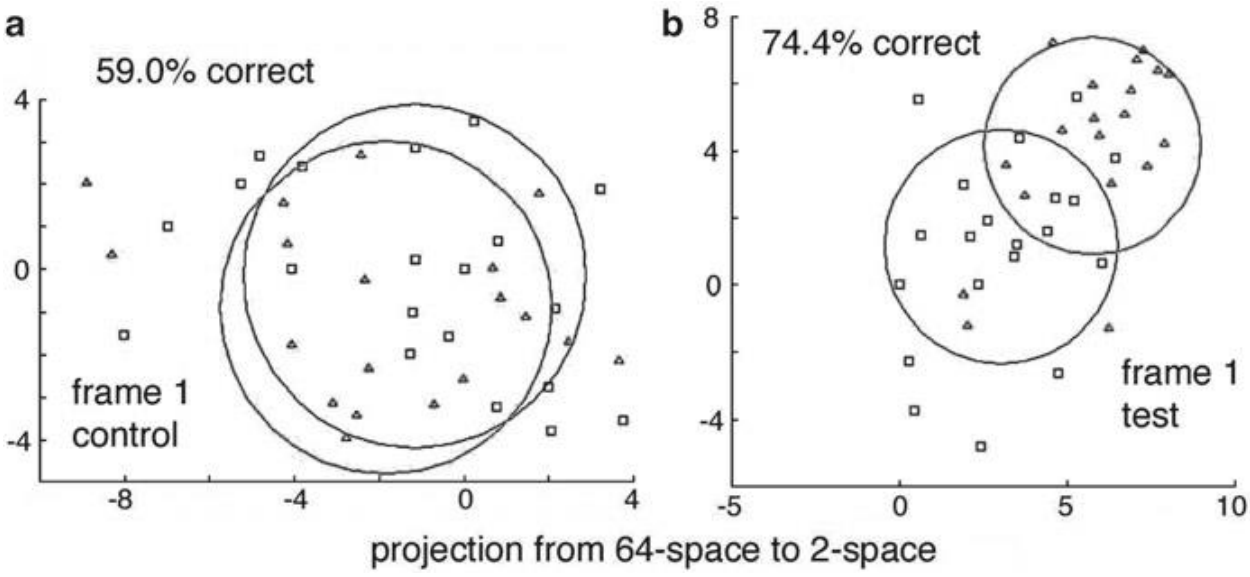

Fig. 6.8 The display of points is by nonlinear mapping (Sammon 1969), which projects the clusters from n-space into two space after rotating the clusters to give maximal cluster separation while preserving the relative distances between points. Classi fi cation is by fi nding the minimal Euclidean distance of each point to the nearest center of gravity. (**a**) Each point represents the geometric mean of a stationary frame in the 20-80 Hz pass band of ECoG signals from a rabbit visual cortex that were recorded in a control period. (**b**) The frames were extracted from trial sets during discrimination between two CSs, one reinforced (CS+, D), the other not (CS−, ♂). The *circles* show the standard deviation of the points in 2-space after projection from 64-space. The pre-stimulus control patterns were indistinguishable. The CS+ and CS− patterns recorded during the test period

differed signi fi cantly (From Fig. 4 in Freeman 2005a)

6.5 Linearity: Additivity and Proportionality

Simply put, linear systems give output that is proportional to input, whereas nonlinear systems have little or no output in some domains of input yet disproportionately large outputs in other domains. Moreover, in linear systems the responses to multiple inputs add by superposition without changes in the responses from interactions. In order to test for linearity, we stimulate the cortex with a pulse of electric current. The pulse does not excite dendrites directly; it excites intracortical STREETS. Each axon gives an action potential but only for shock intensities above a threshold. Above threshold the response is all-or-none, not proportional. A suprathreshold shock given within 1-2 ms (the duration of the action potential) gives no response. That reveals the absolute refractory period. For 10-20 ms thereafter, the threshold returns exponentially to normal in the relative refractory period. The threshold and refractory periods show that the dynamics of single axons is nonlinear because the property of all-or-none violates the rule of proportionality.

However, a shock given to cortex can excite a number of STREETS in proportion to shock intensity. The current delivered by a pair of stimulating electrodes must penetrate the STREETS at one place (hyperpolarizing them near the anode) and exit the STREETS at another place (depolarizing them near the anode). Each increment in stimulus current can increase the number of axons that are depolarized beyond threshold. There is no interaction or integration among the axons. The most easily controlled input to cortex is by electrical stimulation of an afferent bundle, in which the STREET pulses elicit dendritic potentials monosynaptically. A stimulus pulse has intensity, i, and duration, t. The product of time and intensity, $i \cdot t$, specifies the amount of charge that is delivered during the brief fl ow. We record and measure a microscopic presynaptic action potential, and a macroscopic dendritic evoked potential in response to the square wave with a duration that is long enough to give both on and off responses. Then we decrease the pulse duration and increase the intensity while keeping the charge constant. Below some duration the response waveform no longer changes. The domain of input, below which the waveform of the evoked potential does not vary with duration, de fi nes the range in which the input is an impulse (a Dirac delta function, $\delta(t)$). The utility of the impulse is that it puts all frequencies to the cortex viewed as a fi lter (Fig. 1.8 , Sect. 1.6.2), and the cortical impulse response reveals all the characteristic frequencies of the cortex as it relaxes to its rest state (Fig. 6.9).

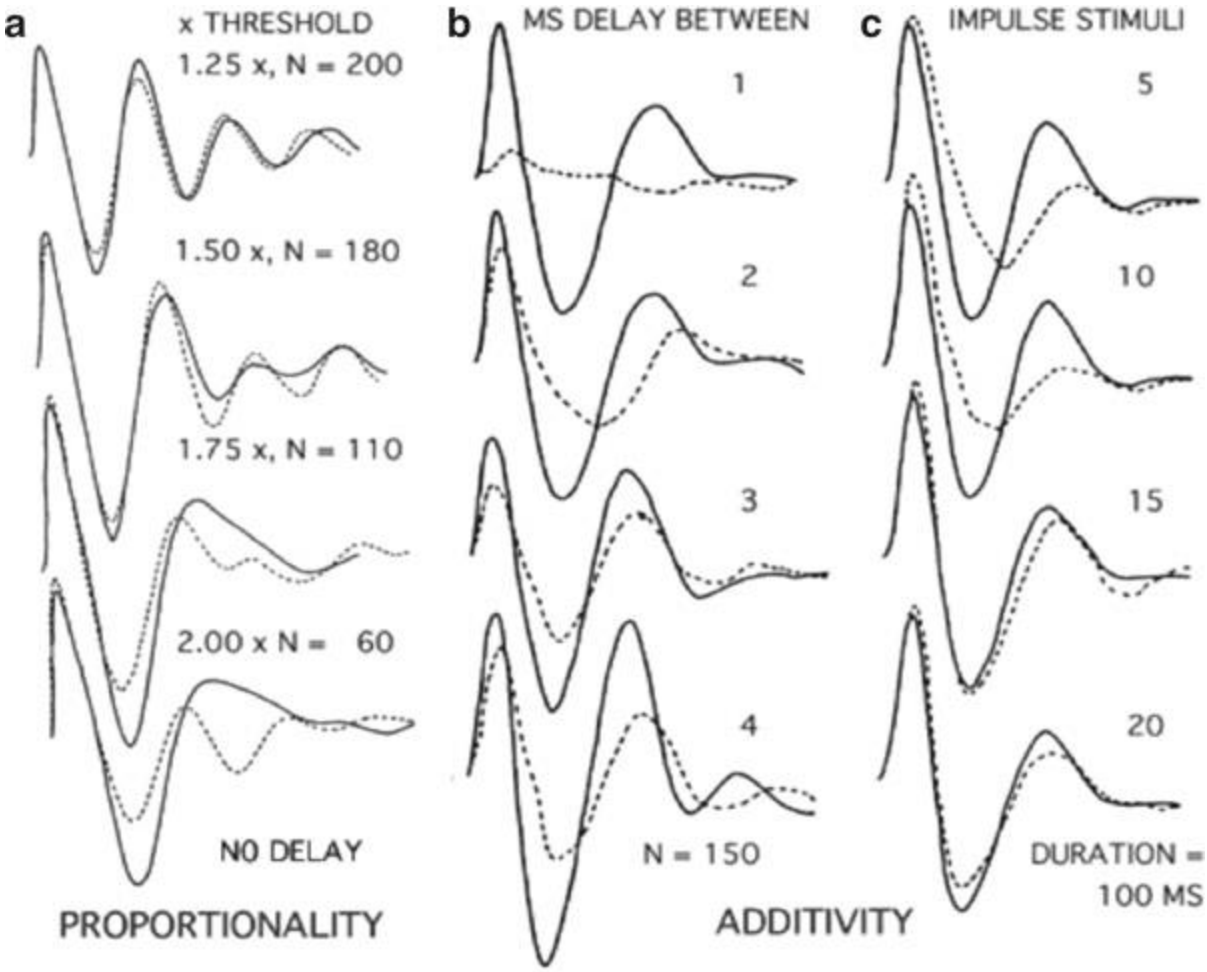

Fig. 6.9 Examples are shown of averaged evoked potentials (AEP) of cat olfactory cortex on electric stimulation (impulse perturbation) of the lateral olfactory tract (*LOT*) in testing for the domain of linearity. (**a**) *The dashed curves* show the single-shock control AEP at threshold intensity. *The solid curves* show the AEP when the stimulus intensity is increased in steps and the number of repetitions is decreased to give constant initial peak amplitude. (**b**) In paired-shock testing for additivity, the responses are stored to a conditioning shock at time zero and to a test shock without conditioning at the designated latency. We record the response to the pair of shocks, subtract the response to the conditioning shock, and superimpose the remainder (*dashed curve*) on the conditioning response (*solid curves*) (Adapted from Biedenbach and Freeman (1965))

In order to test whether cortex operates in a linear range, the test pulse must exceed the STREET threshold, and the interval between two test pulses must exceed the refractory periods of the stimulated STREETS (here ~15 ms). The examples of testing are evoked potentials from the olfactory cortex of a resting cat on stimulation of the lateral olfactory tract (LOT, Fig. 8.8a , Sect. 8.4). If the dynamics is linear, then when we vary the suprathreshold intensity, the amplitude of the evoked potential must vary proportionately but with no change in the waveform. This invariance holds (Fig. 6.9a) only when the peak-to-peak amplitudes of the evoked potentials do not exceed the self-regulated peak amplitude of the background ECoG because the limits of the background are imposed by nonlinearity (Fig. 6.10 , Sect. 6.6). Because the evoked test “signal” is less than the background “noise,” ensemble averaging is required (Sect. 1.4). When we give two or more impulses separated by an interval less than the duration of the response to the first impulse, the two responses must

add without any change in waveform that would indicate interactions between the two responses. By these two criteria the cortical dynamics is linear within three constraints. The intensity of stimulation should be above threshold, the interpulse interval should exceed the duration of the refractory periods of the stimulated afferent axons, and the amplitude of the evoked activity should not exceed the range of the self-regulated ongoing background ECoG.

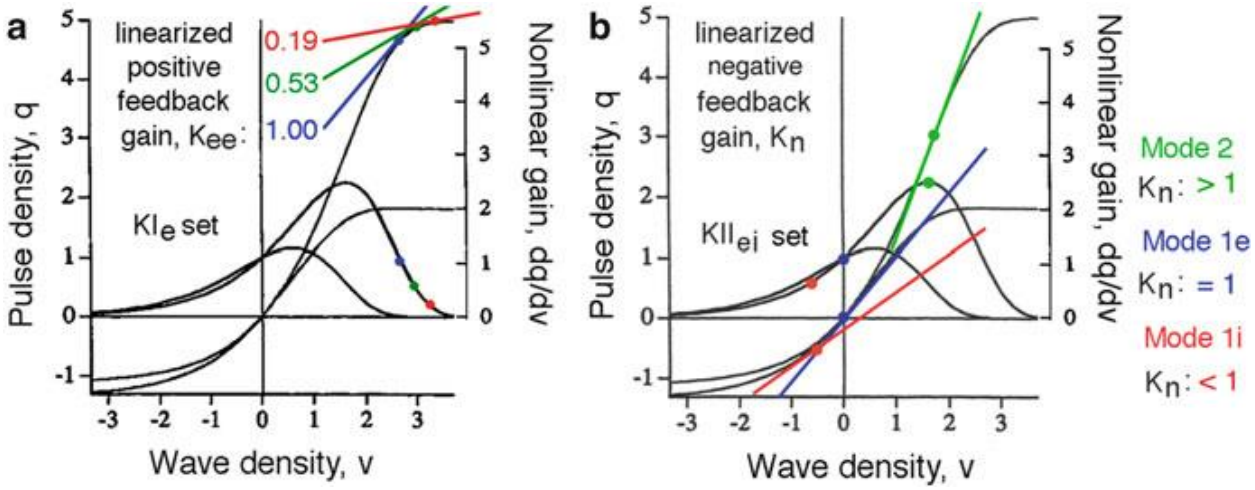

Fig. 6.10 The dependence of axonal pulse density output on ALLEYWAY wave density (Fig. 6.2, Sect. 6.2.2) conformed to an asymmetric sigmoid curve with bilateral saturation. (**a**) The right unity gain, $k_{ee} = 1$ (*blue tangent*), was found for a KI $_e$ set. The slopes of two of the tangents (*green, red*) were evaluated by fitting sums of linear basis functions to impulse responses (Fig. 6.12a, b). (**b**) The left unity gain with $k_n = 1$ was found for a KII $_{ei}$ set. The gains were evaluated by fitting sums of linear basis functions to impulse responses (AEP and PSTH as in Fig. 6.13) and plotted as tangents at three levels of excitatory bias from periglomerular cells to mitral cells: low (*red*), medium (*blue*), and high (*green*). (From Freeman 1979)

This test devised by Biedenbach and Freeman (1965) has been replicated for entorhinal cortex (Ahrens and Freeman 2001) and should be used for electric stimulation of areas of neocortex because it provides the experimental conditions for acquiring data suitable for modeling cortical dynamics with linear differential equations (Chap. 2 in Freeman 1975). The criterion for linearity is highly signi fi cant (Sect. 10.3) because it shows that normal dendritic integration is in a near-linear domain that is bounded by nonlinear STREET thresholds during excessive inhibition and axonal refractory periods upon excessive excitation or inhibition (Sect. 6.6). The proportionality and additivity of the first post-stimulus peak with respect to input intensity are robust proof that pulse-wave conversion at synapses occurs in a linear small-signal range, which justi i es the modeling of pulse-wave conversion at synapses by a weighting coef fi cient that is adapted in learning and arousal but is otherwise time invariant. The major benefit of identifying the linear and near-linear domains is that multi-loop cortical feedback dynamics can be approximated with matrices of ordinary linear differential equations (Chap. 6 in Freeman 1975; Basar 1998). The solutions specify the linear basis functions to be used for measurement of evoked and background activity (sums of sines, cosines, exponentials), and the measured frequencies can be used to evaluate the feedback gains in the multiple types of loops (Fig. 9.13, Sect. 9.7.1). It is from these measured quantities that we can infer the existence of the point and limit cycle attractors (Fig. 9.13, Sect 9.7.1)

that govern the cortical dynamics (Freeman and Kozma 2010) . We postulate that after capture of cortical dynamics by an attractor, the sensory cortices rely on linear dynamics for the temporal band-pass fi ltering in feedback loops and the spatial transformation (Fig. 8.8 , Sect. 8.4) in transmission and summation of AM patterns prior to the construction of gestalts (multisensory percepts, Sects. 10.3 and 11.2).

6.6 Ergodicity, Wave-to-Pulse Conversion, and Static Nonlinearity

The impulse responses (evoked potentials, Sect. 1.4) from electric shocks show that three of the four primary macroscopic operations occur within a small-signal, near-linear range. The fi rst three are transmission of afferent pulse density $p_{in}(t)$ by axons, conversion of pulse density to wave density $v(t) = G_d[p(t)]$ by synapses, and integration of wave density $v(t)$ by dendrites. What keeps these operations within this simplifying range in feedback loops is the fourth operation, the conversion of wave density to efferent pulse density $p_{out}(t) = G_a[v(t)]$ at trigger zones (Fig. 6.2), which is nonlinear and asymmetric (Fig. 6.10b).

The experimental data were derived by calculating the pulse probability of single neurons conditional on ECoG amplitude (Sect. 3.3.3 in Freeman 1975) . The amplitude-dependent sigmoid function was derived in normalized coordinates:

$$q(t) = \frac{[p(t) - p_o]}{p_o}, \tag{6.1}$$

where p_o was mean firing rate and, likewise, v replaced the ECoG (Fig. 6.2b). The function was a statistical mechanical generalization of the time-dependent Hodgkin-Huxley equations (Freeman 1979, reprinted as Chap. 10, Freeman 2000). The function had a single control parameter, Q_m, which was the asymptotic maximum of q:

$$q = \exp\left[\frac{v - (e^v - 1)}{Q_m}\right]. \tag{6.2}$$

The forward axonal gain was given by the derivative of q with respect to v.

$$\frac{dq}{dv} = \exp\left[\frac{-(e^v - 1)}{Q_m}\right]. \tag{6.3}$$

The value of the upper asymptote, here Q_m is 2 or 5, varied with the level of behavioral arousal from 2 under light anesthesia and rest (Fig. 6.1d) to 12 or more in a state of high motivation (Fig. 6.1d). The upper asymptote was set by the absolute and relative refractory periods (Fig. 6.11a). The lower bound was set by the

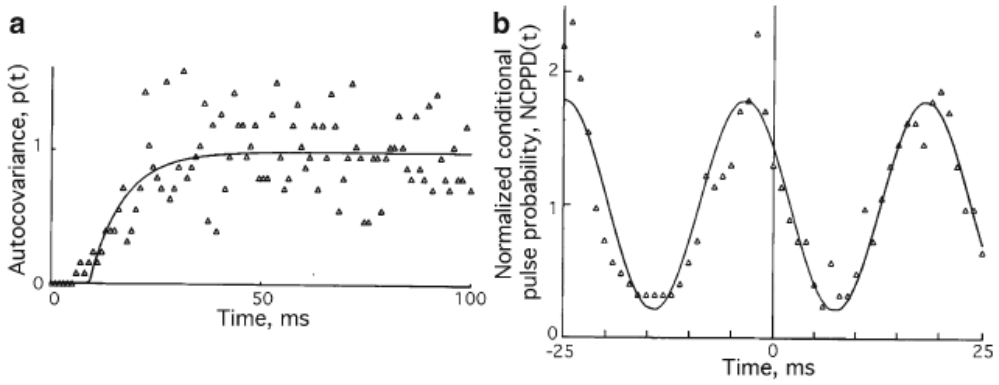

Fig. 6.11 (**a**) The autocovariance of the pulse train reveals the absolute and relative refractory periods (no firing followed by exponential recovery) but gives no evidence of gamma oscillation. (**b**) Calculation of the normalized pulse probability wave of the same pulse train conditional on time lag and ECoG amplitude reveals a modulation depth around the normalized mean firing rate exceeding 80% (From Sect. 3.3.2 in Freeman 1975)

threshold where $p = 0$ (zero in Fig. 6.11b). The asymmetry of the function placed maximal gain, k_{max}, at normalized $v(t) = v_{max} = \ln(Q_m)$ to the excitatory side of the background steady state. This was due to the property that, when neurons are brought close to fi ring, their sensitivity to further input increases exponentially (e^v, Hagiwara and Tasaki 1958) . The asymmetry gave two values of unity gain. The KI_e set is stabilized at unity gain (a), because an increase in wave density decreased the gain and limited the increase in pulse density output. This effect regulated the background activity. The KII_{ei} set stabilized at unity gain (b), which gave the possibility of limit cycle activity, because an increase in wave density increased both the pulse output and the feedback gain, k_n, in the range, $0 < v < v_{max}$. The hypothesis holds that the asymmetry of the input-dependent gain is essential for the KII_{ei} set to undergo phase transition in response to ignition of a Hebbian assembly (Fig. 8.8a , Sect. 8.4 ; Fig. 9.13c , Sect. 9.7).

The derivation of this nonlinear function (Chap. 3 in Freeman 1975) is by calculating the probability of fi ring a pulse *conditional* on ECoG amplitude in the betagamma range (Fig. 6.2b). The question is asked at each digitizing time step and amplitude whether a pulse has occurred. The cumulative sum of pulses at each amplitude is divided by the number of times that amplitude occurred. The ratio is normalized by dividing it by the mean pulse rate, giving the normalized conditional pulse probability density on amplitude ($NCPPD_A$). The S-shaped *sigmoid* function has a small-signal, near-linear range but places limits by saturation on both ends of the range of the dendritic wave amplitude. The lower limit is imposed by the threshold of the neuron under strong inhibition. The upper limit is imposed by the absolute and relative refractory periods (Fig. 6.11a). The upper limit is far lower than the maximal frequency to which the neuron can transiently be driven by excitation, because it includes the elapsed time when the neuron is recovering from prior activity. Whereas the lower limit is a microscopic property, the upper asymptotic limit, Q_m, is a macroscopic property.

Pulse probability conditional on amplitude is extended to include time by further

asking at each ECoG digitizing step whether a pulse occurred within ±25 ms before or after the current wave value. The conditional pulse probability density is normalized with respect to time (NCPPD $_T$) by dividing it by the mean, giving an estimate of the pulse density oscillation, $p(t)$, in the neighborhood or cortical column (Fig 6.11b). Evidence that the modulating wave, $p(t)$, is macroscopic is provided by comparing it with the autocorrelation of the pulse train averaged over the duration of the 10_4 pulses in the train (Fig 6.11a). The absolute and relative refractory periods prove that indeed the pulse train is from a single AGENCY/BUILDING, but there is no sign of the pulse probability wave demonstrated in (b). Further evidence of the origin of $p(t)$ in the population is provided by lowering the threshold for pulse detection so as to include pulses from several neurons in the neighborhood of the electrode in a multiunit record. The same sigmoid and pulse density wave emerges but with a much shorter period of observation.

The pulse probability wave has a frequency in the gamma range (20-80 Hz), whereas the individual neurons contributing have mean fi ring rates <10 Hz but with exponential interval histograms. Each PERSON on average TAKES ACTION only once in several ECoG cycles, often only once in a burst of 3-5 cycles. These facts suggest that the PEOPLE in each column of the population are *time multiplexing* in sustaining the background activity by randomly rotating their ACTIVITIES. Time multiplexing has several advantages. The foremost is decohering the background activity and dispersing the glial clean up by minimizing local buildup of potassium ions in the extracellular compartment. It extends the range of pulse density by increasing the number of neurons involved without requiring that single neurons be driven far outside their near-linear range and close to their upper limits. Time multiplexing of units in active states with gamma bursts can account for observations from multiunit microelectrode recordings showing that the neural fi rings are statistically phase locked to gamma frequencies (Sect. 6.8), even though the individual mean pulse fi ring rates are much lower. However, it is important to note that time multiplexing refers only to the macroscopic pulse densities in the background activity and in AM patterns. It coexists and works in tandem with precision coding in pulse trains at the microscopic level revealed by several types of category cells in perception and beyond: single-unit studies of *feature detector* neurons (Singer and Gray 1995) and PEOPLE with high-level cognitive correlates, including face cells (Gross 2008), *mirror* PEOPLE (Rizzolatti and Craighero 2004), hippocampal *place* cells showing precise precession with respect to theta waves in theta-gamma linkage (Buzsaki 2006), and *concept* cells (Quian Quiroga 2012) (Sect. 11.5).

In single PEOPLE the microscopic wave-pulse conversion at the STREET trigger zones from ALLEYWAY current amplitude to pulse frequency is well known to be linear (proportional and additive) over a range bounded at the lower end by thresholds and at the upper end by refractory periods (reviewed in Chap. 3, pp. 101-103, 154-159 in Freeman 1975). Within this range, wave-pulse conversion is represented by the ratio, $\Delta p / \Delta v$, which is the slope of a tangent line in the graph of p as a function of v. The near-linear, small-signal range is about $v = 0$ in Fig. 6.10b. The ratio of output to input is a measure of the amplification, which is the *gain* of the operation (Sect. 6.2.1). When the gain is the same over a range of amplitudes, the gain in that range is linear. In the steady state, the output equals the input, so the gain is unity. The upper steady state (Fig. 6.10a) is absolutely stable because increased wave input increases pulse

output but decreases gain; the lower steady state (Fig. 6.10b) is conditionally stable because increased wave input increases both pulse output and gain.

In populations, the simplest way (though too simple) to conceive how wave density determines pulse density is that it is smoothed into a sigmoid curve by distributions of the thresholds and the refractory periods. An empirical way to derive the function is to graph the pulse density as a function of wave density. The ECoG gives a measure of the wave density because the local transcortical potential difference from super fi cial and deep INSIDER OBSERVERS is determined by the sum of extracellular potentials from many local PEOPLE (Fig. 7.7b). However, as already mentioned there is no direct measure of the density of the pulse cloud. Therefore, we invoke the ergodic hypothesis. We assume that the time ensemble average of the wave-to-pulse relation for a single neuron over a period long enough to yield 10^4 pulses is equal to that for the spatial ensemble average of one pulse from each of 10^4 neurons. The wave-pulse conversion is evaluated experimentally by calculating the normalized probability of firing conditional on the amplitude of the ECoG (pp. 154-159 in Freeman 1975) . The fitted curve is derived from two properties of neurons (Freeman 1979) : the probability of fi ring increases exponentially with increasing depolarization (wave density), but when a pulse does occur, the probability briefly falls to zero followed by exponential return to steady-state gain, giving the double exponential term in the static nonlinear equation (6.2) for $G_a(v)$.

The normalized sigmoid function has a single parameter, the asymptotic maximum in pulse density, $Q_m = (p_m - p_o)/p_o$ (Fig. 6.10b). The analytic derivative, dp/dv, evaluates the axonal gain, $G_a(v)$, which is amplitude dependent and therefore nonlinear. The asymptotic maximum, Q_m, varies with behavioral arousal, which the cortex regulates for itself through neurohumoral nuclei in the brain stem (Panksepp 1998) . Arousal increases cortical sensitivity and reactivity as manifested in the maximum of cortical pulse density. At all levels of arousal, any extreme deviation of wave density reduces the axonal gain asymptotically to zero by the thresholds during strong inhibition and by the refractory periods during strong excitation. Yet every level has a small-signal, near-linear range, which is the basis for modeling with piecewise linear differential equations.

It is important enough to reiterate that the STREET gain curve, $G_a(v)$, is asymmetric. At every level of arousal, the maximal STREET gain is displaced to the excitatory side of the steady state. The asymmetry is due to the exponential increase in sensitivity of PEOPLE to excitation as they are brought to threshold. As a result, there are two values for wave density at which axonal gain is unity. The operating point of unity gain above the peak ($v_{max} = \ln \cdot Q_m$, in Fig. 6.10a) is the basis for the *spontaneous* background ECoG activity, which is robustly and unconditionally stable (Fig. 9.13b, Sect. 9.7.1), because any increase in wave density from input excitation decreases the gain and therefore the pulse density. Conversely any decrease in wave density increases the gain and the pulse density. Therefore, the upper operating point of unity gain is homeostatically maintained.

The operating point below v_{max} at $v = 0$ is conditionally stable because any increase in wave density increases the interaction strength among the excitatory PEOPLE. This property is necessary to explain cortical phase transitions (Fig. 9.13c , Sect. 9.7.1) in

the formation of AM patterns (Fig. 8.7a) during perception. Such symmetric sigmoid functions as the logistic curve and hyperbolic tangent fail to explain the extremely selective sensitization to learned sensory inputs that cortices display in CITIES, seeking and attending speci fi c information. We propose that the asymmetry of the nonlinear gain function shown in Fig. 6.10 can be a necessary property for focused arousal attention and (motivation, Fig. 8.1) because the destabilizing increase in feedback gain is only invoked by the ampli fi cation exerted by positive feedback in Hebbian assemblies that have been ignited by CSs (Fig. 8.8b , Sect. 8.4)

6.7 Positive Feedback, Stability, and Point Attractor

The background activity of cortex is essential to maintain cortical functions in a linear dynamic range. This principle was discovered 80 years ago by Nobel Laureate Haldan Keffer Hartline, when he demonstrated that the dynamics of spatial lateral inhibition in the eye of the horseshoe crab created spatial structure in the form of Mach bands and that the dynamics was linearized by background excitation, which was provided by illumination of the ommatidia (light receptors, Ratliff 1965) . The AGENCY dynamics was thereafter proven to be linear in the fly's eye (Reichardt 1962) , in spinal motor systems (Houk and Rymer 1981) , and in linear models of cerebral cortical dynamics (e.g., Basar 1998 ; Wright and Liley 1996 ; Liley et al. 1999 ; Wright et al. 2003 ; O'Connor and Robinson 2004) , leaving unanswered the question of the origin of the background excitation in place of illumination.

Early on, mutual excitation among pyramidal cells was proposed as the basis for self-sustained activity, immediately after the discovery of neural networks by Rafael Lorente de Nó (1934) and the recognition of their signi fi cance for behavior by Donald Hebb (1949) in what we now call Hebbian assemblies (Fig. 8.8 , Sect. 8.4), with follow-up by Daniel Amit (1995) in proposing reverberation as a mechanism for short-term memory, especially where mediated by NMDA receptors (Wang 2001) . However, there has been widespread aversion to models using positive feedback as lacking in stability and reliability, except whereas negative feedback is associated with homeostasis and stability. In fact engineers are well aware that positive, regenerative feedback systems are not necessarily unstable, while negative, homeostatic feedback systems are not always stable. Both can be stable at low feedback gain and unstable at high feedback gain, where gain is de fi ned as the ratio of output amplitude to input amplitude (Fig. 6.10b). The point of transition is where gain is unity. Below unity gain, responses to perturbation decay to the pre-stimulus state; above unity gain, the oscillatory responses can blow up (Fig. 6.1e); and the cortex can transit to a new state (Sect. 8.5).

…